Analysis of Two- and Three-dimensional Flow Separation

by

Olivier Grunberg

B.S. in Mathematics, University of Paris VII, France (2000)
M.S. in Fundamental Sciences, Ecole Polytechnique, France (2002)

Submitted to the Department of Mechanical Engineering
in partial fulfillment of the requirements for the degree of

Master of Science in Mechanical Engineering

at the

MASSACHUSETTS INSTITUTE OF TECHNOLOGY

February 2004

Signature of Author .....
Department of Mechanical Engineering
December 19, 2003

Certified by .....
George Haller
Associate Professor
Thesis Supervisor

Accepted by .....
Ain A. Sonin
Professor of Mechanical Engineering
Chairman, Department Committee on Graduate Students

Analysis of Two- and Three-dimensional Flow Separation

by

Olivier Grunberg

Submitted to the Department of Mechanical Engineering
on December 19, 2003, in partial fulfillment of the
requirements for the degree of
Master of Science in Mechanical Engineering

Abstract

Prandtl (1904) showed that streamlines in a steady flow past a two-dimensional streamlined body separate from the boundary where the skin friction (or wall shear) vanishes and admits a negative gradient. Although commonly thought otherwise, these separation conditions are purely kinematic: They can be derived for any two-dimensional steady vector field that conserves mass (see, e.g. Shariff, Pulliam, and Ottino 1991).

Haller (2002) managed to extend the Lagrangian separation theory to compressible two-dimensional velocity fields with general time dependence. Specifically, he defines unsteady flow separation as a material instability induced by an unstable manifold of a distinguished boundary point. In this general context, the unstable manifold is a time-dependent material line that shrinks to the separation point in backward time. In forward time, the unstable manifold attracts and ejects particles from a vicinity of the boundary.

Using the above Lagrangian definition, the above kinematic separation theory renders mathematically exact Eulerian criteria for the location of time-dependent unstable manifolds. The theory only assumes local mass conservation and regularity for the unsteady velocity field.

After recalling the main points of Haller's theory, we apply it to a specific model: a two-dimensional pitching airfoil. We first analyze the flow around the airfoil, and show how, under certain conditions, separation happens on the upper part of this airfoil. Next we consider the unsteady flow conditions, and determine the shape of the separation profile emanating from the wing. At that point, we also outline a new approach to the control of separation.

In the second part of this thesis, we extend Haller's two-dimensional separation theory to three-dimensional flows, treating the case of open and closed separation separately.

Next, we use a method developed by Perry and Chong (1986) to derive expansions of the Navier-Stokes equations that we use as models of three-dimensional separation. We verify our theory on those models.

Finally we discuss new results on genuinely three-dimensional aspects of flow separation: open and closed separation, separation lines and separation surfaces.

Thesis Supervisor: George Haller
Title: Associate Professor

Acknowledgements

First and foremost, I would like to express my sincere and deep gratitude to my advisor, Professor George Haller, for his guidance, advice and encouragement throughout the course of this work. His enthusiasm for the topic was greatly inspirational. I am also thankful to Dr. François Lekien, who, as a postdoctoral fellow in my laboratory, gave me really interesting suggestions, and his contributions are very much appreciated.

I am also grateful to Professor Jean Salençon for introducing me to the world of Mechanical Engineering. I have never had such an interesting teacher, and he is the reason why I am now doing Mechanical Engineering.

I also wish to thank my lab-mate of research, Dr. Weijiu Liu, my office mates of research, Amit Surana and Reza Alam, my office mates, Raul Coral Pinto, Jae Jeen Choi, Siavash Yazdanfar, Mac Schwager and Dan Macumber, and my roommates, François Impens, Fabien Sorin, Florent Brunet, Raphaël Tardy and Emmanuel Abbe, for their help and friendly support.

While at MIT, I received financial help from an AFOSR Grant. This support is gratefully acknowledged.

Finally, my utmost gratitude is due to my parents and to my two brothers for their support, and particularly to my fiancée, Nathalie, for her unconditional support, love and affection.

Contents

List of Figures

Introduction

Preliminaries

The theory of separation was initiated by Ludwig von Prandtl in 1904 who showed that streamlines in a steady flow past a two-dimensional streamlined body separate from the boundary where the skin friction vanishes and admits a negative gradient. If we define $y = 0$ to be the flat boundary of a two-dimensional steady velocity field $(u(x,y), v(x,y))$, the skin friction τ_w along the wall must satisfy a set of conditions at a separation point $(p, 0)$:

$$\begin{aligned} \tau_w(p) &= \nu\rho(p,0)\, u_y(p,0) = 0, \\ \tau_w'(p) &= \nu\rho(p,0)\, u_{xy}(p,0) < 0, \end{aligned} \tag{1}$$

where ν is the kinematic viscosity and ρ is the density of the fluid.

For a long time, these conditions have been considered the definition of separation, until Rott (1956), Moore (1958) and Sears & Telionis (1971) proved that zero skin friction does not caracterize separation in unsteady flows. This lead to a change of the definition of separation for unsteady flows and yielded the Moore-Rott-Sears (MRS) principle. This principle, however, requires that we know the separation speed; indeed, Williams (1977) and Van Dommelen (1981) explained why this principle is difficult to apply.

Van Dommelen (1981) and Van Dommelen & Shen (1982) were the first to study unsteady boundary-layer separation in Lagrangian coordinates. The computational simplifications rendered by this method revealed that unsteady separation is in essence Lagrangian. Cowley, Van Dommelen & Lam (1990) showed that separation is caracterized by contraction towards a point, accompanied by a spiky expansion in the wall-normal direction at that point. The Lagrangian notion of separation was further studied by Peridier (1995), Cassel, Smith & Walker (1996), Degani, Walker & Smith (1998). Formal asymptotic expansions for Van Dommelen's singularity in the boundary-layer equations have been obtained by Cowley (1983) and Van Dommelen & Cowley (1990).

Although boundary-layer separation has been numerically studied very accurately, no satisfying theory has been formulated. Moreover, because separation occurs both for low and high Reynolds numbers, one should be able to study separation without solving the boundary-layer equations. Indeed, Sears & Telionis (1975) pointed out the need for an unsteady separation definition that does not depend on boundary layers. Moreover, Cowley et al. (1990) stressed that an ideal separation definition which would be independent of the coordinate system. Finally, active flow control forced Wu, Tramel, Zhu & Yin (2000) to seek a separation criterion that only uses quantities obtained along the boundary.

The conditions (1) are purely kinematic: They can be derived for any two-dimensional steady vector field that conserves mass, as shown by Shariff, Pulliam & Ottino (1991). Moreover, the Lagrangian definition of steady separation has the above three ingredients, and was the starting point of Shariff et al. (1991): For two-dimensional, incompressible, time-periodic flows, the separation point is a fixed point with an unstable manifold for the Poincaré map associated with the flow. They showed that unsteady separation takes place where the time-average of the skin friction vanishes. Yuster & Hackborn (1997) re-derived this result in more rigorous terms for near-steady, time-periodic, incompressible flows, and Hackborn, Ulucakli & Yuster (1997) verified it experimentally. The latter authors, however, also showed that the principle of zero-mean-skin-friction fails for compressible time-periodic flows.

Haller (2002) analyzed the steady flow separation as an instability in the Lagrangian frame, which is due to the presence of a distinguished fixed point (the separation point) with an unstable manifold. This manifold acts as an attracting material line that collects and transports particles away from the wall. The distinguished fixed point is degenerate due to the no-slip boundary conditions, and hence its location and stability cannot be predicted from linearization. Prandtl's first condition in (1) gives a necessary condition for the existence of such a degenerate fixed point, while (1) as a whole gives a sufficient set of conditions for the existence of an unstable manifold. Haller then extended the Lagrangian separation definition of Shariff et al. (1991) to compressible two-dimensional velocity fields with general time dependence. Specifically, one can define unsteady flow separation as a *material instability due to an unstable manifold emanating from a fixed boundary point.* Then unstable manifold is a time-dependent material line that shrinks to the separation point in backward time. In forward time, the unstable manifold attracts and repels particles from a vicinity of the boundary.

Using the above Lagrangian definition, Haller (2002) derive mathematically exact Eulerian criteria that locate the separation point. Due to nonhyperbolicity of fixed points on a no-slip wall, classical dynamical systems methods for locating their unstable manifolds fail to apply. To overcome these limitations of classical invariant manifold theory, Haller (2002) uses a novel nonlinear technique that gives both the location and the shape of unstable manifolds, that are named *separation profiles.* This approach only assumes local mass conservation and regularity for the unsteady velocity field.

We show on a practical example the validity of the above theory: The analysis of separation over a pitching airfoil is a matter of interest to the aerodynamics community. We then consider a relevant example of an airfoil: a NACA 0012. We change periodically its angle of attack, and use a Navier-Stokes solver (developed by Hesthaven 1998) to derive the flow around the airfoil. Using Haller's formulae restricted to the upper surface of the airfoil allows us to analyze aperiodic separation.

As fluid flows are rarely two-dimensional, the matter of three-dimensional separation has received a lot of interest for decades. Different definitions of separation have been proposed, some highly contentious.

Legendre (1956) and Lighthill (1963) were the first to introduce a theoretical treatment of three-dimensional separation. Without proposing a theory that would predict 3D steady separation, they describe separation with geometrical arguments. The topological classification of Chapman (1986) distinguishes a great number of separation shapes, contrary to the relative simplicity of two-dimensional separation geometry. Here we show in figure 0-1 three basic shapes of separation: saddle-sink, saddle-saddle and saddle-focus.

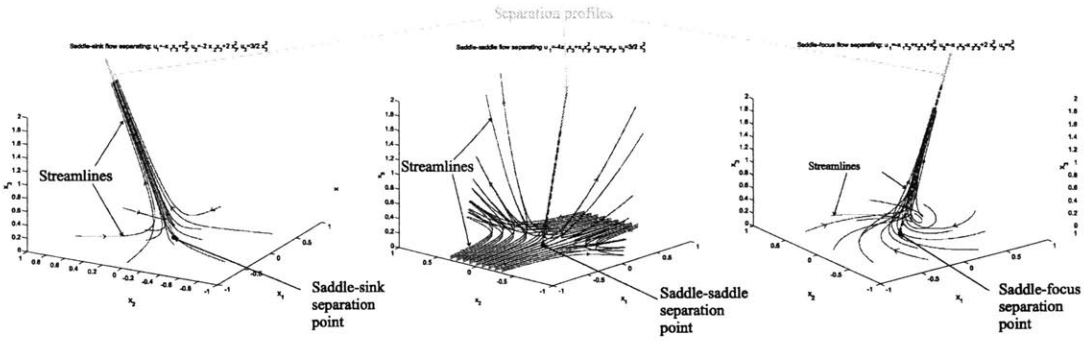

Figure 0-1: Three basic shapes of separation: saddle-sink, saddle-saddle and saddle-focus.

Further work by Wang (1970) introduced the concept of open separation: contrary to the two-dimensional case, one can observe separation (along a surface) while there is no observed specific separation point. First highly criticized, this concept has been adopted by others (see Wang 1983 for details). One can now define steady separation as a breakaway of particles from the wall. Closed separation occurs at a zero skin friction point, which acts as a distinguished separation point (and may also be part of a separation surface). By contrast, open separation does not occur at a zero skin friction point: there is no distinguished separation point but a separation surface, whose intersection with the wall (the separation line) is a skin friction line.

A similar definition for any unsteady flow has, however, always been missing. Here we define closed separation as a case of separation (particles breaking away from the wall) where there is at least one distinguished separation point; we call the separation open when there is no such point. When the flow is steady, the two definitions coincide.

Later work has concentrated on the experimental verifications of the geometrical concepts of three-dimensional separation, which are of vital importance in a wide range of engineering applications. For instance, separation drives the formation of vortices over a surface, as explained by Wu & Gu (1987). One can also study the transition to turbulence and fully developed turbulence of various wall-bounded flows. A lot of related numerical computations have been performed by Legendre and Werlé (Délery 2001).

With the increasing development of computational fluid dynamics, one needs a quantitative criterion to characterize separation. As for now, only a topological theory has been introduced: the critical point theory of Perry & Chong (1987), which classifies steady separation points in geometrical terms; an analysis of the topology of pressure surfaces (Tobak and Coon 1996) which links separation surfaces to pressure surfaces; and a vorticity dynamics theory (Wu et al. 2000) which analyzes the on-wall signatures of separation, and shows that closed separation occurs at zero skin friction points. These theories generally describe the flow in an Eulerian way, and only focus on steady incompressible flows. The ideas they introduce are qualitative and geometric, and only apply to steady flows. So far, an understanding of three-dimensional unsteady separation has been missing, and no theory has ever been presented.

In his previous work on two-dimensional separation, Haller (2002) analyzed unsteady 2D separation; his theory is here extended to three-dimensional unsteady separation. The main

result is that fixed closed separation takes place where the weighted backward-time average of the skin friction remains uniformly bounded. The weight function in the average is just the squared reciprocal of the fluid density. We also introduce the concept of *effective separation points* at which the finite-time mean of the skin friction vanishes. Numerically, these points converge to the fixed separation points.

To validate this new theory, we derive some three-dimensional separated flow models using a concept developed by Perry & Chong (1986). We present the three basic shapes caracterizing steady closed separation: saddle-sink, saddle-saddle and saddle-focus separation, showing how the predicted separation profile fits the observed shape of separation. Then we develop a new model: a separation bubble, with an interesting pattern of separation. We study different kinds of unsteadiness on this model: periodic and quasiperiodic.

Finally, we explain the current limits of our theory and propose further extensions.

Thesis outline

The outline of this thesis is as follows.

In chapter 1, we review the kinematic theory of 2D unsteady separation from Haller (2002) and apply it to a relevant example. The first part of this chapter is mostly intended to recall the concepts of separation, separation point and separation profile. The second part of chapter 1 focuses on the validation of the theory in the unsteady case: we analyze the flow around a two-dimensional pitching airfoil, and show how, under certain conditions, separation happens on the upper part of this airfoil. We shall also develop some concepts for the control of separation.

In chapter 2, we extend Haller's theory of separation to three-dimensional flows. We define closed and open separation, then concentrate on closed separation. We still use the concepts of separation point, separation profile or moving separation.

In chapter 3, we use a method developed by Perry & Chong (1986) to introduce physically relevant incompressible expansions of the Navier-Stokes equations to be used as models of three-dimensional separation. These flow models allow us to verify our separation theory on relevant steady, periodic and quasiperiodic examples. We first introduce a steady model that contains the three separation patterns one typically observes: saddle-sink, saddle-saddle and saddle focus. Secondly, we present a three-dimensional model of a separation bubble flow, both for the steady and the unsteady cases. On this model, we illustrate the usual concepts of three-dimensional unsteady separation points and profiles. In addition, we also explain the genuinely three-dimensional concepts of separation lines and separation surfaces.

In chapter 4, we focus on a new approach to separation lines and surfaces. We discuss initial results for these objects, and outline the next steps to be taken in their study.

Finally, we present our conclusions.

In appendix A, we derive the proofs and formulae used in our three-dimensional separation theory.

In appendix B, we present details of the arguments used in the validation of the three-dimensional theory.

Chapter 1

Location and shape of aperiodic separation over a pitching airfoil

1.1 Introduction

The objective of this chapter is to visualize the points and angles of separation in an unsteady flow over a pitching airfoil. This method can be applied to a wide range of vehicles, such as passenger cars, submarines, etc.

The pitching airfoil is investigated as an example to detect and control dynamic stall. Problems involving unsteady separation over aerodynamic boundary layers are usually modeled as nominally two-dimensional flows over a moving airfoil. As explained by Sinha et al. (1997), such models contain the essential characteristics of dynamic stall on helicopter rotors, where stall occurs during the pitch-up motion of the blade of a rotor. Particles can separate from the upper part of the airfoil, which causes fatigue failure in the blade control mechanisms, as well as loss of lift.

The above problem has been studied experimentally by Pal et al. (1997) and numerically by Okong'o & Knight (1997), but a full understanding of stall has not been achieved. More recently, Kuo & Hsieh (2001) analyzed the structure of separation over a pitching airfoil using vortex visualization. New simulations and experiments by Magil et al. (2001), Reuster & Baeder (2001) and Emblemsvag et al. (2002) aim to control separation over pitching airfoils. Here we shall use Haller's (2002) criteria for separation to analyze separation over a pitching airfoil.

The organization of this chapter is as follows. We first recall the main points of Haller's theory in § 1.2. Then we present an airfoil model, and study separation over it in § 1.3. We finally present our conclusions in § 1.4.

1.2 Brief Review of Separation Criteria

1.2.1 Introduction

For convenience, we briefly recall criteria developed by Haller (2002) for unsteady separation points and angles. Consider a two-dimensional velocity field $\mathbf{v}(x,y,t) = (u(x,y,t), v(x,y,t))$,

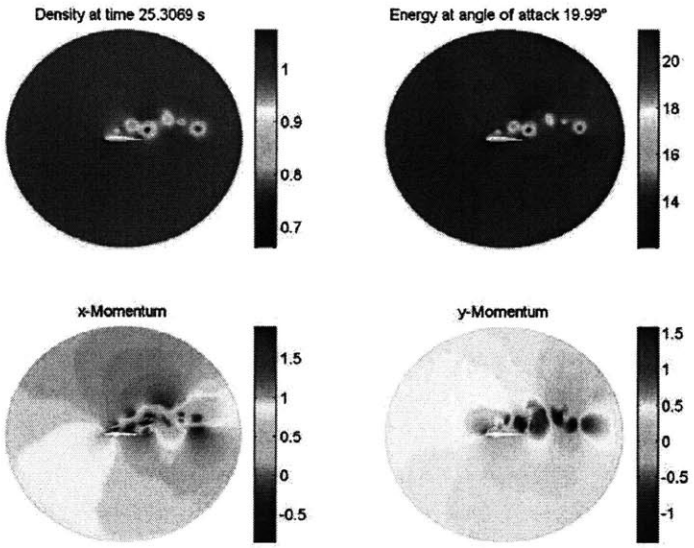

Figure 1-1: Flow over a pitching airfoil.

with the induced fluid particle motion satisfying

$$\dot{x} = u(x, y, t), \qquad \dot{y} = v(x, y, t).$$

Assume further that a boundary is present in the flow at $y = 0$ with the no-slip boundary conditions

$$u(x, 0, t) = v(x, 0, t) = 0.$$

We also assume that no sinks or sources are present at separation, and hence the continuity equation

$$\rho_t + \nabla \cdot (\rho \mathbf{v}) = 0 \tag{1.1}$$

holds for the density $\rho(x, y, t)$ in a neighborhood of a separation point $(x, y) = (\gamma, 0)$.

We seek a time-dependent material line $\mathcal{M}(t)$–the *separation profile*–that collects and ejects fluid particles from a vicinity of the boundary. As a material line, $\mathcal{M}(t)$ is anchored to a boundary point γ due to the no-slip boundary conditions. In dynamical systems terms, $\mathcal{M}(t)$ is an unstable manifold for a fixed point of the $y = 0$ boundary.

Suppose the separation profile is represented by a time-dependent graph

$$x = \gamma + yF(y, t),$$

where the constant γ denotes the separation location to be determined later. Suppose that

$F(y,t)$ has a series expansion

$$F(y,t) = f_0(t) + yf_1(t) + \cdots,$$

where

$$f_0(t) = F(0,t), \quad f_1(t) = F_y(0,t).$$

Thus, the angle φ of separation at time t_0 with the x-axis is

$$\varphi = \arctan \frac{1}{f_0(t_0)}.$$

The explicit criteria and formulae for the point and profile of separation are as follow.

1.2.2 Non-flat boundary

Assuming now that the velocity field satisfies no-slip boundary conditions along a boundary $\mathcal{B}$, we want to find a necessary condition for separation at a point whose relative location is fixed on the non-flat boundary. If the boundary is represented by a differentiable graph $y = h(x)$, as indicated in figure 1-2, we transform the velocity field to a canonical form by letting

$$\xi = x, \qquad \eta = y - h(\xi). \tag{1.2}$$

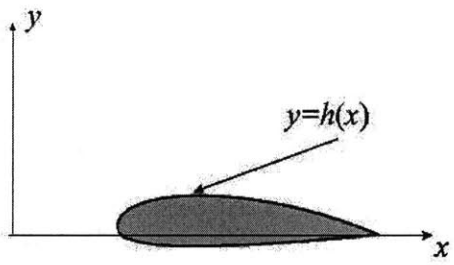

Figure 1-2: Separation over a non-flat boundary.

Compressibility or incompressibility is unaffected by the change of coordinates $(x,y) \mapsto (\xi,\eta)$. We only need to apply the previous change of variables in all separation formulae given below.

1.2.3 Necessary Condition

The necessary condition for the separation point $\gamma(t_0)$ at time t_0 is

$$\frac{d}{dT}\left\langle \int_{t_0}^{t_0-T} \frac{u_y(\gamma(t_0),0,s)}{\rho(\gamma(t_0),0,s)}\, ds \right\rangle_{T=0} = 0, \qquad \frac{d}{dT}\left\langle \int_{t_0}^{t_0-T} \frac{d}{dx}\frac{u_y(\gamma(t_0),0,s)}{\rho(\gamma(t_0),0,s)}\, ds \right\rangle_{T=0} > 0. \tag{1.3}$$

These two conditions represent an extension of Prandtl's necessary criteria to moving separation. Here $\langle g \rangle (x, t_0, \cdot)$ is a low-order polynomial least-square fit to sampled values of $g(x, t_0, \cdot)$ over a T interval as large as possible. This practically means a least-square polynomial fit for g values up to $T = t_0 - t_{00}$, where t_{00} is the earliest time at which velocity data is available. For a faithful approximation of $\langle g \rangle$, the order of the least-square polynomial should be low relative to the number of sampled values for g. The slope $f_0(t_0)$ of the separation profile at $t = t_0$ is given by

$$f_0(t_0) = \frac{\rho(t_0)\frac{d}{dT}\left\langle \int_{t_0}^{t_0-T} \left[\frac{b_y(\tau)-a_x(\tau)}{\rho(\tau)} \int_{t_0}^{\tau} \frac{a(s)}{\rho(s)}\, ds + b_x(\tau) \left(\int_{t_0}^{\tau} \frac{a(s)}{\rho(s)}\, ds \right)^2 - \frac{a_y(\tau)}{\rho^2(\tau)} \right] d\tau \right\rangle_{T=0}}{\frac{d}{dT}\left\langle \int_{t_0}^{t_0-T} \left[\frac{a_x(\tau)-b_y(\tau)}{\rho(\tau)} - 2b_x(\tau) \int_{t_0}^{\tau} \frac{a(s)}{\rho(s)}\, ds \right] d\tau \right\rangle_{T=0}}, \quad (1.4)$$

where

$$\begin{aligned} a(t) &= u_y(\gamma, 0, t), \\ a_x(t) &= u_{xy}(\gamma, 0, t), \\ a_y(t) &= \frac{1}{2} u_{yy}(\gamma, 0, t), \\ b(t) &= v_y(\gamma, 0, t), \\ b_x(t) &= v_{xy}(\gamma, 0, t), \\ b_y(t) &= \frac{1}{2} v_{yy}(\gamma, 0, t), \\ \rho(t) &= \frac{1}{2} \rho(\gamma, 0, t). \end{aligned}$$

1.2.4 Sufficient Condition

First, for the present time t_0, we compute the effective separation point $\gamma_{eff}(t, t_0)$ for all available $t < t_0$, which is obtained via the formula

$$\int_{t_0}^{t} \frac{u_y(\gamma_{eff}, 0, \tau)}{\rho(\gamma_{eff}, 0, \tau)}\, d\tau = 0. \quad (1.5)$$

We then identify the upper and lower bounds

$$\gamma_+(t, t_0) = \sup_{s \in [t, t_0)} \gamma_{eff}(s, t_0), \qquad \gamma_-(t, t_0) = \inf_{s \in [t, t_0)} \gamma_{eff}(s, t_0),$$

on $\gamma_{eff}(t, t_0)$. Let the maximal x distance travelled by $\gamma_{eff}(s, t_0)$ over the interval $[t, t_0)$ be denoted by

$$\delta(t, t_0) = \gamma_+(t, t_0) - \gamma_-(t, t_0),$$

which is the length of the interval

$$I(t, t_0) = \left[\gamma_-(t, t_0), \gamma_+(t, t_0) \right].$$

One can then prove the existence of finite-time separation at the point

$$\gamma(t_0) = \frac{1}{2}\left[\gamma_+(t_0 - T_m(t_0), t_0) + \gamma_-(t_0 - T_m(t_0), t_0)\right], \tag{1.6}$$

where $T_m(t_0)$ is the smallest time for which

$$\frac{1}{2}\delta(t, t_0)\int_{t_0 - T_m(t_0)}^{t_0} \max_{x \in I(t_0 - T_m(t_0), t_0)} |u_{xy}(x, 0, t)| \; dt = 1, \tag{1.7}$$

$$\max_{x \in I(t_0 - T_m(t_0), t_0)} u_{xy}(x, 0, t) < 0, \quad t \in [t_0 - T_m(t_0), t_0].$$

The above conditions distinguish one finite-time unstable manifold out of the infinitely many near the moving separation point.

The moving separation slope is given by the formula

$$f_0(t_0) = \frac{\rho(t_0)\int_{t_0 - T_m(t_0)}^{t_0}\left[\frac{b_y(\tau) - a_x(\tau)}{\rho(\tau)}\int_{t_0}^{\tau}\frac{a(s)}{\rho(s)}\,ds + b_x(\tau)\left(\int_{t_0}^{\tau}\frac{a(s)}{\rho(s)}\,ds\right)^2 - \frac{a_y(\tau)}{\rho^2(\tau)}\right]d\tau}{\int_{t_0 - T_m(t_0)}^{t_0}\left[\frac{a_x(\tau) - b_y(\tau)}{\rho(\tau)} - 2b_x(\tau)\int_{t_0}^{\tau}\frac{a(s)}{\rho(s)}\,ds\right]d\tau}. \tag{1.8}$$

1.3 Separation over a pitching airfoil

1.3.1 Model

The first part of this work consists of defining the airfoil to be studied. We consider the most common airfoil, the NACA 0012. In such an airfoil of the National Advisory Committee for Aeronautics with four digits, say MPXX, the digit M represents the maximum value of the mean line in hundredths of the chord, P represents the chordwise position of the maximum camber in tenths of the chord, and the number XX is the maximum thickness in percent of the chord.

The equation of the upper boundary of this airfoil is given by

$$y = l(x) = 0.17735\sqrt{x} - 0.075597x - 0.212836x^2 + 0.17363x^3 - 0.06254x^4.$$

The lower boundary is symmetric. We translate this airfoil to place it in the middle of our numerical grid. The length of the airfoil is one; it is placed in the center of a circle of radius 3, as shown in figure 1-3.

1.3.2 Aperiodic flow

When the inflow is steady, the flow developing near the airfoil is periodic or quasiperiodic, with vortices behind the airfoil. When the inflow is periodic, the developing flow tends to be aperiodic. In the latter case, we periodically (period = 10s) change the angle of attack of the airfoil between -5 to +15 degrees. Under such flow conditions, the airfoil is said to be pitching.

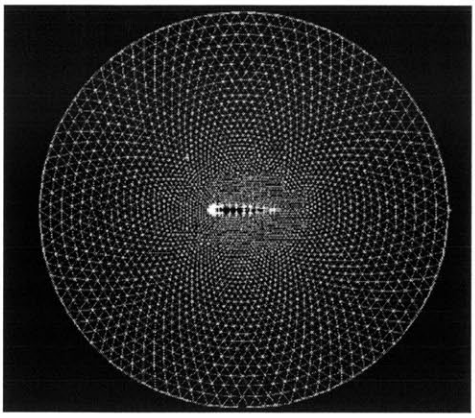

Figure 1-3: Mesh of the pitching airfoil.

1.3.3 Separation

We use a Navier-Stokes solver developed by Hesthaven (1998) to generate the velocity field around the airfoil. We then use the method explained in § 1.2 to find the zero skin friction points, and evaluate the sufficient and necessary separation points. Figure 1-6 underlines the difference between the zero skin friction points and the separation points.

Computation

We use both the necessary and the sufficient criteria in Section 1.2 to determine the approximate points and angles of separation. For the necessary condition, we use a third-order polynomial least-square fit to extract the mean components. Figure 1-4 shows that such a fit well captures the profiles of sampled values of $\int_{t_0}^{t_0-T} \frac{u_y(\gamma(t_0),0,s)}{\rho(\gamma(t_0),0,s)}\, ds$ and
$\int_{t_0}^{t_0-T} \left[\frac{b_y(\tau)-a_x(\tau)}{\rho(\tau)} \int_{t_0}^{\tau} \frac{a(s)}{\rho(s)}\, ds + b_x(\tau) \left(\int_{t_0}^{\tau} \frac{a(s)}{\rho(s)}\, ds \right)^2 - \frac{a_y(\tau)}{\rho^2(\tau)} \right] d\tau$, respectively.

For the sufficient condition, the time scale T is determined by (1.7) and is shown in figure 1-5.

Visualization of separation

We compute the approximate points and angles of separation through formulae (1.4) and (2.5), as shown in figure 1-6. We track the particles and show the zero skin friction points, and the necessary and sufficient separation points along with their slopes (see the legend of the figure for explanation). We conclude that our formulae give a good approximation of the separation point and angle. Indeed, the two separating lines are close to the exact separation profile along which the spikes of fluid particles are formed. Furthermore, we see that the zero skin friction point is not the point of separation; this disproves the common belief that the zero skin friction point is the point of separation in unsteady flows.

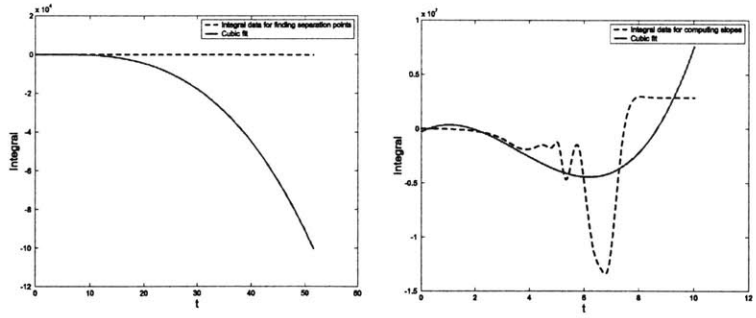

Figure 1-4: Third-order polynomial least-square fit to sampled values of $\int_{t_0}^{t_0-T} \frac{u_y(\gamma(t_0),0,s)}{\rho(\gamma(t_0),0,s)}\, ds$ and $\int_{t_0}^{t_0-T} \left[\frac{b_y(\tau)-a_x(\tau)}{\rho(\tau)} \int_{t_0}^{\tau} \frac{a(s)}{\rho(s)}\, ds + b_x(\tau) \left(\int_{t_0}^{\tau} \frac{a(s)}{\rho(s)}\, ds \right)^2 - \frac{a_y(\tau)}{\rho^2(\tau)} \right] d\tau$, respectively.

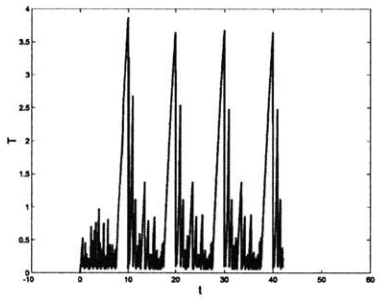

Figure 1-5: Time-scale determined by (1.7) for the sufficient condition in the separation simulation.

1.3.4 Control of separation

A next step of this analysis will be, instead of looking at separation, trying to control it. We still need an efficient device capable of controlling the phenomenon of separation, which creates losses of drag and lift.

Wang et al. (2003) established a feedback control law to control separation in two-dimensional shear flows. Work by Salman et al. (2002) established a feedback control law for Stokes flows, noting that the same control law fails for Navier-Stokes flows. This failure is due to inertia-related delays in real flows, as explained by Insperger (2003). Later work has concentrated on implementing delays in the controller; preliminary results by Lekien et al. (2003) are promising.

1.4 Conclusion

We have performed numerical simulations for real-time monitoring of separation points and angles in the unsteady pitching of an airfoil. These simulations showed Haller's criteria for

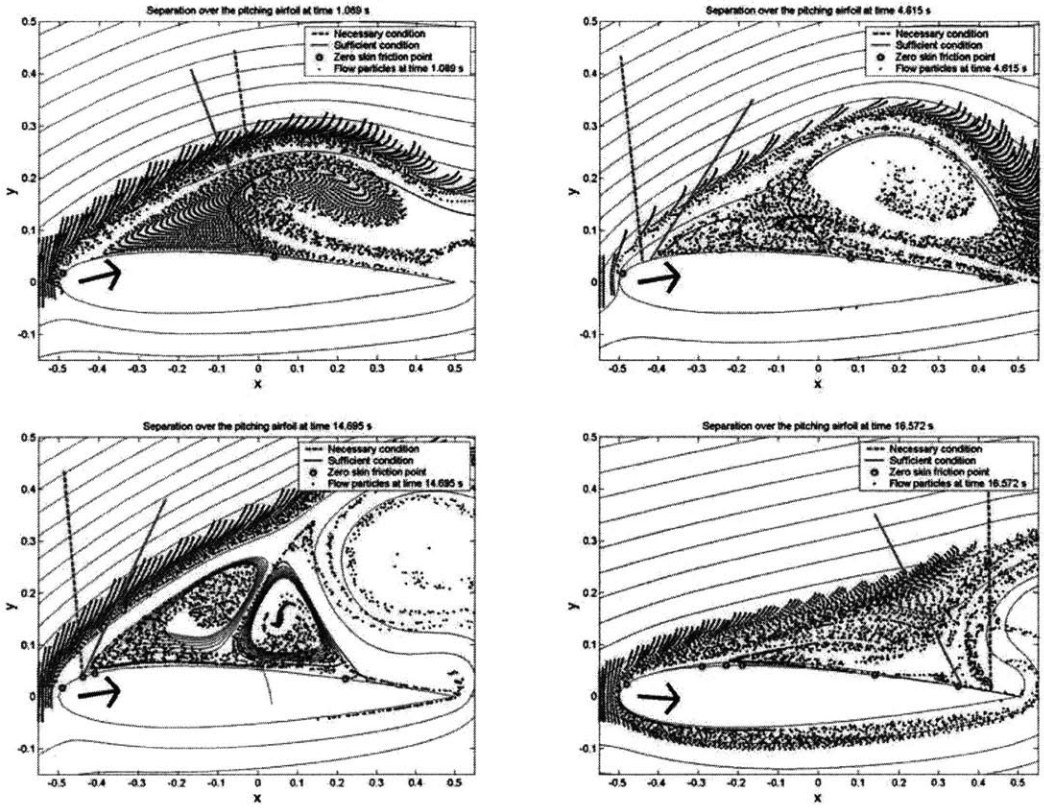

Figure 1-6: Separation over the pitching airfoil.

separation in two-dimensional unsteady flow to be accurate. We have also found that the zero skin friction point is not the point of separation, and that the behavior of the separation point depends on the flow. If the flow is periodic, or quasiperiodic, the separation point is fixed; If the flow is aperiodic, the separation point appears to move, but its motion is unrelated to that of the zero skin friction point.

Chapter 2

Kinematic theory of three-dimensional unsteady flow separation

2.1 Introduction

In his work on two-dimensional separation, Haller (2002) analyzed unsteady 2D separation as a *material instability due to an unstable manifold emanating from a fixed boundary point* and extended Prandtl's formulae to any unsteady flow: He derived mathematically exact Eulerian criteria that locate the separation point and obtained both the location and the shape of the unstable manifolds that generate the *separation profiles.*

As explained in the introduction, Wang (1970) introduced the concept of open separation: contrary to the two-dimensional case, one can observe separation (along a surface) while there is no observed specific separation point. We define closed separation as a case of separation (particles breaking away from the wall) where there is at least one distinguished separation point; we call the separation open when there is no such point. When the flow is steady, our definition coincide with Wang's.

Haller's theory is here extended to three-dimensional unsteady separation. The main result is that fixed closed separation takes place where the weighted backward-time average of the skin friction remains uniformly bounded. The weight function in the average is just the squared reciprocal of the fluid density.

The organization of this chapter is as follows. We first derive necessary conditions for fixed compressible separation in § 2.2, where we also give a first-order approximation for a general compressible separation profile. Section 2.2 also contains equivalent Lagrangian and density-independent formulations of our criteria, as well as a version for moving boundaries. We show how the theory simplifies for incompressible flows in § 2.3, and exploit this simplification to derive a third order approximation for incompressible separation profiles. In § 2.4 we give a kinetic version of the separation criteria for Navier-Stokes flows, and in § 2.5 we formulate sufficient conditions for sharp unsteady separation. Section 2.6 explores how our fixed separation criteria simplify to steady, time-periodic and quasiperiodic flows. Unsteady reattachment is discussed in § 2.7, and we deal with the difficult problem of moving separation in § 2.8. We will

finally present our conclusions and some open problems in § 2.9.

2.2 Fixed unsteady separation

2.2.1 Set-up

Let us consider a three-dimensional unsteady velocity field

$$\mathbf{v}(x,y,z,t) = (u(x,y,z,t), v(x,y,z,t), w(x,y,z,t)),$$

which admits a boundary at $z = 0$, with

$$u(x,y,0,t) = v(x,y,0,t) = w(x,y,0,t) = 0. \tag{2.1}$$

To distinguish the velocity components parallel to the boundary, we shall use the shorthand notation $\mathbf{x} = (x,y)$ and

$$\mathbf{u}(\mathbf{x},z,t) = (u(x,y,z,t), v(x,y,z,t)), \qquad w(\mathbf{x},z,t) = w(x,y,z,t).$$

Fluid particle motions satisfy the three-dimensional system of differential equations of motion

$$\dot{x} = u(x,y,z,t), \qquad \dot{y} = v(x,y,z,t), \qquad \dot{z} = w(x,y,z,t), \tag{2.2}$$

or, briefly,

$$\dot{\mathbf{x}} = \mathbf{u}(\mathbf{x},z,t), \qquad \dot{z} = w(\mathbf{x},z,t),$$

We seek a time-dependent material line $\mathcal{M}(t)$–the *separation profile*–that collects and ejects fluid particles from a vicinity of the boundary. We also seek a surface of separation which attracts all particles away from the wall. The separation profile is a material curve that attracts all fluid particles within the separation surface. The separation surface may be degenerate: It may just coincide with $\mathcal{M}(t)$. An example of this type of separation is given by tornado-type vortex formation near the boundary.

To exclude degenerate or unphysical cases of separation, we shall only consider separation profiles with the following properties:

1. The separation profile is *unique*: no other separation profiles emerges from the same boundary point.
2. The separation profile is *transverse*, i.e., $\mathcal{M}(t)$ is not tangent to the boundary.
3. The separation profile is *regular* up to nth order: $\mathcal{M}(t)$ admits n derivatives ($n \geq 1$) that remain uniformly bounded at $y = 0$ for all times.

2.2.2 Assumptions

Assuming that no sinks or sources are present at separation, the continuity equation

$$\rho_t + \nabla \cdot (\rho \mathbf{v}) = 0 \tag{2.3}$$

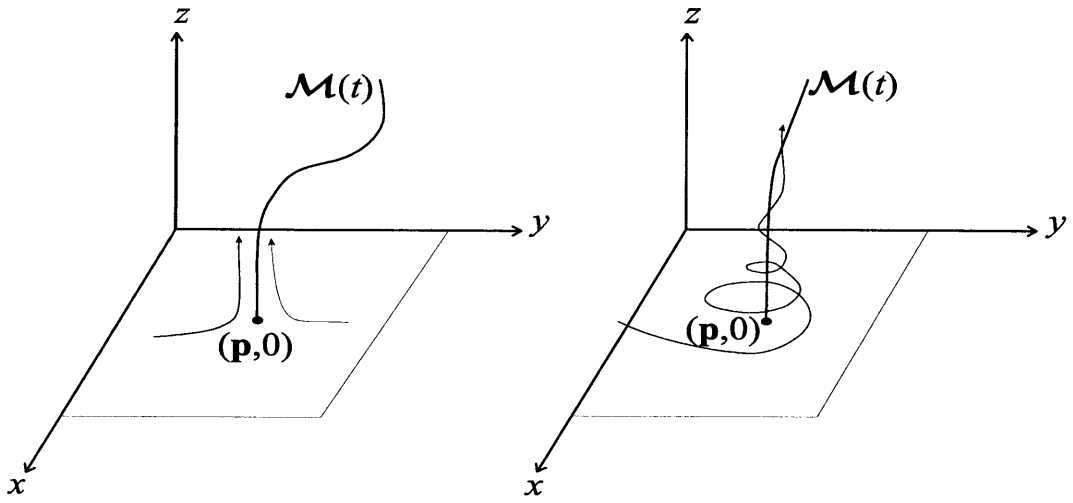

Figure 2-1: Unsteady separation profiles emanating from separation points (**p**,0) viewed as a time-dependent material line that guides particles away from the wall.

is satisfied in a neighborhood of a separation point $(\mathbf{x}, z) = (\gamma, 0)$. The no-slip boundary conditions at $z = 0$ simplifies the continuity equation to

$$\rho_t(\mathbf{x}, 0, t) + \rho(\mathbf{x}, 0, t) w_z(\mathbf{x}, 0, t) = 0$$

at boundary points and implies

$$\rho(\mathbf{x}, 0, t) = \rho(\mathbf{x}, 0, t_0) e^{-\int_{t_0}^{t} w_z(\mathbf{x},0,s)\, ds}. \tag{2.4}$$

Differentiation of (2.4) with respect to x and y gives the wall-tangential density gradient evolution

$$\rho_{\mathbf{x}}(\mathbf{x}, 0, t) = \rho_{\mathbf{x}}(\mathbf{x}, 0, t_0) e^{-\int_{t_0}^{t} w_z(\mathbf{x},0,s)\, ds} - \rho(\mathbf{x}, 0, t_0) e^{-\int_{t_0}^{t} w_z(\mathbf{x},0,s)\, ds} \int_{t_0}^{t} w_{\mathbf{x}z}(\mathbf{x}, 0, s)\, ds. \tag{2.5}$$

Here and in later formulae, the subscript $\mathbf{x}$ refers to the gradient operation with respect to the variables x and y.

As the density of the fluid should remain bounded from below and from above for all times along the boundary, for appropriate $\rho_2 > \rho_1 > 0$ and for all t,

$$0 < \rho_1 \leq \rho(\mathbf{x}, 0, t) \leq \rho_2 < \infty \tag{2.6}$$

must hold along the boundary region of interest.

We also assume that the tangential density gradient along the boundary remains uniformly

bounded near the separation point for all times:

$$\left| \int_{t_0}^{t} w_{\mathbf{x}z}(\mathbf{x}, 0, s)\, ds \right| \leq K_1 < \infty, \tag{2.7}$$

for an appropriate constant K_1, for any time t, and for all $\mathbf{x}$ values near $\boldsymbol{\gamma}$.

Assumptions (2.6)-(2.7) hold automatically for incompressible flows, because for such flows,

$$w_z(\mathbf{x}, 0, t) \equiv 0, \qquad w_{\mathbf{x}z}(\mathbf{x}, 0, t) \equiv 0.$$

2.2.3 Equation for the separation profile

We rewrite the velocity field in a form more suitable for separation studies. The no-slip boundary condition simplifies the velocity filed (2.2) to

$$\dot{\mathbf{x}} = z\mathbf{A}(\mathbf{x}, z, t), \qquad \dot{z} = zB(\mathbf{x}, z, t), \tag{2.8}$$

where we define the quantities

$$\mathbf{A}(x, y, z, t) = \int_0^1 \mathbf{u}_z(\mathbf{x}, s\, z, t)\, ds, \qquad B(\mathbf{x}, z, t) = \int_0^1 w_z(\mathbf{x}, s\, z, t)\, ds. \tag{2.9}$$

Fixed unsteady separation occurs if a boundary point $\mathbf{p} = (\boldsymbol{\gamma}, 0)$ admits an unstable manifold $\mathcal{M}(t)$ not tangent to the boundary: then we locally represent this manifold

$$\mathbf{x} = \boldsymbol{\gamma} + z\mathbf{G}(z, t).$$

Changing to the new horizontal coordinates $\boldsymbol{\xi} = \mathbf{x} - \boldsymbol{\gamma}$, we seek the following representation for the separation profile:

$$\boldsymbol{\xi} = z\mathbf{G}(z, t). \tag{2.10}$$

Substitution of (2.10) into (2.8) yields

$$z\left[(B(\boldsymbol{\gamma} + z\mathbf{G}, z, t)\mathbf{G} + z\mathbf{G}_z) + \mathbf{G}_t - \mathbf{A}(\boldsymbol{\gamma} + z\mathbf{G}, z, t)\right] = 0. \tag{2.11}$$

As the separation profile is continuously differentiable, the bracketed expression in (2.11) must vanish for all $z \geq 0$. (It is zero for $z > 0$, and continuity implies that it also vanishes at $z = 0$.) Then (2.12) implies that the separation profile must satisfy the partial differential equation

$$\mathbf{G}_t = \mathbf{A}(\boldsymbol{\gamma} + z\mathbf{G}, z, t) - B(\boldsymbol{\gamma} + y\mathbf{G}, z, t)\left(\mathbf{G} + z\mathbf{G}_z\right). \tag{2.12}$$

We call this equation the separation equation; we use it to deduce necessary criteria for separation, then for devising approximations to the separation profile at any order. These approximations are obtained from a series expansion

$$\mathbf{G}(z, t) = \mathbf{g}_0(t) + z\mathbf{g}_1(t) + \frac{1}{2}z^2\mathbf{g}_2(t) + \frac{1}{6}z^3\mathbf{g}_2(t)\ldots, \tag{2.13}$$

where

$$\mathbf{g}_0(t) = \mathbf{G}(0,t), \qquad \mathbf{g}_1(t) = \mathbf{G}_z(0,t), \qquad \mathbf{g}_2(t) = \mathbf{G}_{zz}(0,t).$$

2.2.4 Necessary conditions for separation

We first simplify our notation and set

$$\mathbf{a}(t) = \mathbf{A}(\boldsymbol{\gamma},0,t), \qquad b(t) = B(\boldsymbol{\gamma},0,t), \qquad \rho(t) = \rho(\boldsymbol{\gamma},0,t),$$

where $(\boldsymbol{\gamma},0)$ indicates the separation point we wish to characterize. Then the density satisfies

$$\rho(t) = \rho(t_0)e^{-\int_{t_0}^{t} b(s)\,ds}. \tag{2.14}$$

When we set $z = 0$ in the separation equation (2.12), we obtain the linear differential equation

$$\dot{\mathbf{g}}_0(t) = -b(t)\mathbf{g}_0(t) + \mathbf{a}(t), \tag{2.15}$$

whose general solution can be written

$$\mathbf{g}_0(t) = \mathbf{g}_0(t_0)\frac{\rho(t)}{\rho(t_0)} + \rho(t)\int_{t_0}^{t} \frac{\mathbf{a}(s)}{\rho(s)}\,ds, \tag{2.16}$$

using (2.14).

Recall that $(\mathbf{g}_0(t))_1$ is the tangent of the angle that the separation profile encloses with the wall-normal direction at $\boldsymbol{\xi} = \mathbf{0}$, $z = 0$, in the x-direction, $(\mathbf{g}_0(t))_2$ is the tangent of the angle in the y-direction. Fixed separation takes place at $\mathbf{x} = \boldsymbol{\gamma}$, if $\mathbf{g}_0(t)$ remains bounded in backward time. By assumption (2.6), the first term on the right-hand side of (2.16) and the $\rho(t)$ factor in the second term are both bounded in backward time. Therefore, a necessary condition for separation is the boundedness of the integral of the second term in (2.16). Using the skin friction field

$$\tau(\mathbf{x},t) = \nu\rho(\mathbf{x},0,t)\mathbf{u}_z(\mathbf{x},0,t), \tag{2.17}$$

we express this boundedness requirement

$$\limsup_{t\to-\infty}\left|\int_{t_0}^{t} \frac{\tau(\boldsymbol{\gamma},0,s)}{\rho^2(\boldsymbol{\gamma},0,s)}\,ds\right| < \infty, \tag{2.18}$$

or, equivalently,

$$\limsup_{t\to-\infty}\left|\int_{t_0}^{t} \frac{\mathbf{u}_z(\boldsymbol{\gamma},0,s)}{\rho(\boldsymbol{\gamma},0,s)}\,ds\right| < \infty. \tag{2.19}$$

Just as Prandtl's first two-dimensional separation condition, (2.18) is also satisfied at any point of a fluid at rest, which shows the need for a second condition to describe separation. A second necessary condition turns out to be

$$\lim_{t\to-\infty}\left\|\int_{t_0}^{t}\left[\frac{\mathbf{a}_{\mathbf{x}}(s) - b_z(s)\mathbf{I}}{\rho(s)} - \int_{t_0}^{s}\frac{\mathbf{a}(r)\otimes b_{\mathbf{x}}(s) + b_{\mathbf{x}}(s)\cdot\mathbf{a}(r)\mathbf{I}}{\rho(r)}\,dr\right]ds\right\| = \infty, \tag{2.20}$$

as we show in appendix A.1. Here $\mathbf{a}(r)\otimes b_{\mathbf{x}}(s)$ refers to the matrix defined as $[\mathbf{a}\otimes b_{\mathbf{x}}]_{ij} =$

$(\mathbf{a})_i\,(b_{\mathbf{x}})_j$. Condition (2.20) ensures that all material lines emanating from boundary points near γ converge to the wall in backward time, a feature that flows at rest do not admit.

2.2.5 Effective separation points

The theoretical necessary condition (2.18) is not suitable for computation. To derive an equivalent condition, we again recall that material lines emanating from any boundary point near $(\gamma, 0)$ align with the boundary as $t \to -\infty$. By formula (2.16), this asymptotic alignment in backward time is only possible if, for all small enough $|\mathbf{x} - \gamma|$ with $\mathbf{x}$ different from γ,

$$\limsup_{t\to-\infty} \left| \int_{t_0}^{t} \frac{\mathbf{u}_z(\mathbf{x}, 0, s)}{\rho(\mathbf{x}, 0, s)}\, ds \right| = +\infty.$$

Defining the integral

$$\mathbf{i}_t(\mathbf{x}) = \int_{t_0}^{t} \frac{\mathbf{u}_z(\mathbf{x}, 0, s)}{\rho(\mathbf{x}, 0, s)}\, ds,$$

we see in the same way as in the two-dimensional case, that $\mathbf{i}_t(\mathbf{x})$ must admit at least one zero that approaches γ as t approaches $-\infty$. As a result, defining the *effective separation point* $\gamma_{eff}(t, t_0)$ via the formula

$$\boxed{\int_{t_0}^{t} \frac{\mathbf{u}_z(\gamma_{eff},0,s)}{\rho(\gamma_{eff},0,s)}\, ds = \mathbf{0},} \tag{2.21}$$

we obtain

$$\gamma = \lim_{t\to-\infty} \gamma_{eff}(t, t_0). \tag{2.22}$$

We do not prove the existence of the effective separation point (2.21) here; we simply postulate it and find that it works perfectly well in rigorous computations. Equations (2.21) and (2.22) give a practical algorithm for computing fixed unsteady separation points at time t_0 from velocity data. For a past time t with $|t - t_0|$ large enough, one computes the integral in $\mathbf{i}_t(x)$ in the whole plane and finds one effective separation point $\gamma_{eff}(t, t_0)$. By (2.22), this effective separation point will converge to the real separation point γ as $t \to -\infty$.

Two remarks are in order. First, it turns out that fixed separation points of time-periodic or time-quasiperiodic flows are exactly computable from finite-time velocity data without the use of effective separation points (cf. § 2.6). Second, taking the limit $t \to -\infty$ in our formulae does not require solving for the velocity field in backward time: It requires computing longer and longer backward-time averages from the available velocity data as the current time t_0 progresses.

2.2.6 Direction of separation

To obtain an expression for the direction of fixed unsteady separation, we first differentiate (2.12) with respect to z and set $z = 0$ to obtain the differential equation

$$\dot{\mathbf{g}}_1 = \mathbf{a}_z + (\mathbf{a}_{\mathbf{x}} - b_z\mathbf{I})\,\mathbf{g}_0 - (b_{\mathbf{x}} \cdot \mathbf{g}_0)\,\mathbf{g}_0 - 2b\mathbf{g}_1. \tag{2.23}$$

Our notation here is consistent with that of the previous sections; for instance, we have $\mathbf{a}_{\mathbf{x}}(t) = \mathbf{A}_{\mathbf{x}}(\gamma, 0, t)$ and $\mathbf{g}_1(t) = \mathbf{G}_z(0, t)$.

Using the density formula (2.14), we write the solution of the above linear ODE in the form

$$\mathbf{g}_1(t) = \mathbf{g}_1(t_0)\frac{\rho^2(t)}{\rho^2(t_0)} + \int_{t_0}^{t} \frac{\rho^2(t)}{\rho^2(s)} \left[\mathbf{a}_z(s) + (\mathbf{a}_{\mathbf{x}}(s) - b_z(s)\mathbf{I})\,\mathbf{g}_0(s) - (b_{\mathbf{x}}(s)\cdot\mathbf{g}_0(s))\,\mathbf{g}_0(s)\right] ds, \tag{2.24}$$

where $\mathbf{I}$ denotes the 2×2 identity matrix. For a second-order separation profile (i.e., for a profile of bounded curvature), the above solution must be bounded as $t \to -\infty$. As we show in appendix A.1, this boundedness requirement leads to the following formula for the slope of the separation profile at $t = t_0$:

$$\mathbf{g}_0(t_0) = -\lim_{t\to-\infty}\left[\int_{t_0}^{t} \mathbf{Q}(s,t_0,t)\,ds\right]^{-1} \int_{t_0}^{t} \mathbf{p}(s,t_0)\,ds, \tag{2.25}$$

where we define

$$\begin{aligned}
\mathbf{p}(s,t_0) &= \frac{\mathbf{a}_z(s)}{\rho^2(s)} + \frac{\mathbf{a}_{\mathbf{x}}(s) - b_z(s)\mathbf{I}}{\rho(s)} \int_{t_0}^{s} \frac{\mathbf{a}(r)}{\rho(r)}\,dr - b_{\mathbf{x}}(s)\left(\int_{t_0}^{s} \frac{\mathbf{a}(r)}{\rho(r)}\,dr\right)^2, \\
\mathbf{Q}(s,t_0,t) &= \frac{1}{\rho(t_0)}\left[\frac{\mathbf{a}_{\mathbf{x}}(s) - b_z(s)\mathbf{I}}{\rho(s)} - \int_{t_0}^{s} \frac{\mathbf{a}(r)\otimes b_{\mathbf{x}}(s) + b_{\mathbf{x}}(s)\cdot\mathbf{a}(r)\mathbf{I}}{\rho(r)}\,dr\right].
\end{aligned} \tag{2.26}$$

Similar expressions can be derived for higher-order derivatives of $\mathbf{G}(z,t)$ in a recursive fashion by further differentiating the separation equation (2.12) with respect to z at $z = 0$.

2.2.7 Density-independent formulation

Using the density relation (2.4), we can express the density in terms of the integral of $w_z(\gamma,0,t)$, and obtain a density-independent formulation of our separation theory. In this formulation, assumptions (2.6) and (2.7) are expressed as

$$\left|\int_{t_0}^{t} w_z(x,0,s)\,ds\right| \le K_0 < \infty, \qquad \left|\int_{t_0}^{t} w_{\mathbf{x}z}(x,0,\tau)\,d\tau\right| \le K_1 < \infty,$$

and the separation criteria (2.18) and (2.20) are replaced by

$$\limsup_{t\to-\infty}\left|\int_{t_0}^{t} e^{\int_{t_0}^{\tau} w_z(\gamma,0,s)\,ds}\mathbf{u}_z(\gamma,0,\tau)\,d\tau\right| < \infty \tag{2.27}$$

and

$$\begin{aligned}
\lim_{t\to-\infty}\Bigg\| &\int_{t_0}^{t} e^{\int_{t_0}^{\tau} w_z(\gamma,0,s)\,ds}\,(\mathbf{a}_{\mathbf{x}}(s) - \mathbf{I}b_z(s)) \\
&- \left(\int_{t_0}^{\tau} e^{\int_{t_0}^{s} w_z(\gamma,0,s)\,ds}(\mathbf{a}(r)\otimes b_{\mathbf{x}}(s) + b_{\mathbf{x}}(s)\cdot\mathbf{a}(r)\mathbf{I})\,dr\right) ds\Bigg\| = \infty.
\end{aligned} \tag{2.28}$$

Similarly, effective separation points are defined by the formula

$$\int_{t_0}^{t} e^{\int_{t_0}^{\tau} w_z(\gamma_{eff},0,s)\,ds}\mathbf{u}_z(\gamma_{eff},0,\tau)\,d\tau = \mathbf{0}. \tag{2.29}$$

The separation slope and curvature, as well as higher order derivatives of the separation profile can all be expressed in purely kinematic terms using the density relation (2.4). We shall use the above density-independent formulation in deriving separation conditions for moving boundaries in § 2.2.8.

2.2.8 Separation on moving boundaries of general shape

Let us assume now that the velocity field (2.8) satisfies no-slip boundary conditions along a boundary $\mathcal{B}(t)$ which is not flat and steady but moves with velocity $\mathbf{v}_{\mathcal{B}}(t) = (\mathbf{u}_{\mathcal{B}}(t), w_{\mathcal{B}}(t))$. Thus we would like to find a necessary condition for separation at a point whose relative location is fixed on the moving boundary. As the previous formulae are not directly applicable, we need to transform them.

If at time t_0 the boundary–say, a moving airfoil–is represented by a differentiable graph $z = h(\mathbf{x})$, then at a later time t the boundary satisfies

$$z - \int_{t_0}^{t} w_{\mathcal{B}}(s)\, ds = h(\mathbf{x} - \int_{t_0}^{t} \mathbf{u}_{\mathcal{B}}(s)\, ds),$$

as indicated in figure 2-2.

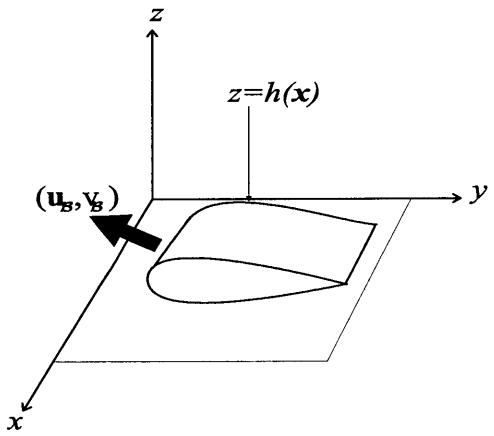

Figure 2-2: Moving boundary.

Then we transform the velocity field to the canonical form (2.2) by setting

$$\boldsymbol{\xi} = \mathbf{x} - \int_{t_0}^{t} \mathbf{u}_{\mathcal{B}}(s)\, ds, \qquad \eta = z - h(\boldsymbol{\xi}) - \int_{t_0}^{t} w_{\mathcal{B}}(s)\, ds. \tag{2.30}$$

In terms of the $(\boldsymbol{\xi}, \eta)$ coordinates, fluid particle motions satisfy

$$\dot{\boldsymbol{\xi}} = \hat{\mathbf{u}}(\boldsymbol{\xi}, \eta, t), \qquad \dot{\eta} = \hat{w}(\boldsymbol{\xi}, \eta, t),$$

with the new velocity field

$$\begin{aligned}
\hat{\mathbf{u}}(\boldsymbol{\xi},\eta,t) &= u(\boldsymbol{\xi}+\int_{t_0}^{t}\mathbf{u}_{\mathcal{B}}(s)\,ds,\eta+h(\boldsymbol{\xi})+\int_{t_0}^{t}w_{\mathcal{B}}(s)\,ds,t)-\mathbf{u}_{\mathcal{B}}(t),\\
\hat{w}(\boldsymbol{\xi},\eta,t) &= w(\boldsymbol{\xi}+\int_{t_0}^{t}\mathbf{u}_{\mathcal{B}}(s)\,ds,\eta+h(\boldsymbol{\xi})+\int_{t_0}^{t}w_{\mathcal{B}}(s)\,ds,t)-w_{\mathcal{B}}(t)-h'(\boldsymbol{\xi})\cdot\hat{\mathbf{u}}(\boldsymbol{\xi},\eta,t).
\end{aligned}$$

The transformed velocity field $(\hat{\mathbf{u}},\hat{w})$ satisfies the boundary conditions

$$\hat{\mathbf{u}}(\mathbf{x},0,t)=0,\qquad \hat{w}(\mathbf{x},0,t)=0. \tag{2.31}$$

Furthermore,

$$\operatorname{Tr}\hat{\mathbf{u}}_{\boldsymbol{\xi}}+\hat{w}_{\eta}=\operatorname{Tr}\mathbf{u}_{\mathbf{x}}+h'\cdot\mathbf{u}_z+w_z-h'\cdot\mathbf{u}_z=\operatorname{Tr}\mathbf{u}_{\mathbf{x}}+w_z,$$

which corresponds to the continuity equation (2.36), thus compressibility or incompressibility is unaffected by the change of coordinates $(\mathbf{x},z)\mapsto(\boldsymbol{\xi},\eta)$.

Because

$$\begin{aligned}
\hat{\mathbf{u}}_{\eta}(\boldsymbol{\xi},\eta,t) &= \mathbf{u}_z(\boldsymbol{\xi}+\int_{t_0}^{t}\mathbf{u}_{\mathcal{B}}(s)\,ds,\eta+h(\boldsymbol{\xi})+\int_{t_0}^{t}w_{\mathcal{B}}(s)\,ds,t), \qquad (2.32)\\
\hat{w}_{\eta}(\boldsymbol{\xi},\eta,t) &= w_z(\boldsymbol{\xi}+\int_{t_0}^{t}\mathbf{u}_{\mathcal{B}}(s)\,ds,\eta+h(\boldsymbol{\xi})+\int_{t_0}^{t}w_{\mathcal{B}}(s)\,ds,t)-h'(\boldsymbol{\xi})\cdot\hat{\mathbf{u}}_{\eta}(\boldsymbol{\xi},\eta,t),
\end{aligned}$$

the density-independent necessary condition (2.27)–applied in the $(\boldsymbol{\xi},\eta)$ coordinates–takes the form

$$\boxed{\limsup_{t\to-\infty}\left|\int_{t_0}^{t}\mathbf{E}(\boldsymbol{\gamma},\tau,t)\,\mathbf{u}_z(\boldsymbol{\gamma}+\int_{t_0}^{\tau}\mathbf{u}_{\mathcal{B}}(s)\,ds,\ h(\boldsymbol{\gamma})+\int_{t_0}^{\tau}w_{\mathcal{B}}(r)\,dr,\tau)\ d\tau\right|<\infty,} \tag{2.33}$$

where

$$\begin{aligned}
E(\gamma,\tau,t) &= \exp\int_{t_0}^{\tau}\Big[w_z(\gamma+\int_{t_0}^{s}\mathbf{u}_{\mathcal{B}}(r)\,dr,h(\boldsymbol{\gamma})+\int_{t_0}^{s}w_{\mathcal{B}}(r)\,dr,s)\\
&\qquad -h'(\boldsymbol{\gamma})\cdot\mathbf{u}_z(\gamma+\int_{t_0}^{s}\mathbf{u}_{\mathcal{B}}(r)\,dr,h(\boldsymbol{\gamma})+\int_{t_0}^{s}w_{\mathcal{B}}(r)\,dr,s)\Big]\,ds\,. \qquad (2.34)
\end{aligned}$$

As in the case of flat boundaries, we locate the separation point on general boundaries by computing the effective separation point $\boldsymbol{\gamma}_{eff}(t,t_0)$ for $|t-t_0|$ large enough from the formula

$$\boxed{\int_{t_0}^{t}E(\boldsymbol{\gamma}_{eff},\tau,t)\,\mathbf{u}_z(\gamma+\int_{t_0}^{\tau}\mathbf{u}_{\mathcal{B}}(s)\,ds,\ h(\boldsymbol{\gamma}_{eff})+\int_{t_0}^{\tau}w_{\mathcal{B}}(r)\,dr,\tau)\ d\tau=\mathbf{0}.} \tag{2.35}$$

To evaluate the second necessary condition (2.28) in the present $(\boldsymbol{\xi},\eta)$ coordinates, we compute the second derivatives

$$\hat{\mathbf{u}}_{\boldsymbol{\xi}\eta}(\boldsymbol{\xi},\eta,t),\quad \hat{w}_{\boldsymbol{\xi}\eta}(\boldsymbol{\xi},\eta,t),\quad \hat{w}_{\eta\eta}(\boldsymbol{\xi},\eta,t),$$

in terms of the original velocity field from (2.32). With these expressions, the second separation

condition (2.28) becomes a straightforward but lengthy condition, which we omit here for brevity.

2.3 Fixed unsteady separation in incompressible flows

In this section, we consider incompressible flows, and show how our theory for fixed unsteady separation simplifies in this case. (We also derive a general third-order approximation for the separation profile.)

2.3.1 Set-up

Consider again the velocity field (2.2), but which also satisfies the incompressibility condition

$$\operatorname{Tr} \mathbf{u}_{\mathbf{x}} + w_z = 0. \tag{2.36}$$

The no-slip boundary conditions again enable us to rewrite the velocity field in the form (2.8), with the equivalent incompressibility condition

$$z \operatorname{Tr} \mathbf{A}_{\mathbf{x}} + B + zB_z = 0.$$

Setting $z = 0$ in this equation gives $B(\mathbf{x}, 0, t) \equiv 0$, thus we can further rewrite the velocity field in the form

$$\dot{\mathbf{x}} = zA(\mathbf{x}, z, t), \qquad \dot{z} = z^2 C(\mathbf{x}, z, t), \tag{2.37}$$

where we have

$$C(\mathbf{x}, z, t) = \int_0^1 \int_0^1 w_{zz}(\mathbf{x}, spz, t) p \, dp \, ds. \tag{2.38}$$

Enforcing the incompressibility condition (2.36) for system (2.37) yields

$$z \left(\operatorname{Tr} \mathbf{A}_{\mathbf{x}} + 2C + zC_z \right) = 0. \tag{2.39}$$

Away from the boundary, i.e., for $z > 0$, this relation between the functions $\mathbf{A}$ and C implies

$$\operatorname{Tr} \mathbf{A}_{\mathbf{x}} + 2C + zC_z = 0. \tag{2.40}$$

Because $\mathbf{A}_{\mathbf{x}}$, C, and C_z are continuous, this last equation extends to $z = 0$. Therefore, (2.40) must hold all over the fluid, including the boundary.

In our arguments, we will work with the incompressible canonical velocity field (2.37) for simplicity. Alternatively, one could work with the compressible canonical form (2.8) and use the incompressibility condition (2.40), but that approach would quickly lead to intractably complex expressions.

2.3.2 Equation for the separation profile

As in the compressible case, we want to express the unsteady separation profile as an unstable manifold satisfying $\boldsymbol{\xi} = \mathbf{x} - \boldsymbol{\gamma} = z\mathbf{G}(z, t)$. Differentiating in time and substituting this relation

into (2.37) implies

$$z\left[\mathbf{A}(z\mathbf{G}+\boldsymbol{\gamma},z,t)-zC(z\mathbf{G}+\boldsymbol{\gamma},z,t)\ (\mathbf{G}+z\mathbf{G}_z)-\mathbf{G}_t\right]=0.$$

By continuity, the bracketed expression must vanish for all $z \geq 0$, which yields

$$\mathbf{A}(z\mathbf{G}+\boldsymbol{\gamma},z,t)-zC(z\mathbf{G}+\boldsymbol{\gamma},z,t)\ (\mathbf{G}+z\mathbf{G}_z)-\mathbf{G}_t=0. \tag{2.41}$$

Applying the incompressibility relation to the compressible separation equation (2.12), we also recover (2.41).

2.3.3 Necessary conditions for separation

We now write the constant term in the Taylor expansion of the incompressible relation (2.41) and obtain the differential equation

$$\dot{\mathbf{g}}_0=\mathbf{a}.$$

We integrate this equation to obtain

$$\mathbf{g}_0(t)=\mathbf{g}_0(t_0)+\int_{t_0}^{t}\mathbf{a}(\tau)\,d\tau. \tag{2.42}$$

As at the point $(\boldsymbol{\gamma},0)$ we require $\mathbf{g}_0(t)$ to be bounded in backward time, we obtain the first necessary condition:

$$\boxed{\limsup_{t\to-\infty}\left|\int_{t_0}^{t}\mathbf{u}_z(\boldsymbol{\gamma},0,\tau)\,d\tau\right|<\infty.} \tag{2.43}$$

Re-applying the ideas in (2.20) and the proof of appendix A.1, we obtain the second necessary condition at fixed separation points:

$$\boxed{\lim_{t\to-\infty}\left\|\int_{t_0}^{t}(\mathbf{a}_{\mathbf{x}}(\boldsymbol{\gamma},0,\tau)+\mathbf{I}\,\mathrm{Tr}\,\mathbf{a}_{\mathbf{x}}(\boldsymbol{\gamma},0,\tau)/2)d\tau\right\|=\infty.} \tag{2.44}$$

2.3.4 Effective separation points

As the separation criterion (2.43) is unsuitable for direct computations, we still use the effective separation point principle. Effective separation points are now defined as

$$\int_{t_0}^{t}\mathbf{u}_z(\boldsymbol{\gamma}_{eff}(t_0,t),0,s)\ ds=\mathbf{0}. \tag{2.45}$$

They approximate the location of the actual flow separation. Our argument for the convergence of effective separation points to actual separation points applies here again.

2.3.5 Separation profile up to third order

We now give explicit formulae for the time-dependent coefficients of the cubic separation profile

$$\mathbf{x}=\boldsymbol{\gamma}+\mathbf{g}_0(t)z+\mathbf{g}_1(t)z^2+\frac{1}{2}\mathbf{g}_2(t)z^3. \tag{2.46}$$

These coefficients are tedious to compute for the compressible case, but they become manageable in the incompressible case. As we show in appendix A.2, the coefficients at time t_0 satisfy

$$\begin{aligned} \mathbf{g}_0(t_0) &= -\lim_{t\to-\infty}\left[\int_{t_0}^{t}(\mathbf{a}_{\mathbf{x}}(s)+\frac{1}{2}\mathbf{I}\,\mathrm{Tr}\,\mathbf{a}_{\mathbf{x}}(s))\,ds\right]^{-1} \\ &\quad\times\int_{t_0}^{t}[\mathbf{a}_z(s)+(\mathbf{a}_{\mathbf{x}}(s)+\frac{1}{2}\mathbf{I}\,\mathrm{Tr}\,\mathbf{a}_{\mathbf{x}}(s))\int_{t_0}^{s}\mathbf{a}(r)\,dr]\,ds, \end{aligned} \tag{2.47}$$

$$\begin{aligned} \mathbf{g}_1(t_0) &= -\lim_{t\to-\infty}\left[2\int_{t_0}^{t}(\mathbf{a}_{\mathbf{x}}(s)+\mathbf{I}\,\mathrm{Tr}\,\mathbf{a}_{\mathbf{x}}(s))ds\right]^{-1} \\ &\quad\times\int_{t_0}^{t}\left[\mathbf{a}_{zz}(\tau)+2\left[\mathbf{a}_{\mathbf{x}z}(\tau)+\frac{1}{3}\mathbf{I}\,\mathrm{Tr}\,\mathbf{a}_{\mathbf{x}z}(\tau)\right]\mathbf{g}_0(\tau)\right. \\ &\quad+[[\mathbf{a}_{\mathbf{xx}}(\tau)+(\mathrm{Tr}\,\mathbf{a}_{\mathbf{x}}(\tau))_{\mathbf{x}}\cdot\mathbf{I}]\,\mathbf{g}_0(\tau)]\,\mathbf{g}_0(\tau) \\ &\quad\left.+2\,[\mathbf{a}_{\mathbf{x}}(\tau)+\mathbf{I}\,\mathrm{Tr}\,\mathbf{a}_{\mathbf{x}}(\tau)]\times\int_{t_0}^{\tau}\left[\mathbf{a}_z(s)+\left(\mathbf{a}_{\mathbf{x}}(s)+\frac{1}{2}\mathbf{I}\,\mathrm{Tr}\,\mathbf{a}_{\mathbf{x}}(s)\right)\mathbf{g}_0(s)\right]\,ds\right]\,d\tau, \end{aligned} \tag{2.48}$$

$$\begin{aligned} \mathbf{g}_2(t_0) &= -\lim_{t\to-\infty}\left[3\int_{t_0}^{t}(\mathbf{a}_{\mathbf{x}}(s)+\frac{3}{2}\mathbf{I}\,\mathrm{Tr}\,\mathbf{a}_{\mathbf{x}}(s))ds\right]^{-1} \\ &\quad\times\int_{t_0}^{t}\left[\mathbf{a}_{zzz}(\tau)+3\left[\mathbf{a}_{\mathbf{x}zz}(\tau)+\frac{1}{4}\mathbf{I}\,\mathrm{Tr}\,\mathbf{a}_{\mathbf{x}zz}(\tau)\right]\mathbf{g}_0(\tau)\right. \\ &\quad+\left[\left(\mathbf{a}_{\mathbf{xxx}}(\tau)\mathbf{g}_0(\tau)+\frac{3}{2}(\mathrm{Tr}\,\mathbf{a}_{\mathbf{x}}(\tau))_{\mathbf{xx}}\mathbf{g}_0\cdot\mathbf{I}\right)\mathbf{g}_0(\tau)\right]\mathbf{g}_0(\tau) \\ &\quad+3\left[\left(\mathbf{a}_{\mathbf{xx}z}(\tau)+\frac{2}{3}(\mathrm{Tr}\,\mathbf{a}_{\mathbf{x}z}(\tau))_{\mathbf{x}}\cdot\mathbf{I}\right)\mathbf{g}_0(\tau)\right]\mathbf{g}_0(\tau) \\ &\quad+3\left[\left[\left(\mathbf{a}_{\mathbf{xx}}(\tau)+\frac{3}{2}(\mathrm{Tr}\,\mathbf{a}_{\mathbf{x}}(\tau))_{\mathbf{x}}\cdot\mathbf{I}\right)\mathbf{g}_0(\tau)\right]\mathbf{g}_1(\tau)\right. \\ &\quad\left.+\left[\left(\mathbf{a}_{\mathbf{xx}}(\tau)+\frac{3}{2}(\mathrm{Tr}\,\mathbf{a}_{\mathbf{x}}(\tau))_{\mathbf{x}}\cdot\mathbf{I}\right)\mathbf{g}_1(\tau)\right]\mathbf{g}_0(\tau)\right]+6\left(\mathbf{a}_{\mathbf{x}z}(\tau)+\frac{2}{3}\,\mathrm{Tr}\,\mathbf{a}_{\mathbf{x}z}(\tau)\mathbf{I}\right)\mathbf{g}_1(\tau) \\ &\quad+3\left[\mathbf{a}_{\mathbf{x}}(\tau)+\frac{3}{2}\mathbf{I}\,\mathrm{Tr}\,\mathbf{a}_{\mathbf{x}}(\tau)\right]\int_{t_0}^{\tau}\left[\mathbf{a}_{zz}(s)+2\left[\mathbf{a}_{\mathbf{x}z}(s)+\frac{1}{3}\mathbf{I}\,\mathrm{Tr}\,\mathbf{a}_{\mathbf{x}z}(s)\right]\mathbf{g}_0(s)\right. \\ &\quad\left.\left.+[[\mathbf{a}_{\mathbf{xx}}(s)+(\mathrm{Tr}\,\mathbf{a}_{\mathbf{x}}(s))_{\mathbf{x}}\cdot\mathbf{I}]\,\mathbf{g}_0(s)]\,\mathbf{g}_0(s)+2\,[\mathbf{a}_{\mathbf{x}}(s)+\mathbf{I}\,\mathrm{Tr}\,\mathbf{a}_{\mathbf{x}}(s)]\,\mathbf{g}_1(s)]\,ds\right]\,d\tau. \end{aligned} \tag{2.49}$$

2.4 Unsteady separation from pressure and skin friction

In order to monitor and control unsteady separation in experiments, one needs separation criteria phrased in terms of physically measurable quantities. Here we present a formulation of our separation theory in terms of pressure, skin friction, density, and viscosity measured along the wall.

Using the skin friction (or wall-shear) $\boldsymbol{\tau}(x,t)$, we have already expressed the first separation condition (2.19) in (2.18). For some $t<t_0$, we compute the effective separation point from the

equation

$$\int_{t_0}^{t} \frac{\boldsymbol{\tau}(\gamma_{eff}(t,t_0),s)}{\rho^2(\gamma_{eff}(t,t_0),0,s)}\, ds = 0.$$

For incompressible flows, the effective separation point coincides with the point of zero mean-skin-friction. For compressible flows, however, the zero-mean-skin-friction rule is generally inadequate as a true separation indicator: To obtain a good estimate for the separation location, one needs to use $1/\rho^2$ as a weight function when integrating the skin friction in time.

For incompressible flows, the second separation criterion (2.20) also admits a simple kinetic formulation. Differentiating equation (2.17) with respect to $\mathbf{x}$, we obtain

$$\boldsymbol{\tau}'(\mathbf{x},t) = \tau(\mathbf{x},t)\rho_{\mathbf{x}}(\mathbf{x},0)/\rho(\mathbf{x},0) + \nu\rho(\mathbf{x},0)\mathbf{u}_{\mathbf{x}z}(\mathbf{x},0,t),$$

from which we express and substitute $\mathbf{u}_{\mathbf{x}z}$ into (2.44) to obtain the second condition

$$\lim_{t\to-\infty} \left\| \int_{t_0}^{t} [(\boldsymbol{\tau}'(\mathbf{x},\tau)\rho(\mathbf{x},0) - \tau(\mathbf{x},\tau)\rho_{\mathbf{x}}(\mathbf{x},0)) + \mathbf{I}\,\mathrm{Tr}(\boldsymbol{\tau}'(\mathbf{x},\tau)\rho(\mathbf{x},0) - \tau(\mathbf{x},\tau)\rho_{\mathbf{x}}(\mathbf{x},0))/2] d\tau \right\| = \infty.$$

The separation slope formula also admits a purely kinetic form for incompressible flows: along the no-slip boundary $z = 0$, the incompressible Navier-Stokes equations imply

$$p_{\mathbf{x}}(\mathbf{x},0,t)/\rho(\mathbf{x},0) = \nu\mathbf{u}_{zz}(x,0,t),$$

with $p(\mathbf{x},z,t)$ denoting the pressure. Combining the above formulae with the definition of $\mathbf{a}(\boldsymbol{\gamma},t)$, we can write the slope

$$\begin{aligned} \mathrm{g}_0(t_0) \;=\; & -\lim_{t\to-\infty} \Big[\int_{t_0}^{t} [(\boldsymbol{\tau}'(\mathbf{x},s)\rho(\mathbf{x},0) - \tau(\mathbf{x},s)\rho_{\mathbf{x}}(\mathbf{x},0)) \\ & + \mathbf{I}\,\mathrm{Tr}(\boldsymbol{\tau}'(\mathbf{x},s)\rho(\mathbf{x},0) - \tau(\mathbf{x},s)\rho_{\mathbf{x}}(\mathbf{x},0))/2] ds \Big]^{-1} \times \int_{t_0}^{t} [p_{\mathbf{x}}(\mathbf{x},0,s)/2\nu\rho(\mathbf{x},0) \\ & + [(\boldsymbol{\tau}'(\mathbf{x},s)\rho(\mathbf{x},0) - \tau(\mathbf{x},s)\rho_{\mathbf{x}}(\mathbf{x},0)) + \mathbf{I}\,\mathrm{Tr}(\boldsymbol{\tau}'(\mathbf{x},s)\rho(\mathbf{x},0) - \tau(\mathbf{x},s)\rho_{\mathbf{x}}(\mathbf{x},0))/2] \\ & \times \int_{t_0}^{s} \frac{\boldsymbol{\tau}(\mathbf{x},r)}{\rho(\mathbf{x},0)}\, dr]\, ds. \end{aligned} \tag{2.50}$$

If the initial density of the incompressible fluid is equal to a constant ρ_0 along the wall, then the kinetic separation simplifies to

$$\begin{aligned} \mathrm{g}_0(t_0) \;=\; & -\lim_{t\to-\infty} \left[\int_{t_0}^{t} [\boldsymbol{\tau}'(\mathbf{x},s) + \mathbf{I}\,\mathrm{Tr}\,\boldsymbol{\tau}'(\mathbf{x},s)/2] ds \right]^{-1} \\ & \times \int_{t_0}^{t} \left[\frac{p_{\mathbf{x}}(\mathbf{x},0,s)}{2\nu\rho_0^2} + [\boldsymbol{\tau}'(\mathbf{x},s) + \mathbf{I}\,\mathrm{Tr}\,\boldsymbol{\tau}'(\mathbf{x},s)/2] \int_{t_0}^{s} \frac{\boldsymbol{\tau}(\mathbf{x},r)}{\rho_0^2}\, dr \right] ds. \end{aligned} \tag{2.51}$$

Formulae (2.18) and (2.50) show that for incompressible flows, the separation location and slope can both be monitored from pressure and skin friction sensors distributed along the wall.

2.5 Sufficient conditions for sharp separation

So far we have only looked for necessary features of fixed unsteady separation: if separation takes place at the point $(\gamma, 0)$, then conditions (2.18) and (2.20) must hold. We are now looking for sufficient conditions: when slightly stronger conditions are satisfied, one obtains the existence of a time-dependent nonlinear separation profile linked to a boundary point, the separation point.

We first note that condition (2.18) is general enough to allow for *weak separation*: a scenario whereby particles near the separation point may turn back towards the wall for finite periods of time, and are only ejected from a vicinity of the wall asymptotically. Such weak separation behavior is atypical: In observed fluid motion, once started, separation tends to be *sharp*, which means that particles in a vicinity of the separation point move away always in the same direction from the wall.

We establish here a sufficient criterion for sharp separation. To avoid lengthy technical arguments, we also assume that the flow is incompressible. As we prove in appendix A.3, sharp incompressible separation takes place if the first necessary condition

$$\limsup_{t\to-\infty} \left| \int_{t_0}^{t} \mathbf{u}_z(\boldsymbol{\gamma}, 0, s)\, ds \right| < \infty \tag{2.52}$$

and a stronger version of the second criterion (2.44) both hold. This stronger criterion requires both $\operatorname{Tr} \mathbf{a}_\mathbf{x}$ to be negative and uniformly bounded away from zero for all times, and at the same time the matrix $\mathbf{a}_\mathbf{x}$ to be uniformly bounded:

$$\operatorname{Tr} \mathbf{a}_\mathbf{x}(\boldsymbol{\gamma}, 0, t) \;<\; -c_0 < 0, \tag{2.53a}$$

$$\|\mathbf{a}_\mathbf{x}(\boldsymbol{\gamma}, 0, t)\| \;\leq\; M, \tag{2.53b}$$

where the norm refers to the maximum of the matrix over the sphere of radius 1. For details of the argument, we refer the reader to appendix A.3.

As a simple Taylor expansion shows, the quantity $w_{zz}(\boldsymbol{\gamma}, 0, t) = -\operatorname{Tr} \mathbf{a}_\mathbf{x}(\boldsymbol{\gamma}, 0, t)$ is the dominant term in the instantaneous strength of separation. Requiring it to be strictly positive for all times ensures continued ejection of particles (sharp separation) from a vicinity of the wall. By contrast, the incompressible necessary condition (2.44) is less restrictive, and hence allows for weak separation.

2.6 Separation in flows with simple time-dependence

We now evaluate our results for three simple classes of flows that produce fixed separation: steady, time-periodic and quasiperiodic flows. In all three cases, separation points and profiles turn out to be exactly computable from finite-time velocity data, and hence the use of effective separation points is unnecessary. Even these special cases are important, because no related results are available in the literature.

2.6.1 Steady flows

Assumptions

Considering a steady compressible flow with a horizontal no-slip boundary at $z = 0$, the continuity equation (2.3) yields

$$\rho(\mathbf{x}, 0) w_z(\mathbf{x}, 0) = 0.$$

As the density cannot vanish along the boundary, we obtain

$$w_z(\mathbf{x}, 0) = 0, \tag{2.54}$$

and differentiating this expression with respect to $\mathbf{x}$, we have

$$w_{\mathbf{x}z}(\mathbf{x}, 0) = 0. \tag{2.55}$$

Thus the two assumptions (2.6)-(2.7) are satisfied for steady flows.

Separation criteria

In steady flows the density $\rho(\mathbf{x}, z)$ is constant in time, then the first separation condition (2.18) can be transformed to

$$\lim_{t \to -\infty} \left| \int_t^{t_0} \mathbf{u}_z(\boldsymbol{\gamma}, 0)\, ds \right| = \lim_{t \to -\infty} |\mathbf{u}_z(\boldsymbol{\gamma}, 0)(t_0 - t)| < \infty,$$

which is equivalent to

$$\mathbf{u}_z(\boldsymbol{\gamma}, 0) = 0. \tag{2.56}$$

Differentiating the continuity equation (2.3) with respect to z, we obtain

$$\rho(\boldsymbol{\gamma}, 0) \left[\operatorname{Tr} \mathbf{u}_{\mathbf{x}z}(\boldsymbol{\gamma}, 0) + w_{zz}(\boldsymbol{\gamma}, 0) \right] = 0,$$

which implies the equality

$$\operatorname{Tr} \mathbf{u}_{\mathbf{x}z}(\boldsymbol{\gamma}, 0) = -w_{zz}(\boldsymbol{\gamma}, 0). \tag{2.57}$$

Then the second separation criterion (2.44) becomes

$$\begin{aligned} & \lim_{t \to -\infty} \left\| \int_{t_0}^{t} (\mathbf{u}_{\mathbf{x}z}(\gamma, 0) + \mathbf{I} \operatorname{Tr} \mathbf{u}_{\mathbf{x}z}(\boldsymbol{\gamma}, 0)/2) d\tau \right\| \\ = & \lim_{t \to -\infty} \| \mathbf{u}_{\mathbf{x}z}(\gamma, 0) + \mathbf{I} \operatorname{Tr} \mathbf{u}_{\mathbf{x}z}(\boldsymbol{\gamma}, 0)/2 \| \, (t - t_0) = \infty, \end{aligned} \tag{2.58}$$

implying $\| \mathbf{u}_{\mathbf{x}z}(\gamma, 0) + \mathbf{I} \operatorname{Tr} \mathbf{u}_{\mathbf{x}z}(\boldsymbol{\gamma}, 0)/2 \| \neq 0$, which is equivalent to

$$\mathbf{u}_{\mathbf{x}z}(\gamma, 0) \neq 0. \tag{2.59}$$

Separation profile

From formula (2.25) we can write and simplify the slope:

$$\begin{aligned} \mathbf{g}_0(t_0) &= -\lim_{t\to-\infty}\left[\int_{t_0}^{t}[\mathbf{a}_{\mathbf{x}}(s)-b_z(s)\mathbf{I}]\,ds\right]^{-1}\int_{t_0}^{t}\mathbf{a}_z(s)ds \\ &= -\left[\mathbf{u}_{\mathbf{x}z}(\boldsymbol{\gamma},0)+\mathbf{I}\,\mathrm{Tr}\,\mathbf{u}_{\mathbf{x}z}(\boldsymbol{\gamma},0)/2\right]^{-1}\mathbf{u}_{zz}(\boldsymbol{\gamma},0), \end{aligned} \tag{2.60}$$

where we have used (2.56) and (2.57). Higher-order approximations for steady separation profiles can be derived following the previous analysis.

Steady examples

They are developed in chapter 3: a saddle-sink, a saddle-saddle, a saddle-focus (§ 3.3.2) and a closing bubble (§ 3.4.4). We also develop a method to analytically calculate all the orders of separation and the real separation profile in appendix B.2.1.

2.6.2 Time-periodic flows

Assumptions

If we suppose that the velocity field $\mathbf{v}=(\mathbf{u},w)$ is T-periodic in time, then $\mathbf{v}$ and its derivatives admit Fourier expansions in time. In particular, $w_z(\mathbf{x},z,t)$ can be written as the sum of a time-independent mean and a time-dependent oscillating part:

$$w_z(\mathbf{x},z,t)=\bar{w}_z(\mathbf{x},z)+\tilde{w}_z(\mathbf{x},z,t),$$

where we have

$$\bar{w}_z(\mathbf{x},z)=\frac{1}{T}\int_0^T w_z(\mathbf{x},z,t)\,dt, \qquad \int_0^T \tilde{w}_z(\mathbf{x},z,t)\,dt=0.$$

The first major assumption in our fixed separation study was (2.6), which now takes the particular form

$$\limsup_{t\to-\infty}\left|\int_{t_0}^{t} w_z(\mathbf{x},0,s)\,ds\right| = \limsup_{t\to-\infty}\left|\bar{w}_z(\mathbf{x},0)\,(t-t_0)+\int_{t_0}^{t}\tilde{w}_z(\mathbf{x},0,s)\,ds\right| < \infty. \tag{2.61}$$

As $\tilde{w}_z(\mathbf{x},z,t)$ is a zero-mean periodic function of t, the integral $\int_{t_0}^{t}\tilde{w}_z(\mathbf{x},0,s)\,ds$ is a zero-mean periodic function of t, and remains bounded for all t. Then, in view of the density formula (2.4), assumption (2.6) can be expressed as

$$\int_0^T w_z(\boldsymbol{\gamma},0,t)\,dt=0. \tag{2.62}$$

Without this last assumption, the density at the separation point would tend to zero or

infinity. Repeating the above principle for (2.7), we obtain

$$\int_0^T w_{\mathbf{x}z}(\boldsymbol{\gamma}, 0, t)\, dt = 0, \tag{2.63}$$

which prevents the unbounded growth of the wall-tangential density gradient at the point of separation.

Separation criteria

Under assumption (2.62), the first separation condition (2.18) becomes

$$\limsup_{t\to-\infty} \left| \int_{t_0}^t \frac{\mathbf{u}_z(\boldsymbol{\gamma}, 0, s)}{\rho(\boldsymbol{\gamma}, 0, s)}\, ds \right| < \infty. \tag{2.64}$$

The integrand in this condition is again a T-periodic function, and this integral can only remain bounded if

$$\boxed{\int_0^T \frac{\mathbf{u}_z(\boldsymbol{\gamma},0,t)}{\rho(\boldsymbol{\gamma},0,t)}\, dt = 0.} \tag{2.65}$$

We now have a general criterion for separation in two-dimensional time-periodic flows.

For incompressible time-periodic flows, the relevant first separation criterion is (2.43), which simplifies to

$$\int_0^T \mathbf{u}_z(\boldsymbol{\gamma}, 0, t)\, dt = 0. \tag{2.66}$$

To evaluate the second separation criterion, we again split the integrand in (2.20) into a mean and an oscillating part. For the criterion to be satisfied, we need the mean to be nonzero:

$$\boxed{\int_0^T \left[\frac{\mathbf{a}_{\mathbf{x}}(t) - b_z(t)\mathbf{I}}{\rho(t)} - \int_{t_0}^t \frac{\mathbf{a}(s) \otimes b_{\mathbf{x}}(t) + b_{\mathbf{x}}(t) \cdot \mathbf{a}(s)\mathbf{I}}{\rho(s)}\, ds \right] dt \neq 0} \tag{2.67}$$

must hold for all t_0. For incompressible flows, this criterion simplifies to

$$\int_0^T [\mathbf{a}_{\mathbf{x}}(t) + \mathbf{I}\,\mathrm{Tr}\,\mathbf{a}_{\mathbf{x}}(t)/2]\, dt \neq 0, \tag{2.68}$$

as one readily deduces from (2.44).

Time-periodic flows illustrate that the lim sup operation cannot be replaced by lim in the separation criterion (2.18). Indeed, at a fixed separation point $\boldsymbol{\gamma}$, formula (2.61) becomes

$$\limsup_{t\to-\infty} \left| \int_{t_0}^t \mathbf{u}_z(\boldsymbol{\gamma}, 0, \tau)\, d\tau \right| = \limsup_{t\to-\infty} \left| \int_{t_0}^t \tilde{\mathbf{u}}_z(\boldsymbol{\gamma}, 0, \tau)\, d\tau \right|,$$

and the integrand in this formula will have no limit as $t \to -\infty$ for an unsteady time-periodic velocity field.

Separation profile

Based on the above arguments, all our asymptotic formulae for the derivatives of the separation profile simplify to integrals over one period. For instance, the separation angle formula (2.25) becomes

$$\boxed{\mathbf{g}_0(t_0) = -\left[\int_0^T \mathbf{Q}(s,0,t)\,ds\right]^{-1} \int_0^T \mathbf{p}(s,0)\,ds,} \tag{2.69}$$

where we have defined

$$\begin{aligned}
\mathbf{p}(s,t_0) &= \frac{\mathbf{a}_z(s)}{\rho^2(s)} + \frac{\mathbf{a}_\mathbf{x}(s) - b_z(s)\mathbf{I}}{\rho(s)} \int_{t_0}^s \frac{\mathbf{a}(r)}{\rho(r)}\,dr - b_\mathbf{x}(s)\left(\int_{t_0}^s \frac{\mathbf{a}(r)}{\rho(r)}\,dr\right)^2, \\
\mathbf{Q}(s,t_0,t) &= \frac{1}{\rho(t_0)}\left[\frac{\mathbf{a}_\mathbf{x}(s) - b_z(s)\mathbf{I}}{\rho(s)} - \int_{t_0}^s \frac{\mathbf{a}(r)\otimes b_\mathbf{x}(s) + b_\mathbf{x}(s)\cdot\mathbf{a}(r)\mathbf{I}}{\rho(r)}\,dr\right].
\end{aligned}$$

For incompressible flows, this formula further simplifies from (2.47) to

$$\begin{aligned}
\mathbf{g}_0(t_0) &= -\left[\int_0^T (\mathbf{a}_\mathbf{x}(s) + \mathbf{I}\,\mathrm{Tr}\,\mathbf{a}_\mathbf{x}(s))/2ds\right]^{-1} \\
&\quad \times \int_0^T [\mathbf{a}_z(s) + (\mathbf{a}_\mathbf{x}(s) + \mathbf{I}\,\mathrm{Tr}\,\mathbf{a}_\mathbf{x}(s)/2)\int_0^T \mathbf{a}(r)\,dr]\,ds.
\end{aligned} \tag{2.70}$$

Periodic bubbles

Chapter 3 contains three periodic examples: a closing bubble with moving saddle-foci, a closing bubble with moving saddle-saddles and a non-closing bubble with moving saddle-saddles (§ 3.4.4).

2.6.3 Quasiperiodic flows

Quasiperiodic flows still display simple time-dependence, but it cannot be studied through the repeated iteration of a single period-T map. For this reason, quasiperiodic separation has remained inaccessible to classical dynamical systems methods. Here we show how general separation criteria translate to simple formulae in the quasiperiodic case.

Assumptions

Let $\omega_1, \omega_2, \ldots, \omega_m$ be m numbers that are rationally independent, i.e., admit no vanishing linear combination with rational coefficients. We say that the original velocity field $(\mathbf{u}(\mathbf{x},z,t), w(\mathbf{x},z,t))$ is quasiperiodic in time with frequencies $\omega_1,\ldots,\omega_m$, if we can write

$$\begin{aligned}
\mathbf{u}(\mathbf{x},z,t) &= \mathbf{U}(\mathbf{x},z,\omega_1 t,\ldots,\omega_m t), \\
w(\mathbf{x},z,t) &= W(\mathbf{x},z,\omega_1 t,\ldots,\omega_m t),
\end{aligned}$$

where the functions $\mathbf{U}(\mathbf{x},z,\phi_1,\ldots,\phi_m)$, and $W(\mathbf{x},z,\phi_1,\ldots,\phi_m)$ are 2π-periodic in each of the arguments $\phi_1,\ldots,\phi_m$.

Quasiperiodic velocity fields can be Fourier expanded in terms of the angular arguments ϕ_i, thus we can write

$$\begin{aligned} \mathbf{u}(\mathbf{x},z,t) &= \overline{\mathbf{u}(\mathbf{x},z,t)} + \tilde{\mathbf{u}}(\mathbf{x},z,t), \\ w(\mathbf{x},z,t) &= \overline{w(\mathbf{x},z,t)} + \tilde{w}(\mathbf{x},z,t), \end{aligned}$$

where we define

$$\begin{aligned} \overline{\mathbf{u}(\mathbf{x},z,t)} &= \frac{1}{(2\pi)^m}\int_0^{2\pi}\cdots\int_0^{2\pi}\mathbf{U}(\mathbf{x},z,\phi_1,\ldots,\phi_m)\,d\phi_1\ldots d\phi_m, \\ \overline{w(\mathbf{x},z,t)} &= \frac{1}{(2\pi)^m}\int_0^{2\pi}\cdots\int_0^{2\pi}W(\mathbf{x},z,\phi_1,\ldots,\phi_m)\,d\phi_1\ldots d\phi_m, \end{aligned}$$

and $(\tilde{\mathbf{u}}(\mathbf{x},z,t),\tilde{w}(\mathbf{x},z,t))$ denotes the bounded oscillatory part of the velocity. Just as in the periodic case, we perform a decomposition into mean and oscillating parts for the quantities featured in (2.6)-(2.7), and obtain

$$\overline{w_z(\gamma,0,t)} = 0, \qquad \overline{w_{\mathbf{x}z}(\gamma,0,t)} = 0, \tag{2.71}$$

as the main physical assumptions for our theory. Again, these assumptions ensure the boundedness of the density and the density gradient along the wall.

Separation criteria

Following the arguments we gave in the periodic case, we deduce the two separation criteria

$$\boxed{\overline{\frac{\mathbf{u}_z(\gamma,0,t)}{\rho(\gamma,0,t)}} = 0,} \tag{2.72}$$

$$\boxed{\overline{\frac{\mathbf{a}_{\mathbf{x}}(t) - b_z(t)\mathbf{I}}{\rho(t)} - \int_{t_0}^{t}\frac{\mathbf{a}(s)\otimes b_{\mathbf{x}}(t) + b_{\mathbf{x}}(t)\cdot\mathbf{a}(s)\mathbf{I}}{\rho(s)}\,ds} \neq 0.}$$

Here the second criterion needs to be satisfied for all $t_0 > 0$.

Separation profile

Quasiperiodic separation profiles obey formulae similar to their periodic counterparts. One simply takes the periodic formulae and replaces single phase averaging over $[0,T]$ with multiphase averaging as defined above. We omit these expressions for brevity.

Quasiperiodic compressible closing bubble

In chapter 3, we give a quasiperiodic example of a closing bubble (§ 3.5).

2.7 Unsteady flow reattachment

We view reattachment profiles as material lines that shrink to a single boundary point, the point of reattachment, as $t \to \infty$. Thus, in dynamical systems terms, a reattachment profile is a time-dependent *stable manifold*, or *repelling material line*, as shown in figure 2-3.

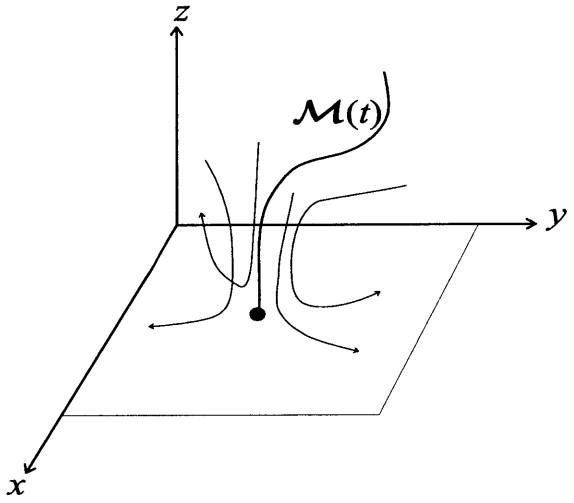

Figure 2-3: Reattachment profile as a time-dependent stable manifold for the point of separation.

Material lines that emanate from generic boundary points become asymptotically tangent to the boundary in the $t \to -\infty$ limit, as shown in figure 2-4. By contrast, all derivatives of fixed reattachment profiles at $z = 0$ stay bounded for all past times.

Effective reattachment points can be defined through the formula

$$\int_{t_0}^{t} \frac{\mathbf{u}_z(\gamma_{eff}(t,t_0),0,s)}{\rho(\gamma(t,t_0),0,s)}\, ds = 0,$$

and they will again converge to actual fixed reattachment points as $t \to -\infty$.

As for a second necessary criterion for unsteady reattachment, we follow the argument in appendix A.1 to find that

$$\boxed{\lim_{t\to-\infty}\left(\int_{t_0}^{t}\left[\frac{\mathbf{a}_{\mathbf{x}}(s)-b_z(s)\mathbf{I}}{\rho(s)} - \int_{t_0}^{s}\frac{\mathbf{a}(r)\otimes b_{\mathbf{x}}(s)+b_{\mathbf{x}}(s)\cdot\mathbf{a}(r)\mathbf{I}}{\rho(r)}\,dr\right]ds\right)\mathbf{n} = \infty}$$

for any $\mathbf{n}$ normal vector leaving the reattachment point. Note that this criterion is slightly different as the separation one: we require convergence to $+\infty$ in any direction leaving the point of reattachment. If the separation point attracts particles in one direction and repels other particles in another direction (which happens for saddle-saddle separation), we have separation. The reason for this difficulty is that all the general shape of separation: separation or reattachment, will depend on the strength of the two phenomena.

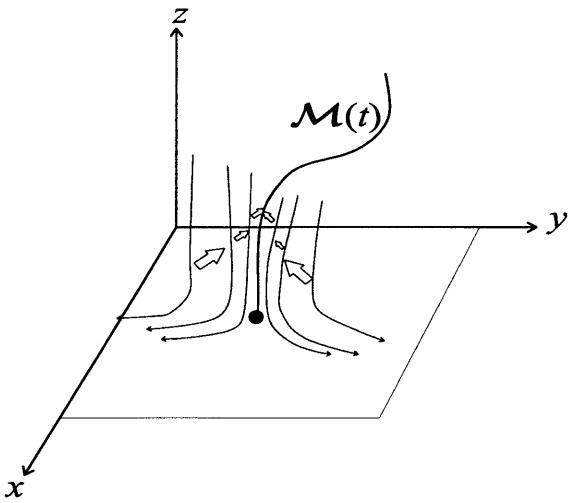

Figure 2-4: Behavior of wall-bound material lines near a reattachment profile in backward time.

Finding the shape of reattachment profiles is more difficult. The reason is that *all* material lines anchored at the reattachment point are attracted to the reattachment profile in backward time, and hence all admit bounded derivatives at $z = 0$ as $t \to -\infty$. The reattachment profile therefore only becomes a distinguished material line with bounded derivatives in the $t \to +\infty$ limit. One may, of course, take the formulae for the separation profile derivatives $\mathbf{g}_k(t)$, change the upper limit of the improper integrals from $-\infty$ to $+\infty$, and obtain formulae for reattachment profile derivatives. This approach, however, is impractical in applications where future velocity data is unavailable.

The above difficulty causes an unavoidable delay in reattachment profile calculations. Exceptions to the above computational difficulties are time-periodic velocity fields, for which formula (2.69) remains valid in the case of reattachment.

2.8 Moving separation

Moving separation points are commonly observed under varying flow conditions, such as increasing Reynolds numbers in a flow past a cylinder. Here we only discuss moving separation along a flat boundary (figure 2-5), because the results extend to general boundaries via the approach of § 2.2.8.

First, we stress that *classical invariant manifolds are inadequate for describing moving separation*: If particles are to separate from the wall along an attracting material line (a classical unstable manifold), then the point of attachment of the material line on the boundary cannot move due to the no-slip boundary condition.

The key to understanding moving separation is a recent development in dynamical systems, the concept of *finite-time invariant manifolds* (Haller & Poje 1998; Haller 2000, 2001 in 2D). A finite-time unstable manifold is a material curve that acts as an unstable manifold for a fixed

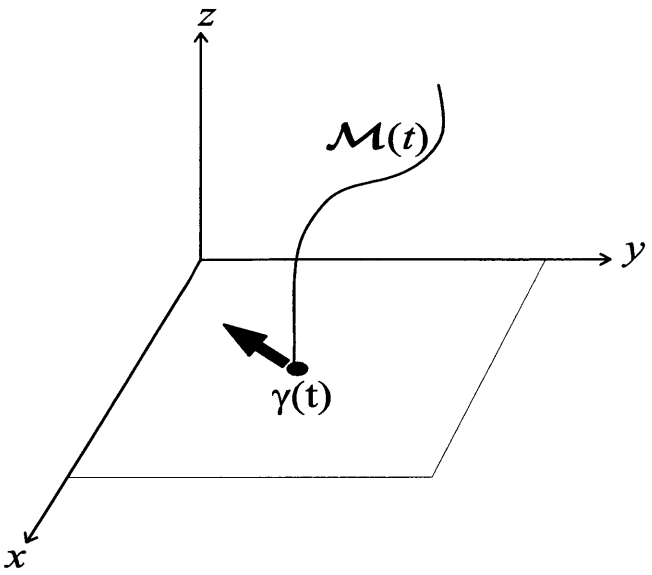

Figure 2-5: Moving separation along a no-slip boundary.

point *only* over a finite time interval $\mathcal{I}$. In more physical terms, a finite-time unstable manifold is a material line that attracts all nearby fluid particles over $\mathcal{I}$.

When a finite-time unstable manifold loses its attracting nature, another nearby material line may become attracting. Then the second material line will act as a separation profile for a while, attracting all nearby material lines, including the one that used to be the separation curve. Later, the second material line may also lose its attracting property, and give its place to a nearby third material line that has just become attracting. If this process repeats itself, one observes a sliding separation point created by attachment points of different material lines, each of which acts as a finite-time separation profile. Below we propose two algorithms to capture moving separation profiles.

2.8.1 Analytic approach

As we show in appendix A.4, moving separation in incompressible flows can be treated analytically as follows. For a present time t_0, one computes the effective separation point $\gamma_{eff}(t, t_0)$ for times $t < t_0$. Let the maximal $\mathbf{x}$ distance travelled by $\gamma_{eff}(t, t_0)$ over the interval $[t, t_0]$ be denoted by

$$\delta(t, t_0) = \max\left(\max_{t\in\mathcal{I}} \gamma_{x,eff}(t, t_0) - \min_{t\in\mathcal{I}} \gamma_{x,eff}(t, t_0), \max_{t\in\mathcal{I}} \gamma_{y,eff}(t, t_0) - \min_{t\in\mathcal{I}} \gamma_{y,eff}(t, t_0)\right).$$

We can then show the existence of a finite-time sharp separation point close to $\gamma_{eff}(t, t_0)$ if

$$\delta(t, t_0) \int_{t_0}^{t} \max_{\mathbf{x}\in I(t,t_0)} \|\mathbf{u}_{\mathbf{x}z}(\mathbf{x}, 0, \tau)\| \, d\tau < \frac{\sqrt{2}}{2}\kappa \max_{\mathbf{x}\in I(t,t_0)} \frac{\|\mathbf{u}_{zz}(t)\|}{\|\mathbf{u}_{\mathbf{x}z}(t)\|}, \tag{2.73}$$

where κ is a constant chosen a priori, *and*

$$\max_{\mathbf{x}\in I(t,t_0)} \mathrm{Tr}\, \mathbf{u}_{\mathbf{x}z}(\mathbf{x},0,t) < 0. \tag{2.74}$$

The supremum $t^*(t_0)$ of the t values satisfying the above inequalities gives a maximal admissible time scale $T_m(t_0) = t^*(t_0) - t_0$ over which all the integrals in our earlier fixed separation formulae should be evaluated to capture moving separation at time t_0.

2.8.2 Harmonics-based approach

Instead of finding a single time scale T_m for the motion of the effective separation point, one can alternatively identify several characteristic time scales from the velocity field itself. Assume that $\mathbf{v}(\mathbf{x},z,t)$ has a limited number of dominant Fourier modes, i.e., its components can be written as

$$\begin{aligned} \mathbf{u}(\mathbf{x},z,t) &= \mathbf{U}(\mathbf{x},z,\omega_1 t,\ldots,\omega_m t) + \mathbf{q}_1(\mathbf{x},z,t), \\ w(\mathbf{x},z,t) &= W(\mathbf{x},z,\omega_1 t,\ldots,\omega_m t) + q_2(\mathbf{x},z,t), \end{aligned}$$

with the terms $\mathbf{q}_1$ and q_2 being small in norm compared to $\mathbf{U}$ and W. Such a decomposition is obtained by fast-Fourier transforming the velocity components, with the result updated continuously.

If $\mathbf{q}_1$ and q_2 indeed remain small, one can view the velocity field as approximately quasi-periodic, and apply the separation criteria and separation-shape formulae derived in § 2.6.3. Specifically, one may compute the effective separation point at time t_0 from the criterion

$$\int_{t_0}^{t_0-2\pi/\omega_m} \cdots \int_{t_0}^{t_0-2\pi/\omega_1} \frac{\mathbf{U}_z(\gamma_{eff}(t_0),0,\omega_1\tau_1,\ldots,\omega_m\tau_m)}{\rho(\gamma_{eff}(t_0),0,\omega_1\tau_1,\ldots,\omega_m\tau_m)}\, d\tau_1 \ldots d\tau_m = 0,$$

following the results of § 2.6.3. Applying the same multi-phase averaging used in our earlier separation formulae will yield quasiperiodic separation profiles that approximate the true separation profile.

2.9 Conclusions

We have described a kinematic theory of three-dimensional unsteady separation that links the formation of a material spike near a no-slip boundary to the existence of an unstable manifold for a distinguished point on the boundary. This theory is frame-independent, and only assumes regularity and mass conservation along the boundary. In particular, the velocity field does not have to solve the boundary-layer equations or the Navier-Stokes equations: it can be an arbitrary numerical, experimental, or model field.

The existence of a wall-bound unstable manifold (separation profile) is guaranteed by Haller (2002) in the two-dimensional case. Here we have extended these criteria in the same mathematically rigorous fashion to three-dimensional, covering separation and reattachment on fixed boundaries. We have also given an algorithm for computing the shape of the unstable manifold via a Taylor expansion. This expansion becomes simpler for incompressible flows, for which we

have obtained a cubic approximation of the separation profile.

While they reveal a frame-independent Lagrangian separation phenomenon, our criteria are fully Eulerian and hence do not require the advection of particles. In addition, the criteria only use quantities computed from distributed pressure and skin-friction measurements along the wall (cf. § 2.4). These features make our kinematic separation theory useful in active flow control problems.

Being purely kinematic, our analysis does not distinguish between laminar and turbulent separation. All criteria we have derived involve time averages of Eulerian quantities on the boundary, and hence are–in principle–computable for turbulent flows. Further work is needed, however, to assess the computational difficulties for turbulent separation.

There are still some open questions about three-dimensional separation that we will discuss in chapter 4.

Chapter 3

Three-dimensional analytical models for unsteady separation

3.1 Introduction

In this chapter, we test the unsteady separation and reattachment formulae of chapter 2 on different types of steady and unsteady flows, derived by a method proposed by Perry & Chong (1986).

This method provides a low-order approximation to particular incompressible separating solutions of the Navier-Stokes equations. Using different patterns of separation, we build models of a wide range of closed-separating flows. These flow models allow a detailed comparison between our theory explained in chapter 2 and actual flow separation displayed by fluid particles. Some of the flows will be steady, others time-periodic.

We will also explain how one can deduct compressible flow expansions from incompressible ones, and build a final flow model that we will analyze under quasiperiodic conditions.

The organization of this chapter is as follows. We first recall the method developed by Perry & Chong to derive flow expansions in § 3.2. We present some characteristic steady models of closed separation in § 3.3. Then we develop and analyze a bubble model in § 3.4, which will experience steady and periodic conditions. We develop a compressible bubble flow in § 3.5, with quasiperiodic conditions, and an aperiodic model in § 3.6. We finally present our conclusions in § 3.7.

3.2 Flow expansion

3.2.1 Velocity field

We fix the origin of the (x_1, x_2, x_3) coordinate system on the $x_3 = 0$ boundary of the flow. The velocity vector $\mathbf{u}(\mathbf{x}, t)$, $\mathbf{x} \equiv \begin{pmatrix} x_1 \\ x_2 \\ x_3 \end{pmatrix} \in \mathbb{R}^2 \times \mathbb{R}^+$, $\mathbf{u} \equiv \begin{pmatrix} u_1 \\ u_2 \\ u_3 \end{pmatrix} \in \mathbb{R}^3$, is sought in the form of an

asymptotic third-order expansion at the origin

$$u_i = A_i + \sum_{j=1}^{3} A_{ij}x_j + \sum_{j,k=1}^{3} A_{ijk}x_j x_k + \sum_{j,k,l=1}^{3} A_{ijkl}x_j x_k x_l + O(4), \tag{3.1}$$

where $O(4)$ represents a homogeneous polynomial of degree $n \geq 4$. The i, j, k, l indices vary from 1 to 3. The vector A_i and the symmetric (in all indices except the first one) tensors A_{ij}, ... depend on time when the flow is unsteady. The number of independent coefficients in (3.1) depends on the order at which we truncate the expansion: For a third-order expansion, we have sixty independent coefficients.

The basic idea of the Perry-Chong procedure is to force the tensor coefficients A_{ij}, ... to satisfy the continuity equation and the boundary conditions. Then we substitute the velocity field into the Navier-Stokes equations to express the pressure gradient, whose regularity gives additional differential equations for the coefficients. Finally, we select the remaining coefficients depending on the type of separation we want to observe.

3.2.2 Equations

Continuity equation

We substitute (3.1) into the continuity equation for incompressible flows

$$\sum_{i=1}^{3} \frac{\partial u_i}{\partial x_i} = 0, \tag{3.2}$$

which yields ten equations for the third-order expansion:

$$\sum_{j=1}^{3} A_{jj} = 0, \tag{3.3}$$

$$2A_{iii} + \sum_{j \neq i} A_{jji} = 0, \tag{3.4}$$

$$3A_{iiii} + \sum_{j \neq i} A_{jjii} = 0, \tag{3.5}$$

$$A_{iikl} + 2A_{kkkl} + 2A_{lllk} = 0, \tag{3.6}$$

where $i = 1, 2, 3$, and $i \neq k \neq l$.

Boundary conditions

We define a no-slip boundary condition at the wall

$$u_i(x_1, x_2, 0, t) = 0, \tag{3.7}$$

where $i = 1, 2, 3$. Substituting (3.1) into (3.7), we obtain thirty equations for the coefficients:

$$\begin{aligned} A_i &= 0, && (3.8)\\ A_{i1} &= A_{i2} = 0, && (3.9)\\ A_{i11} &= A_{i12} = A_{i22} = 0, && (3.10)\\ A_{i111} &= A_{i112} = A_{i122} = A_{i222} = 0, && (3.11) \end{aligned}$$

for all i.

Navier-Stokes equations

The Navier-Stokes equations for incompressible, constant-density flow can be written as

$$\frac{\partial u_i}{\partial t} + \sum_{q=1}^{3} u_q \frac{\partial u_i}{\partial x_q} = -\frac{\partial P}{\partial x_i} + \nu \sum_{q=1}^{3} \frac{\partial^2 u_i}{\partial x_q^2}, \tag{3.12}$$

where $i = 1, 2, 3$, $P = p/\rho$ is the kinematic pressure, p is the pressure, ρ is the fluid density, ν is the kinematic viscosity.

Substituting (3.1) into (3.12) and grouping terms of the same order, we determine P_r, the r^{th} derivative of the pressure at the origin. Considering a third-order expansion of the velocity field, we can only determine the gradient of the pressure at first order.

Our expansion has sixty unknowns, and we have forty linear independent equations for the coefficients. By combining all the equations except the Navier-Stokes, there remain only a few undetermined coefficients:

$$\begin{aligned} &A_{13}, A_{23},\\ &A_{113}, A_{213}, A_{123}, A_{223}, A_{313}, A_{323},\\ &A_{1133}, A_{2133}, A_{1123}, A_{2123}, A_{1223}, A_{2223}, A_{1133}, A_{2133}, A_{1233}, A_{2233}, A_{1333}, A_{2333}, \end{aligned}$$

and four equations

$$\begin{aligned} A_{333} &= -\frac{A_{113} + A_{223}}{2},\\ A_{3133} &= -\frac{2A_{1113} + A_{2123}}{2},\\ A_{3233} &= -\frac{2A_{2223} + A_{1123}}{2},\\ A_{3333} &= -\frac{A_{1133} + A_{2233}}{3}. \end{aligned}$$

All other coefficients in the expansion vanish.

Thus our velocity field becomes

$$\begin{aligned}
u_1 &= A_{13}x_3 + A_{113}x_1x_3 + A_{123}x_2x_3 + A_{1123}x_1x_2x_3 \\
&\quad + x_3^2(A_{133} + A_{1133}x_1 + A_{1233}x_2 + A_{1333}x_3), \\
u_2 &= A_{23}x_3 + A_{213}x_1x_3 + A_{223}x_2x_3 + A_{2123}x_1x_2x_3 \\
&\quad + x_3^2(A_{233} + A_{2133}x_1 + A_{2233}x_2 + A_{2333}x_3), \\
u_3 &= A_{313}x_1x_3 + A_{323}x_2x_3 \\
&\quad - x_3^2\left(\frac{A_{113} + A_{223}}{2} + \frac{2A_{1113} + A_{2123}}{2}x_1 + \frac{2A_{2223} + A_{1123}}{2}x_2 + \frac{A_{1133} + A_{2233}}{3}x_3\right).
\end{aligned} \tag{3.13}$$

Substitution of (3.13) into (3.12) gives the pressure gradient at first order:

$$\begin{aligned}
\frac{\partial P}{\partial x_1} &= -\dot{A}_{13}x_3 + \nu[2A_{133} + 2A_{1133}x_1 + 2A_{1233}x_2 + 6A_{1333}x_3], \\
\frac{\partial P}{\partial x_2} &= -\dot{A}_{23}x_3 + \nu[2A_{233} + 2A_{2133}x_1 + 2A_{2233}x_2 + 6A_{2333}x_3], \\
\frac{\partial P}{\partial x_3} &= -\nu\left[A_{113} + A_{223} + (2A_{1113} + A_{2123})x_1 + (2A_{2223} + A_{1123})x_2\right. \\
&\quad \left. + 2\left(A_{1133} + A_{2233}\right)x_3\right].
\end{aligned} \tag{3.14}$$

By equating the cross-derivative terms of P at the origin, we obtain:

$$\begin{aligned}
\frac{\partial}{\partial x_2}\frac{\partial P}{\partial x_1}(0,0,0) = 2\nu A_{1233} &= \frac{\partial}{\partial x_1}\frac{\partial P}{\partial x_2}(0,0,0) = 2\nu A_{2133}, \\
\frac{\partial^2 P}{\partial x_1 \partial x_3} &= -\dot{A}_{13} + 6\nu A_{1333} = -\nu(2A_{1113} + A_{2123}), \\
\frac{\partial^2 P}{\partial x_2 \partial x_3} &= -\dot{A}_{23} + 6\nu A_{2333} = -\nu(2A_{2223} + A_{1123}),
\end{aligned}$$

which implies:

$$A_{1233} = A_{2133}, \tag{3.15}$$

$$\dot{A}_{13} = \nu(6A_{1333} + 2A_{1113} + A_{2123}), \tag{3.16}$$

$$\dot{A}_{23} = \nu(6A_{2333} + 2A_{2223} + A_{1123}). \tag{3.17}$$

Separation pattern

Some of the coefficients (twelve for the third-order expansion) will be determined by the topological constraints of the separation pattern. The remaining coefficients are free parameters.

Separation profile

Using the theory developed in chapter 2, we shall locate the separation point γ, write down the conditions that the flow has to satisfy at separation, and then derive a second-order approxi-

mation for the separation profile at a time instant t_0 in the form

$$\begin{pmatrix} x_1 \\ x_2 \end{pmatrix} = \gamma + x_3 \mathbf{g}_0(t_0) + x_3^2 \mathbf{g}_1(t_0) + O(x_3^3), \tag{3.18}$$

where $\mathbf{g}_0(t_0)$ and $\mathbf{g}_1(t_0)$ are two-dimensional vectors.

3.3 Separation with linear skin friction field

We first specify the normal derivative of the velocity at the wall to vary according to the equation

$$\begin{pmatrix} \frac{\partial u_1}{\partial x_3} \\ \frac{\partial u_2}{\partial x_3} \end{pmatrix} = \mathbf{K} \begin{pmatrix} x_1 \\ x_2 \end{pmatrix} + \mathbf{F}, \tag{3.19}$$

with

$$\mathbf{K} = \begin{pmatrix} k_{11}(t) & k_{12}(t) \\ k_{21}(t) & k_{22}(t) \end{pmatrix},$$
$$\mathbf{F} = \begin{pmatrix} f_1(t) \\ f_2(t) \end{pmatrix}.$$

Changing the matrix $\mathbf{K}$, we can generate different patterns of separation: saddle-sink, saddle-saddle, or saddle-focus. For instance, $\mathbf{K} = K\mathbf{I}$ generates a single point of zero shear stress at the origin. The skin friction field admits a sink or a source in the x_1-x_2 plane, as shown in figure 3-1.

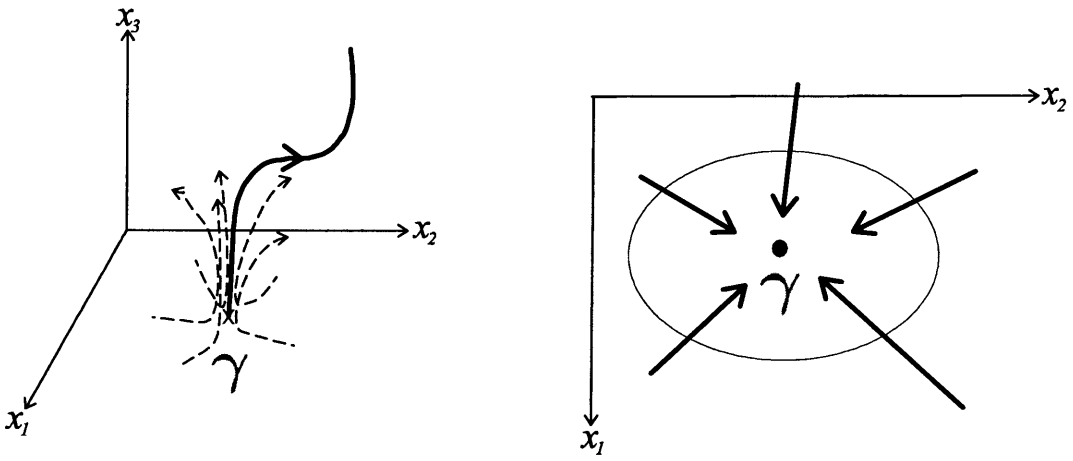

Figure 3-1: Flow emanating from a sink.

Substituting (3.1) into (3.19) yields twelve equations at the third order, with the new para-

meters defined by the components of $\mathbf{K}$ and $\mathbf{F}$:

$$\begin{gathered} A_{13} = f_1, \quad A_{23} = f_2, \\ A_{113} = k_{11}, \quad A_{223} = k_{22}, \\ A_{123} = k_{12}, \quad A_{213} = k_{21}, \\ A_{1113} = A_{1123} = A_{1223} = A_{2113} = A_{2123} = A_{2223} = 0. \end{gathered}$$

With all the previous equations, the velocity field simplifies to

$$\boxed{\begin{aligned} u_1 &= f_1 x_3 + k_{11} x_1 x_3 + k_{12} x_2 x_3 + x_3^2(\alpha + A_{1133} x_1 + A_{1233} x_2 + \frac{\dot{f}_1}{6\nu} x_3), \\ u_2 &= f_2 x_3 + k_{21} x_1 x_3 + k_{22} x_2 x_3 + x_3^2(\beta + A_{1233} x_1 + A_{2233} x_2 + \frac{f_2}{6\nu} x_3), \\ u_3 &= -\frac{k_{11} + k_{22}}{2} x_3^2 - \frac{A_{1133} + A_{2233}}{3} x_3^3, \end{aligned}} \tag{3.20}$$

with still nine unknown coefficients. These coefficients determine the shape of separation we wish to study in our model. The coefficients $\alpha = A_{133}$ and $\beta = A_{233}$ will determine the direction of separation.

3.3.1 Analysis of the separation pattern

To simplify our notation, we define $\mathbf{x} = \begin{pmatrix} x_1 \\ x_2 \end{pmatrix}$, $z = x_3$, $\mathbf{u} = \begin{pmatrix} u_1 \\ u_2 \end{pmatrix}$, $w = u_3$. A separation point will be denoted by $\boldsymbol{\gamma} = \begin{pmatrix} \gamma_1 \\ \gamma_2 \end{pmatrix}$.

The velocity field (3.20) admits only one point of zero skin friction on the x_1-x_2 wall, $\begin{pmatrix} x_1 \\ x_2 \end{pmatrix} = -\mathbf{K}^{-1}\mathbf{F}$. Thus we expect only one separation point for this flow. A necessary condition for separation at $\boldsymbol{\gamma}$ is

$$\limsup_{t \to -\infty} \left| \int_{t_0}^{t} \mathbf{u}_z(\boldsymbol{\gamma}, 0, s)\, ds \right| < \infty$$

in the incompressible case, as shown in (2.43). In our current setting, this condition takes the form

$$\limsup_{t \to -\infty} \left| \int_{t_0}^{t} \mathbf{F}(s)\, ds + \left(\int_{t_0}^{t} \mathbf{K}(s)\, ds \right) \boldsymbol{\gamma} \right| < \infty. \tag{3.21}$$

The second condition for incompressible separation is given by (2.44) or

$$\lim_{t \to -\infty} \left\| \int_{t_0}^{t} \left[\mathbf{u}_{\mathbf{x}z}(\boldsymbol{\gamma}, 0, s) + \frac{1}{2} \mathbf{I} \operatorname{Tr} \mathbf{u}_{\mathbf{x}z}(\boldsymbol{\gamma}, 0, s) \right] ds \right\| = \infty$$

in the general case, and it simplifies here to

$$\lim_{t \to -\infty} \left\| \int_{t_0}^{t} \left[\mathbf{K} + \frac{1}{2} \mathbf{I} \operatorname{Tr}(\mathbf{K}) \right] (s)\, ds \right\| = \infty. \tag{3.22}$$

By (2.47), the separation slope satisfies

$$\begin{aligned}\mathbf{g}_0(t_0) &= -\lim_{t\to-\infty}\left[\int_{t_0}^{t}\left(\mathbf{u}_{\mathbf{x}z}(\boldsymbol{\gamma},0,s)+\frac{1}{2}\mathbf{I}\,\mathrm{Tr}\,\mathbf{u}_{\mathbf{x}z}(\boldsymbol{\gamma},0,s)\right)\,ds\right]^{-1}\\ &\times\int_{t_0}^{t}\left[\frac{1}{2}\mathbf{u}_{zz}(\boldsymbol{\gamma},0,s)+\frac{1}{2}\left(\mathbf{u}_{\mathbf{x}z}(\boldsymbol{\gamma},0,s)+\frac{1}{2}\mathbf{I}\,\mathrm{Tr}\,\mathbf{u}_{\mathbf{x}z}(\boldsymbol{\gamma},0,s)\right)\int_{t_0}^{s}\mathbf{u}_z(\boldsymbol{\gamma},0,r)\,dr\right]ds,\end{aligned}$$

which simplifies for our velocity field to

$$\begin{aligned}\mathbf{g}_0(t_0) = &-\lim_{t\to-\infty}\left[\int_{t_0}^{t}\begin{pmatrix}\frac{3k_{11}+k_{22}}{2} & k_{12}\\ k_{21} & \frac{k_{11}+3k_{22}}{2}\end{pmatrix}(\tau)\,d\tau\right]^{-1}\\ &\times\int_{t_0}^{t}\left[\begin{pmatrix}\alpha\\ \beta\end{pmatrix}+\begin{pmatrix}A_{1133} & A_{1233}\\ A_{1233} & A_{2233}\end{pmatrix}\boldsymbol{\gamma}\right.\\ &\left.+\begin{pmatrix}\frac{3k_{11}+k_{22}}{2} & k_{12}\\ k_{21} & \frac{k_{11}+3k_{22}}{2}\end{pmatrix}\int_{t_0}^{s}\left(\mathbf{F}(r)+\mathbf{K}(r)\boldsymbol{\gamma}\right)\,dr\right](s)\,ds.\end{aligned}\tag{3.23}$$

Analyzing the next order of separation

$$\begin{aligned}\mathbf{g}_1(t_0) &= -\lim_{t\to-\infty}\left[2\int_{t_0}^{t}\left(\mathbf{u}_{\mathbf{x}z}(\boldsymbol{\gamma},0,s)+\mathbf{I}\,\mathrm{Tr}\,\mathbf{u}_{\mathbf{x}z}(\boldsymbol{\gamma},0,s)\right)\,ds\right]^{-1}\\ &\times\int_{t_0}^{t}\left[\frac{1}{3}\mathbf{u}_{zz}(\boldsymbol{\gamma},0,s)+\left(\mathbf{u}_{\mathbf{x}zz}(\boldsymbol{\gamma},0,s)+\frac{1}{3}\mathbf{I}\,\mathrm{Tr}\,\mathbf{u}_{\mathbf{x}zz}(\boldsymbol{\gamma},0,s)\right)\mathbf{g}_0(\tau)\right.\\ &+\left[\left[\mathbf{u}_{\mathbf{x}\mathbf{x}z}(\boldsymbol{\gamma},0,s)+\left(\mathrm{Tr}\,\mathbf{u}_{\mathbf{x}z}\right)_{\mathbf{x}}(\boldsymbol{\gamma},0,s)\cdot\mathbf{I}\right]\mathbf{g}_0\right]\mathbf{g}_0\\ &+2\left(\mathbf{u}_{\mathbf{x}z}(\boldsymbol{\gamma},0,s)+\mathbf{I}\,\mathrm{Tr}\,\mathbf{u}_{\mathbf{x}z}(\boldsymbol{\gamma},0,s)\right)\\ &\left.\times\int_{t_0}^{s}\left[\frac{1}{2}\mathbf{u}_{zz}(\boldsymbol{\gamma},0,r)+\left(\mathbf{u}_{\mathbf{x}z}(\boldsymbol{\gamma},0,r)+\frac{1}{2}\mathbf{I}\,\mathrm{Tr}\,\mathbf{u}_{\mathbf{x}z}(\boldsymbol{\gamma},0,r)\right)\mathbf{g}_0(r)\right]\,dr\right]\,ds,\end{aligned}$$

we find that:

$$\begin{aligned}\mathbf{g}_1(t_0) &= -\lim_{t\to-\infty}\left[2\int_{t_0}^{t}\left(\mathbf{K}+\mathbf{I}\,\mathrm{Tr}\,\mathbf{K}\right)(\tau)d\tau\right]^{-1}\\ &\times\int_{t_0}^{t}\left(\frac{\dot{\mathbf{F}}}{3\nu}+2\begin{pmatrix}\frac{4A_{1133}+A_{2233}}{3} & A_{1233}\\ A_{1233} & \frac{A_{1133}+4A_{2233}}{3}\end{pmatrix}\mathbf{g}_0+2\begin{pmatrix}2k_{11}+k_{22} & k_{12}\\ k_{21} & k_{11}+2k_{22}\end{pmatrix}\right.\\ &\left.\times\int_{t_0}^{s}\left[\begin{pmatrix}\alpha\\ \beta\end{pmatrix}+\begin{pmatrix}A_{1133} & A_{1233}\\ A_{1233} & A_{2233}\end{pmatrix}\boldsymbol{\gamma}+\begin{pmatrix}\frac{3k_{11}+k_{22}}{2} & k_{12}\\ k_{21} & \frac{k_{11}+3k_{22}}{2}\end{pmatrix}\mathbf{g}_0\right](r)\,dr\right](s)\,ds.\end{aligned}\tag{3.24}$$

To find more details on the tensor term

$$\left[\left[\mathbf{u}_{\mathbf{x}\mathbf{x}z}(\boldsymbol{\gamma},0,s)+\left(\mathrm{Tr}\,\mathbf{u}_{\mathbf{x}z}\right)_{\mathbf{X}}(\boldsymbol{\gamma},0,s)\cdot\mathbf{I}\right]\mathbf{g}_0\right]\mathbf{g}_0,\tag{3.25}$$

the reader may refer to appendix B.1.

3.3.2 Examples

Steady separation

When the flow is steady, the point of zero skin friction is $\boldsymbol{\gamma} = -\mathbf{K}^{-1}\mathbf{F}$ for all times, and we deduce from our criterion that this point is the actual separation point.

The second condition for separation (3.22) at $\boldsymbol{\gamma}$ is then $\mathbf{K}+\frac{1}{2}\mathbf{I}\,\mathrm{Tr}\,(\mathbf{K}) \neq \mathbf{0}$, which is equivalent to

$$\mathbf{K} \neq \mathbf{0}. \tag{3.26}$$

The separation slope (3.23) becomes

$$\mathrm{g}_0 = -\begin{pmatrix} \frac{3k_{11}+k_{22}}{2} & k_{12} \\ k_{21} & \frac{k_{11}+3k_{22}}{2} \end{pmatrix}^{-1} \left[\begin{pmatrix} \alpha \\ \beta \end{pmatrix} + \begin{pmatrix} A_{1133} & A_{1233} \\ A_{1233} & A_{2233} \end{pmatrix} \boldsymbol{\gamma} \right]. \tag{3.27}$$

Finally, we obtain from formula (3.24) the curvature of the separation profile:

$$\begin{aligned} \mathrm{g}_1 \;=\; & \begin{pmatrix} 2k_{11}+k_{22} & k_{12} \\ k_{21} & k_{11}+2k_{22} \end{pmatrix}^{-1} \begin{pmatrix} \frac{4A_{1133}+A_{2233}}{3} & A_{1233} \\ A_{1233} & \frac{A_{1133}+4A_{2233}}{3} \end{pmatrix} \\ & \times \begin{pmatrix} \frac{3k_{11}+k_{22}}{2} & k_{12} \\ k_{21} & \frac{k_{11}+3k_{22}}{2} \end{pmatrix}^{-1} \left[\begin{pmatrix} \alpha \\ \beta \end{pmatrix} + \begin{pmatrix} A_{1133} & A_{1233} \\ A_{1233} & A_{2233} \end{pmatrix} \boldsymbol{\gamma} \right]. \end{aligned} \tag{3.28}$$

We conclude from our analysis that these steady separation patterns depend on the eigenvalues of $\mathbf{K}$, and we differentiate three cases which were physically observed:

-a saddle-sink: $\mathbf{K}$ has two negative eigenvalues of different magnitude (the case of two positive eigenvalues corresponds to reattachment, and cannot exist in our model because we assumed the flow incompressible),

-a saddle-saddle: $\mathbf{K}$ has a positive and a negative eigenvalue,

-a saddle-focus (or tornado): $\mathbf{K}$ has a complex pair of eigenvalues with negative real parts.

Saddle-sink type steady separation

General case In the steady case and in the base of the eigenvectors of $\mathbf{K}$, we can write the matrix $\mathbf{K} = -\begin{pmatrix} \lambda_1 & 0 \\ 0 & \lambda_2 \end{pmatrix}$ with $\lambda_1, \lambda_2 > 0$. In that case, the separation point $\boldsymbol{\gamma}$ satisfies

$$\boldsymbol{\gamma} = \begin{pmatrix} f_1/\lambda_1 \\ f_2/\lambda_2 \end{pmatrix}. \tag{3.29}$$

Then we deduce the slope of the separation profile

$$\mathrm{g}_0 = \begin{pmatrix} \frac{2}{3\lambda_1+\lambda_2} & 0 \\ 0 & \frac{2}{\lambda_1+3\lambda_2} \end{pmatrix} \left[\begin{pmatrix} \alpha \\ \beta \end{pmatrix} + \begin{pmatrix} A_{1133} & A_{1233} \\ A_{1233} & A_{2233} \end{pmatrix} \begin{pmatrix} f_1/\lambda_1 \\ f_2/\lambda_2 \end{pmatrix} \right], \tag{3.30}$$

and the curvature of separation

$$\mathbf{g}_1 = 2\begin{pmatrix} \frac{1}{2\lambda_1+\lambda_2} & 0 \\ 0 & \frac{1}{\lambda_1+2\lambda_2} \end{pmatrix}\begin{pmatrix} \frac{4A_{1133}+A_{2233}}{3} & A_{1233} \\ A_{1233} & \frac{A_{1133}+4A_{2233}}{3} \end{pmatrix} \times \begin{pmatrix} \frac{2}{3\lambda_1+\lambda_2} & k_{12} \\ k_{21} & \frac{2}{\lambda_1+3\lambda_2} \end{pmatrix}\left[\begin{pmatrix} \alpha \\ \beta \end{pmatrix} + \begin{pmatrix} A_{1133} & A_{1233} \\ A_{1233} & A_{2233} \end{pmatrix}\begin{pmatrix} f_1/\lambda_1 \\ f_2/\lambda_2 \end{pmatrix}\right]. \quad (3.31)$$

Analysis of saddle-sink type steady separation Let us consider a steady saddle-sink with $\lambda_1 = 1$, $\lambda_2 = 2$, $\mathbf{F} = \mathbf{0}$, $A_{1233} = 0$, and $A_{1133} = A_{2233} = \delta > 0$. Then the steady flow model (3.20) simplifies to

$$\begin{aligned} u_1 &= -x_1x_3 + (\alpha + \delta x_1)x_3^2, \\ u_2 &= -2x_2x_3 + (\beta + \delta x_2)x_3^2, \\ u_3 &= \frac{3}{2}x_3^2 - \frac{2\delta}{3}x_3^3. \end{aligned} \quad (3.32)$$

For this particular flow, we obtain $\mathbf{g}_0 = 2\begin{pmatrix} \alpha/5 \\ \beta/7 \end{pmatrix}$ and $\mathbf{g}_1 = \frac{4\delta}{3}\begin{pmatrix} \alpha/4 \\ \beta/7 \end{pmatrix}$; trajectories emanating from a vicinity of the separation point follow the separation profile

$$\begin{pmatrix} x_1 \\ x_2 \end{pmatrix} = 2x_3\begin{pmatrix} \frac{1}{5} + \frac{\delta}{6}x_3 & 0 \\ 0 & \frac{1}{7} + \frac{2\delta}{21}x_3 \end{pmatrix}\begin{pmatrix} \alpha \\ \beta \end{pmatrix} + O(x_3^3). \quad (3.33)$$

By releasing particles near the separation point, we verify formula (3.33) in figure 3-2.

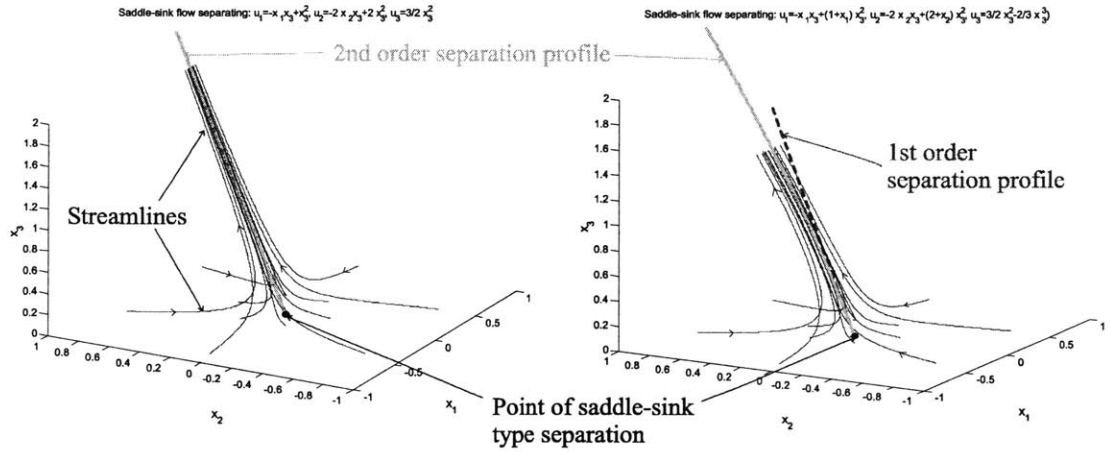

Figure 3-2: Predicted and real saddle-sink separation profiles.

In the steady case, the motion of the particles is given by the streamlines, and we see in the two cases of figure 3-2 that the particles are attracted to a single line, the separation profile,

which is well approximated by our first and second order computations.

The left image shows the case of $\delta = 0$, in which case the flow is simple and the slope is sufficient to approximate the separation profile. The right image shows the case of $\delta = 1$, in which case the curvature of the separation profile is also needed to obtain the shape of separation.

Saddle-saddle type steady separation

General case In the eigenbasis of $\mathbf{K}$, we have $\mathbf{K} = -\begin{pmatrix} \lambda_1 & 0 \\ 0 & -\lambda_2 \end{pmatrix}$ with $\lambda_1, \lambda_2 > 0$. Then the separation point $\boldsymbol{\gamma}$ satisfies

$$\boldsymbol{\gamma} = \begin{pmatrix} f_1/\lambda_1 \\ -f_2/\lambda_2 \end{pmatrix}. \tag{3.34}$$

If $\lambda_2 \neq 3\lambda_1$ and $\lambda_2 \neq \lambda_1/3$, we deduce the slope of the separation profile

$$\mathbf{g}_0 = \begin{pmatrix} \frac{2}{3\lambda_1-\lambda_2} & 0 \\ 0 & \frac{2}{\lambda_1-3\lambda_2} \end{pmatrix} \left[\begin{pmatrix} \alpha \\ \beta \end{pmatrix} + \begin{pmatrix} A_{1133} & A_{1233} \\ A_{1233} & A_{2233} \end{pmatrix} \begin{pmatrix} f_1/\lambda_1 \\ -f_2/\lambda_2 \end{pmatrix} \right], \tag{3.35}$$

and the following order provided that $\lambda_2 \neq 2\lambda_1$ and $\lambda_2 \neq \lambda_1/2$:

$$\begin{aligned} \mathbf{g}_1 \;=\; & 2 \begin{pmatrix} \frac{1}{2\lambda_1-\lambda_2} & 0 \\ 0 & \frac{1}{\lambda_1-2\lambda_2} \end{pmatrix} \begin{pmatrix} \frac{4A_{1133}+A_{2233}}{3} & A_{1233} \\ A_{1233} & \frac{A_{1133}+4A_{2233}}{3} \end{pmatrix} \\ & \times \begin{pmatrix} \frac{2}{3\lambda_1-\lambda_2} & k_{12} \\ k_{21} & \frac{2}{\lambda_1-3\lambda_2} \end{pmatrix} \left[\begin{pmatrix} \alpha \\ \beta \end{pmatrix} + \begin{pmatrix} A_{1133} & A_{1233} \\ A_{1233} & A_{2233} \end{pmatrix} \begin{pmatrix} f_1/\lambda_1 \\ -f_2/\lambda_2 \end{pmatrix} \right]. \end{aligned} \tag{3.36}$$

Analysis of a saddle-saddle type steady separation Let us consider a saddle-saddle with $\lambda_1 = 4$, $\lambda_2 = 1$, $\mathbf{F} = \mathbf{0}$, $A_{1233} = 0$, and $A_{1133} = A_{2233} = \delta < 0$: under these conditions, the model velocity field (3.20) takes the form

$$\begin{aligned} u_1 &= -4x_1x_3 + (\alpha + \delta x_1)x_3^2, \\ u_2 &= x_2x_3 + (\beta + \delta x_2)x_3^2, \\ u_3 &= \frac{3}{2}x_3^2 - \frac{2\delta}{3}x_3^3. \end{aligned} \tag{3.37}$$

For this particular flow, we obtain $\mathbf{g}_0 = 2\begin{pmatrix} \alpha/11 \\ \beta \end{pmatrix}$ and $\mathbf{g}_1 = \frac{10\delta}{3}\begin{pmatrix} 2\alpha/77 \\ \beta \end{pmatrix}$, with the corresponding separation profile

$$\begin{pmatrix} x_1 \\ x_2 \end{pmatrix} = x_3 \begin{pmatrix} \frac{2}{11} + \frac{20\delta}{231}x_3 & 0 \\ 0 & 2 + \frac{10\delta}{3}x_3 \end{pmatrix} \begin{pmatrix} \alpha \\ \beta \end{pmatrix} + O(x_3^3). \tag{3.38}$$

Following the particles near the separation point, we shall check the validity of formula (3.38). For instance, the computation shown in figure 3-3 demonstrates the accuracy of the predicted profile. We observe that the unstable manifold of the separation point divides the plane of separation $x_3 = 0$, and the particles on each side converge to a separation surface whose intersection with $x_3 = 0$ is defined by the stable manifold of the saddle.

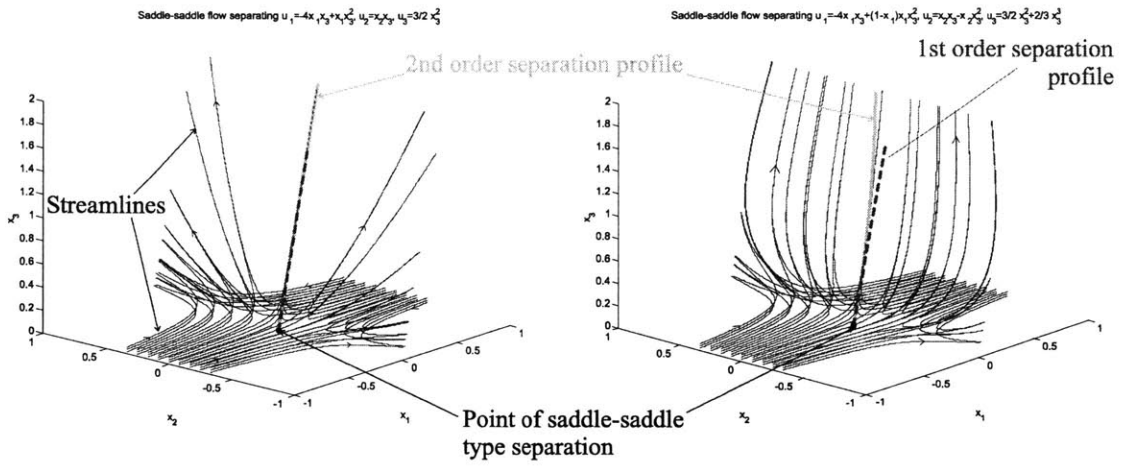

Figure 3-3: Approximate and real separation for the saddle-saddle type separation.

The left image in figure 3-3 shows the case of $\delta = 0$, the right image shows the case of $\delta = -1$, where again the curvature of the separation profile is needed to obtain a good estimate for the shape of separation.

Saddle-focus type steady separation

General case In the eigenbasis of $\mathbf{K}$, we have $\mathbf{K} = -\lambda \begin{pmatrix} \cos\theta & -\sin\theta \\ \sin\theta & \cos\theta \end{pmatrix}$ with $\lambda > 0$ and $\theta \in [-\pi/2; \pi/2] \setminus \{0\}$. In that case, the separation point $\boldsymbol{\gamma}$ satisfies

$$\boldsymbol{\gamma} = \frac{1}{\lambda} \begin{pmatrix} \cos\theta & \sin\theta \\ -\sin\theta & \cos\theta \end{pmatrix} \begin{pmatrix} f_1 \\ f_2 \end{pmatrix}. \tag{3.39}$$

Then we deduce the slope of the separation profile

$$\mathbf{g}_0 = \frac{1}{\lambda} \begin{pmatrix} 2\cos\theta & -\sin\theta \\ \sin\theta & 2\cos\theta \end{pmatrix}^{-1} \left[\begin{pmatrix} \alpha \\ \beta \end{pmatrix} + \begin{pmatrix} A_{1133} & A_{1233} \\ A_{1233} & A_{2233} \end{pmatrix} \boldsymbol{\gamma} \right], \tag{3.40}$$

and the curvature of the profile

$$\begin{aligned} \mathbf{g}_1 \;=\; & \frac{1}{\lambda^2} \begin{pmatrix} 3\cos\theta & -\sin\theta \\ \sin\theta & 3\cos\theta \end{pmatrix}^{-1} \begin{pmatrix} \frac{4A_{1133}+A_{2233}}{3} & A_{1233} \\ A_{1233} & \frac{A_{1133}+4A_{2233}}{3} \end{pmatrix} \\ & \times \begin{pmatrix} 2\cos\theta & -\sin\theta \\ \sin\theta & 2\cos\theta \end{pmatrix}^{-1} \left[\begin{pmatrix} \alpha \\ \beta \end{pmatrix} + \begin{pmatrix} A_{1133} & A_{1233} \\ A_{1233} & A_{2233} \end{pmatrix} \boldsymbol{\gamma} \right]. \end{aligned} \tag{3.41}$$

Analysis of a simple case of saddle-focus Let us consider the steady saddle-focus flow such as $\lambda = \sqrt{2}$ and $\theta = \frac{\pi}{4}$: Thus $\mathbf{K} = -\begin{pmatrix} 1 & -1 \\ 1 & 1 \end{pmatrix}$, and we choose again $\mathbf{F} = \mathbf{0}$, $A_{1233} = 0$, and $A_{1133} = A_{2233} = \delta < 0$. Under these conditions, the model velocity field (3.20) takes the form

$$\begin{aligned} u_1 &= -x_1x_3 + x_2x_3 + (\alpha + \delta x_1)x_3^2, \\ u_2 &= -x_1x_3 - x_2x_3 + (\beta + \delta x_2)x_3^2, \\ u_3 &= x_3^2 - \frac{2\delta}{3}x_3^3. \end{aligned} \tag{3.42}$$

For this particular flow, we obtain $\mathbf{g}_0(t_0) = \frac{1}{5}\begin{pmatrix} 2 & 1 \\ -1 & 2 \end{pmatrix}\begin{pmatrix} \alpha \\ \beta \end{pmatrix}$ and $\mathbf{g}_1 = \frac{\delta}{6}\begin{pmatrix} 1 & 1 \\ -1 & 1 \end{pmatrix}\begin{pmatrix} \alpha \\ \beta \end{pmatrix}$; trajectories emanating from a vicinity of the separation point follow the separation profile

$$\begin{pmatrix} x_1 \\ x_2 \end{pmatrix} = x_3 \begin{pmatrix} \frac{2}{5} + x_3\frac{\delta}{6} & \frac{1}{5} + x_3\frac{\delta}{6} \\ -\frac{1}{5} - x_3\frac{\delta}{6} & \frac{2}{5} + x_3\frac{\delta}{6} \end{pmatrix} \begin{pmatrix} \alpha \\ \beta \end{pmatrix} + O(x_3^3). \tag{3.43}$$

By comparing streamlines of this flow and the predicted separation profile at first and second order, we validate formula (3.43) in figure 3-4.

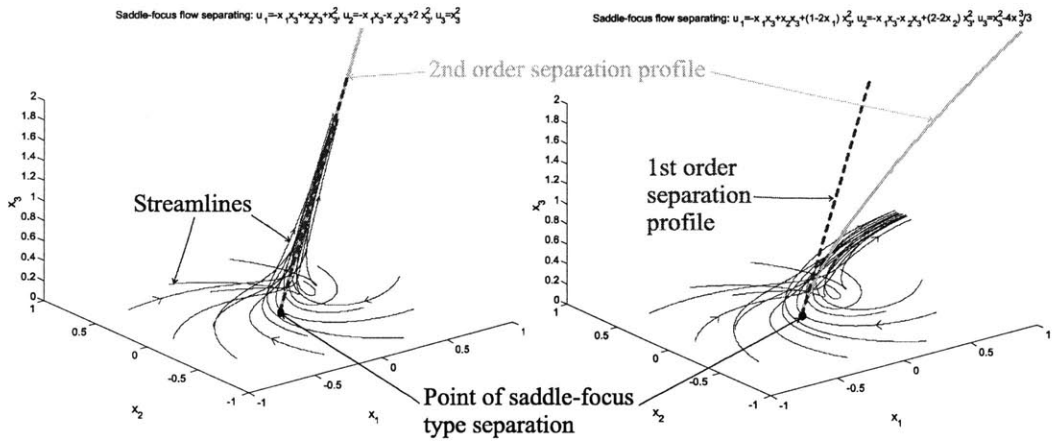

Figure 3-4: Visualization of the separation in the case of saddle-focus.

The left image in 3-4 shows the case of $\delta = 0$, the right image shows the case of $\delta = 2$. We analyze in appendix B.2.2 the accuracy of the separation profile.

3.3.3 Preliminary conclusion

In conclusion, we have introduced three models of typical separation patterns. We have validated chapter 2's theory with our steady models, and we have brought out the theoretical difficulties of the saddle-focus separation profile, which requires more consideration.

3.4 Three-dimensional separation bubble

3.4.1 Motivation

The linear skin friction field (3.19) gives a simple yet physically unlikely example. Here we consider a more relevant example, one that models a three-dimensional pattern observed in reality: separation on a car as described by Ahmed, Ramm & Faltin (1984) or separation on wings (Legendre & Werlé, by Délery 2001).

3.4.2 Topology of the separation pattern

We specify a skin friction field that mimicks the separation observed in the references cited above. Let the normal derivative of the velocity on the wall vary according to the equation

$$\mathbf{u}_z = \begin{pmatrix} \left(\frac{x_1 - f_1}{a}\right)^2 + \left(\frac{x_2 - f_2}{b}\right)^2 - 1 \\ -c(x_1 - f_1)(x_2 - f_2) - d(x_2 - f_2) \end{pmatrix}, \tag{3.44}$$

with parameters $a(t), b(t), c(t), d(t) > 0$ and with the functions $f_1(t)$ and $f_2(t)$.

In this case, the skin friction field has a saddle whose unstable manifold terminates in foci. There is another saddle behind the foci, as shown in figure 3-5. By changing the value of the coefficients in (3.44), we can generate different bubble shapes.

For $d = 0$, the foci degenerate into centers: Then the unstable manifold of the first saddle forms an ellipsoid-type arc that connects to the other saddle, encircling the two centers. In practice, such centers are structurally unstable patterns of separation: By adding a small perturbation to $\frac{\partial u_2}{\partial x_3}$, one may destroy the centers and create foci.

Substituting the shear-stress field (3.44) into (3.1) yields twelve equations up to third order:

$$A_{13} = -1 + \left(\frac{f_1}{a}\right)^2 + \left(\frac{f_2}{b}\right)^2, \quad A_{23} = -cf_1f_2 + df_2,$$

$$\begin{aligned} A_{113} &= -\frac{2f_1}{a^2}, & A_{123} &= -\frac{2f_2}{b^2}, \\ A_{213} &= cf_2, & A_{223} &= -d + cf_1, \\ A_{1113} &= \frac{1}{a^2}, & A_{1223} &= \frac{1}{b^2}, \end{aligned}$$

$$A_{1123} = A_{2113} = A_{2223} = 0, \quad A_{2123} = -c.$$

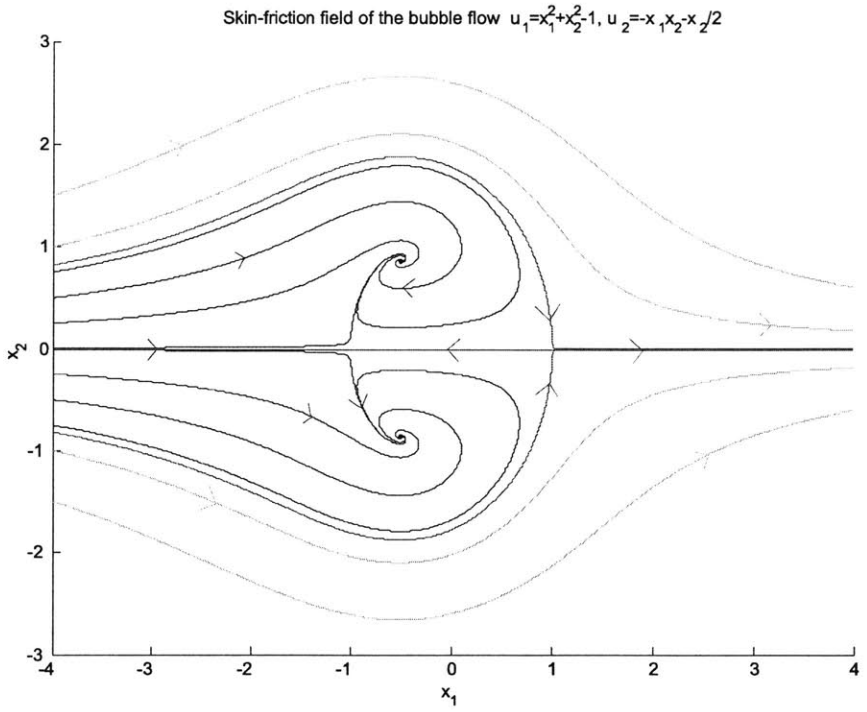

Figure 3-5: Skin friction fied of the separation bubble.

With all these relations, the velocity field takes the form

$$
\begin{aligned}
u_1 &= x_3\left[\left(\frac{x_1-f_1}{a}\right)^2+\left(\frac{x_2-f_2}{b}\right)^2-1\right] \\
&\quad + x_3^2\left[\alpha + A_{1133}x_1 + A_{1233}x_2 + \left[\frac{1}{6\nu}\frac{d}{dt}\left(\left(\frac{f_1}{a}\right)^2+\left(\frac{f_2}{b}\right)^2\right)+\frac{ca^2-2}{6a^2}\right]x_3\right], \\
u_2 &= -x_3\left(c(x_1-f_1)(x_2-f_2)+d(x_2-f_2)\right) \\
&\quad + x_3^2\left[\beta + A_{1233}x_1 + A_{2233}x_2 + \frac{1}{6\nu}\frac{d}{dt}\left(-cf_1f_2+df_2\right)x_3\right], \\
u_3 &= \frac{2f_1+a^2\left(d-cf_1\right)}{2a^2}x_3^2 + \frac{ca^2-2}{2a^2}x_1x_3^2 - \frac{A_{1133}+A_{2233}}{3}x_3^3,
\end{aligned}
\tag{3.45}
$$

with still nine unknown coefficients.

3.4.3 Analysis of the separation

The above flow admits four points of zero skin friction, thus we a priori expect four points of separation. The first condition for separation at $\boldsymbol{\gamma} = \begin{pmatrix} \gamma_1 \\ \gamma_2 \end{pmatrix}$ reads

$$\limsup_{t\to-\infty} \left| \int_{t_0}^{t} \mathbf{u}_z(\boldsymbol{\gamma}, 0, s)\, ds \right| < \infty$$

as shown in (2.43), and is now of the form

$$\limsup_{t\to-\infty} \left| \int_{t_0}^{t} \begin{pmatrix} \left(\dfrac{\gamma_1 - f_1}{a}\right)^2 + \left(\dfrac{\gamma_2 - f_2}{b}\right)^2 - 1 \\ -c(\gamma_1 - f_1)(\gamma_2 - f_2) - d(\gamma_2 - f_2) \end{pmatrix} d\tau \right| < \infty. \tag{3.46}$$

The second condition for incompressible separation is (2.44)

$$\lim_{t\to-\infty} \left\| \int_{t_0}^{t} \left[\mathbf{u}_{\mathbf{x}z}(\boldsymbol{\gamma}, 0, s) + \frac{1}{2}\mathbf{I}\,\mathrm{Tr}\,\mathbf{u}_{\mathbf{x}z}(\boldsymbol{\gamma}, 0, s) \right] ds \right\| = \infty$$

in the general case, and it reads

$$C = \lim_{t\to-\infty} \left\| \int_{t_0}^{t} \begin{pmatrix} \dfrac{(\gamma_1 - f_1)\,(6 - a^2c) - a^2d}{2a^2} & 2\dfrac{\gamma_2 - f_2}{b^2} \\ -c(\gamma_2 - f_2) & \dfrac{(\gamma_1 - f_1)\,(2 - 3a^2c) - 3a^2d}{2a^2} \end{pmatrix} (\tau)\, d\tau \right\| = \infty, \tag{3.47}$$

which we will analyze for each point individually.

The separation slope satisfies (2.47) or

$$\begin{aligned} \mathbf{g}_0(t_0) \;=\; & -\lim_{t\to-\infty} \left[\int_{t_0}^{t} \left(\mathbf{u}_{\mathbf{x}z}(\boldsymbol{\gamma}, 0, s) + \frac{1}{2}\mathbf{I}\,\mathrm{Tr}\,\mathbf{u}_{\mathbf{x}z}(\boldsymbol{\gamma}, 0, s) \right) ds \right]^{-1} \\ & \times \int_{t_0}^{t} \left[\frac{1}{2}\mathbf{u}_{zz}(\boldsymbol{\gamma}, 0, s) + \frac{1}{2} \left(\mathbf{u}_{\mathbf{x}z}(\boldsymbol{\gamma}, 0, s) + \frac{1}{2}\mathbf{I}\,\mathrm{Tr}\,\mathbf{u}_{\mathbf{x}z}(\boldsymbol{\gamma}, 0, s) \right) \int_{t_0}^{s} \mathbf{u}_z(\boldsymbol{\gamma}, 0, r)\, dr \right] ds, \end{aligned}$$

and simplifies for our velocity field to

$$\begin{aligned}
\mathbf{g}_0(t_0) = &- \lim_{t\to-\infty}\left[\int_{t_0}^{t}\begin{pmatrix} \dfrac{(\gamma_1-f_1)(6-a^2c)-a^2d}{2a^2} & 2\dfrac{\gamma_2-f_2}{b^2} \\ -c(\gamma_2-f_2) & \dfrac{(\gamma_1-f_1)(2-3a^2c)-3a^2d}{2a^2}\end{pmatrix} d\tau\right]^{-1} \\
&\times\int_{t_0}^{t}\left[\begin{pmatrix}\alpha\\ \beta\end{pmatrix}+\begin{pmatrix}A_{1133} & A_{1233}\\ A_{1233} & A_{2233}\end{pmatrix}\boldsymbol{\gamma}\right. \\
&+\begin{pmatrix} \dfrac{(\gamma_1-f_1)(6-a^2c)-a^2d}{2a^2} & 2\dfrac{\gamma_2-f_2}{b^2} \\ -c(\gamma_2-f_2) & \dfrac{(\gamma_1-f_1)(2-3a^2c)-3a^2d}{2a^2}\end{pmatrix} \\
&\times\left.\int_{t_0}^{s}\begin{pmatrix}\left(\dfrac{\gamma_1-f_1}{a}\right)^2+\left(\dfrac{\gamma_2-f_2}{b}\right)^2-1\\ -c(\gamma_1-f_1)(\gamma_2-f_2)-d(\gamma_2-f_2)\end{pmatrix} dr\right] ds.
\end{aligned} \tag{3.48}$$

The separation curvature (2.48) or

$$\begin{aligned}
\mathbf{g}_1(t_0) \;=\; &- \lim_{t\to-\infty}\left[2\int_{t_0}^{t}\left(\mathbf{u}_{\mathbf{x}z}(\boldsymbol{\gamma},0,s)+\mathbf{I}\,\mathrm{Tr}\,\mathbf{u}_{\mathbf{x}z}(\boldsymbol{\gamma},0,s)\right)\,ds\right]^{-1} \\
&\times\int_{t_0}^{t}\left[\frac{1}{3}\mathbf{u}_{zz}(\boldsymbol{\gamma},0,s)+\left(\mathbf{u}_{\mathbf{x}zz}(\boldsymbol{\gamma},0,s)+\frac{1}{3}\mathbf{I}\,\mathrm{Tr}\,\mathbf{u}_{\mathbf{x}zz}(\boldsymbol{\gamma},0,s)\right)\mathbf{g}_0(\tau)\right. \\
&+\left[\left[\mathbf{u}_{\mathbf{x}\mathbf{x}z}(\boldsymbol{\gamma},0,s)+(\mathrm{Tr}\,\mathbf{u}_{\mathbf{x}z})_{\mathbf{x}}(\boldsymbol{\gamma},0,s)\cdot\mathbf{I}\right]\mathbf{g}_0\right]\mathbf{g}_0 \\
&+2\left(\mathbf{u}_{\mathbf{x}z}(\boldsymbol{\gamma},0,s)+\mathbf{I}\,\mathrm{Tr}\,\mathbf{u}_{\mathbf{x}z}(\boldsymbol{\gamma},0,s)\right) \\
&\times\left.\int_{t_0}^{s}\left[\frac{1}{2}\mathbf{u}_{zz}(\boldsymbol{\gamma},0,r)+\left(\mathbf{u}_{\mathbf{x}z}(\boldsymbol{\gamma},0,r)+\frac{1}{2}\mathbf{I}\,\mathrm{Tr}\,\mathbf{u}_{\mathbf{x}z}(\boldsymbol{\gamma},0,r)\right)\mathbf{g}_0(r)\right]\,dr\right]\,ds,
\end{aligned}$$

can be written as

$$
\begin{aligned}
\mathbf{g}_1(t_0) \;=\; & -\lim_{t\to-\infty}\left[2\int_{t_0}^{t}\begin{pmatrix} \dfrac{(\gamma_1-f_1)(4-a^2c)-a^2d}{a^2} & 2\dfrac{\gamma_2-f_2}{b^2} \\ -c(\gamma_2-f_2) & 2\dfrac{(\gamma_1-f_1)(1-a^2c)-a^2d}{a^2}\end{pmatrix} d\tau\right]^{-1} \\
& \times\int_{t_0}^{t}\begin{pmatrix} 2\begin{pmatrix} \dfrac{1}{6\nu}\dfrac{d}{dt}\left(\left(\dfrac{f_1}{a}\right)^2+\left(\dfrac{f_2}{b}\right)^2\right)+\dfrac{ca^2-2}{6a^2} \\ \dfrac{1}{6\nu}\dfrac{d}{dt}\left(-cf_1f_2+df_2\right)\end{pmatrix} \\ +2\begin{pmatrix} \frac{4A_{1133}+A_{2233}}{3} & A_{1233} \\ A_{1233} & \frac{A_{1133}+4A_{2233}}{3}\end{pmatrix}\mathbf{g}_0+\begin{pmatrix} \dfrac{4-ca^2}{a^2}(g_{0,1})^2+\dfrac{2}{b^2}(g_{0,2})^2 \\ \dfrac{2-3ca^2}{a^2}g_{0,1}g_{0,2}\end{pmatrix} \\ +2\begin{pmatrix} \dfrac{(\gamma_1-f_1)(4-a^2c)-a^2d}{a^2} & 2\dfrac{\gamma_2-f_2}{b^2} \\ -c(\gamma_2-f_2) & 2\dfrac{(\gamma_1-f_1)(1-a^2c)-a^2d}{a^2}\end{pmatrix} \\ \times\int_{t_0}^{s}\left[\begin{pmatrix}\alpha\\ \beta\end{pmatrix}+\begin{pmatrix} A_{1133} & A_{1233} \\ A_{1233} & A_{2233}\end{pmatrix}\gamma\right. \\ \left.+\begin{pmatrix} \dfrac{(\gamma_1-f_1)(6-a^2c)-a^2d}{2a^2} & 2\dfrac{\gamma_2-f_2}{b^2} \\ -c(\gamma_2-f_2) & \dfrac{(\gamma_1-f_1)(2-3a^2c)-3a^2d}{2a^2}\end{pmatrix}\mathbf{g}_0\right](r)\,dr\Bigg](s)\,ds.
\end{aligned}
\tag{3.49}
$$

3.4.4 Analysis of specific cases

Steady separation bubble

When the flow is steady, the first condition for separation (3.46) at a separation point $\boldsymbol{\gamma} = \begin{pmatrix}\gamma_1\\ \gamma_2\end{pmatrix}$ simplifies to

$$
\begin{pmatrix} \left(\dfrac{\gamma_1-f_1}{a}\right)^2+\left(\dfrac{\gamma_2-f_2}{b}\right)^2-1 \\ -c(\gamma_1-f_1)(\gamma_2-f_2)-d(\gamma_2-f_2)\end{pmatrix}=0. \tag{3.50}
$$

This flow admits four points of zero skin friction, i.e., four possible points of separation:

$$
\begin{aligned}
\boldsymbol{\gamma}^1 &= \begin{pmatrix}-a\\ 0\end{pmatrix}+\mathbf{F}, & \boldsymbol{\gamma}^2 &= \begin{pmatrix}a\\ 0\end{pmatrix}+\mathbf{F}, \\
\boldsymbol{\gamma}^3 &= \begin{pmatrix} -d/c \\ -b\sqrt{1-\left(\frac{d}{ac}\right)^2}\end{pmatrix}+\mathbf{F}, & \boldsymbol{\gamma}^4 &= \begin{pmatrix} -d/c \\ b\sqrt{1-\left(\frac{d}{ac}\right)^2}\end{pmatrix}+\mathbf{F}.
\end{aligned}
\tag{3.51}
$$

Then the second condition for separation (3.47) becomes for each separation point:

$$
\begin{aligned}
C_1 &= \lim_{t\to-\infty}\left\|\int_{t_0}^{t}\begin{pmatrix}\frac{ca^2-ad-6}{2a} & 0\\ 0 & \frac{3ca^2-3ad-2}{2a}\end{pmatrix}d\tau\right\| = \infty,\\
C_2 &= \lim_{t\to-\infty}\left\|\int_{t_0}^{t}\begin{pmatrix}\frac{-ca^2-ad+6}{2a} & 0\\ 0 & \frac{-3ca^2-3ad+2}{2a}\end{pmatrix}d\tau\right\| = \infty,\\
C_3 &= \lim_{t\to-\infty}\left\|\int_{t_0}^{t}\begin{pmatrix}-\frac{d}{a^2}\left(3c+a^2\right) & -\frac{2}{b}\sqrt{1-\left(\frac{d}{ac}\right)^2}\\ cb\sqrt{1-\left(\frac{d}{ac}\right)^2} & -\frac{d}{a^2}\left(c+3a^2\right)\end{pmatrix}d\tau\right\| = \infty,\\
C_4 &= \lim_{t\to-\infty}\left\|\int_{t_0}^{t}\begin{pmatrix}-\frac{d}{a^2}\left(3c+a^2\right) & \frac{2}{b}\sqrt{1-\left(\frac{d}{ac}\right)^2}\\ -cb\sqrt{1-\left(\frac{d}{ac}\right)^2} & -\frac{d}{a^2}\left(c+3a^2\right)\end{pmatrix}d\tau\right\| = \infty,
\end{aligned}
$$

and these expressions simplify to

$$
\begin{aligned}
\begin{pmatrix}\frac{ca^2-ad-6}{2a} & 0\\ 0 & \frac{3ca^2-3ad-2}{2a}\end{pmatrix} &\neq 0,\\
\begin{pmatrix}\frac{-ca^2-ad+6}{2a} & 0\\ 0 & \frac{-3ca^2-3ad+2}{2a}\end{pmatrix} &\neq 0,\\
\begin{pmatrix}-\frac{d}{a^2}\left(3c+a^2\right) & -\frac{2}{b}\sqrt{1-\left(\frac{d}{ac}\right)^2}\\ cb\sqrt{1-\left(\frac{d}{ac}\right)^2} & -\frac{d}{a^2}\left(c+3a^2\right)\end{pmatrix} &\neq 0,\\
\begin{pmatrix}-\frac{d}{a^2}\left(3c+a^2\right) & \frac{2}{b}\sqrt{1-\left(\frac{d}{ac}\right)^2}\\ -cb\sqrt{1-\left(\frac{d}{ac}\right)^2} & -\frac{d}{a^2}\left(c+3a^2\right)\end{pmatrix} &\neq 0,
\end{aligned}
\qquad (3.52)
$$

which are always satisfied because the four parameters a, b, c and d are strictly positive.

The separation slope at a separation point γ is

$$
\begin{aligned}
\mathrm{g}_0 = &-\begin{pmatrix}\frac{(\gamma_1-f_1)(6-a^2c)-a^2d}{2a^2} & 2\frac{\gamma_2-f_2}{b^2}\\ -c(\gamma_2-f_2) & \frac{(\gamma_1-f_1)(2-3a^2c)-3a^2d}{2a^2}\end{pmatrix}^{-1}\\
&\times\left[\begin{pmatrix}\alpha\\ \beta\end{pmatrix}+\begin{pmatrix}A_{1133} & A_{1233}\\ A_{1233} & A_{2233}\end{pmatrix}\gamma\right],
\end{aligned}
$$

which takes the form

$$\mathbf{g}_0^1 = -\begin{pmatrix} \frac{ca^2-ad-6}{2a} & 0 \\ 0 & \frac{3ca^2-3ad-2}{2a} \end{pmatrix}^{-1} \left[\begin{pmatrix} \alpha \\ \beta \end{pmatrix} + \begin{pmatrix} A_{1133} & A_{1233} \\ A_{1233} & A_{2233} \end{pmatrix} \boldsymbol{\gamma} \right], \tag{3.53a}$$

$$\mathbf{g}_0^2 = -\begin{pmatrix} \frac{-ca^2-ad+6}{2a} & 0 \\ 0 & \frac{-3ca^2-3ad+2}{2a} \end{pmatrix}^{-1} \left[\begin{pmatrix} \alpha \\ \beta \end{pmatrix} + \begin{pmatrix} A_{1133} & A_{1233} \\ A_{1233} & A_{2233} \end{pmatrix} \boldsymbol{\gamma} \right], \tag{3.53b}$$

$$\mathbf{g}_0^3 = -\begin{pmatrix} -\frac{3d}{ca^2} & -\frac{2}{b}\sqrt{1-\left(\frac{d}{ac}\right)^2} \\ cb\sqrt{1-\left(\frac{d}{ac}\right)^2} & -\frac{d}{ca^2} \end{pmatrix}^{-1} \times \left[\begin{pmatrix} \alpha \\ \beta \end{pmatrix} + \begin{pmatrix} A_{1133} & A_{1233} \\ A_{1233} & A_{2233} \end{pmatrix} \boldsymbol{\gamma} \right], \tag{3.53c}$$

$$\mathbf{g}_0^4 = -\begin{pmatrix} -\frac{3d}{ca^2} & \frac{2}{b}\sqrt{1-\left(\frac{d}{ac}\right)^2} \\ -cb\sqrt{1-\left(\frac{d}{ac}\right)^2} & -\frac{d}{ca^2} \end{pmatrix}^{-1} \times \left[\begin{pmatrix} \alpha \\ \beta \end{pmatrix} + \begin{pmatrix} A_{1133} & A_{1233} \\ A_{1233} & A_{2233} \end{pmatrix} \boldsymbol{\gamma} \right], \tag{3.53d}$$

at the four separation points.

Finally the separation curvature takes the form

$$\begin{aligned} \mathbf{g}_1 = -&\begin{pmatrix} \frac{(\gamma_1 - f_1)(4-a^2c)-a^2d}{a^2} & 2\frac{\gamma_2 - f_2}{b^2} \\ -c(\gamma_2 - f_2) & 2\frac{(\gamma_1 - f_1)(1-a^2c)-a^2d}{a^2} \end{pmatrix}^{-1} \\ &\times \left[\begin{pmatrix} \frac{ca^2-2}{6a^2} \\ 0 \end{pmatrix} + \begin{pmatrix} \frac{4A_{1133}+A_{2233}}{3} & A_{1233} \\ A_{1233} & \frac{A_{1133}+4A_{2233}}{3} \end{pmatrix} \mathbf{g}_0 \right. \\ &\left. + \frac{1}{2} \begin{pmatrix} \frac{4-ca^2}{a^2}(g_{0,1})^2 + \frac{2}{b^2}(g_{0,2})^2 \\ \frac{2-3ca^2}{a^2} g_{0,1} g_{0,2} \end{pmatrix} \right], \end{aligned}$$

which becomes

$$\mathbf{g}_1^1 = -\begin{pmatrix} \frac{ca^2-ad-4}{a} & 0 \\ 0 & \frac{2ca^2-2ad-2}{a} \end{pmatrix}^{-1} \left[\begin{pmatrix} \frac{ca^2-2}{6a^2} \\ 0 \end{pmatrix} + \begin{pmatrix} \frac{4A_{1133}+A_{2233}}{3} & A_{1233} \\ A_{1233} & \frac{A_{1133}+4A_{2233}}{3} \end{pmatrix} \mathbf{g}_0 + \frac{1}{2} \begin{pmatrix} \frac{4-ca^2}{a^2} \left(g_{0,1}^1\right)^2 + \frac{2}{b^2} \left(g_{0,2}^1\right)^2 \\ \frac{2-3ca^2}{a^2} g_{0,1}^1 g_{0,2}^1 \end{pmatrix} \right], \tag{3.54a}$$

$$\mathbf{g}_1^2 = -\begin{pmatrix} \frac{-ca^2-ad+4}{a} & 0 \\ 0 & \frac{-2ca^2-2ad+2}{a} \end{pmatrix}^{-1} \left[\begin{pmatrix} \frac{ca^2-2}{6a^2} \\ 0 \end{pmatrix} + \begin{pmatrix} \frac{4A_{1133}+A_{2233}}{3} & A_{1233} \\ A_{1233} & \frac{A_{1133}+4A_{2233}}{3} \end{pmatrix} \mathbf{g}_0 + \frac{1}{2} \begin{pmatrix} \frac{4-ca^2}{a^2} \left(g_{0,1}^2\right)^2 + \frac{2}{b^2} \left(g_{0,2}^2\right)^2 \\ \frac{2-3ca^2}{a^2} g_{0,1}^2 g_{0,2}^2 \end{pmatrix} \right], \tag{3.54b}$$

$$\mathbf{g}_1^3 = -\begin{pmatrix} -\frac{4d}{ca^2} & -\frac{2}{b}\sqrt{1-\left(\frac{d}{ac}\right)^2} \\ cb\sqrt{1-\left(\frac{d}{ac}\right)^2} & -\frac{2d}{ca^2} \end{pmatrix}^{-1} \left[\begin{pmatrix} \frac{ca^2-2}{6a^2} \\ 0 \end{pmatrix} + \begin{pmatrix} \frac{4A_{1133}+A_{2233}}{3} & A_{1233} \\ A_{1233} & \frac{A_{1133}+4A_{2233}}{3} \end{pmatrix} \mathbf{g}_0 + \frac{1}{2} \begin{pmatrix} \frac{4-ca^2}{a^2} \left(g_{0,1}^3\right)^2 + \frac{2}{b^2} \left(g_{0,2}^3\right)^2 \\ \frac{2-3ca^2}{a^2} g_{0,1}^3 g_{0,2}^3 \end{pmatrix} \right], \tag{3.54c}$$

$$\mathbf{g}_1^4 = -\begin{pmatrix} -\frac{4d}{ca^2} & \frac{2}{b}\sqrt{1-\left(\frac{d}{ac}\right)^2} \\ -cb\sqrt{1-\left(\frac{d}{ac}\right)^2} & -\frac{2d}{ca^2} \end{pmatrix}^{-1} \left[\begin{pmatrix} \frac{ca^2-2}{6a^2} \\ 0 \end{pmatrix} + \begin{pmatrix} \frac{4A_{1133}+A_{2233}}{3} & A_{1233} \\ A_{1233} & \frac{A_{1133}+4A_{2233}}{3} \end{pmatrix} \mathbf{g}_0 + \frac{1}{2} \begin{pmatrix} \frac{4-ca^2}{a^2} \left(g_{0,1}^4\right)^2 + \frac{2}{b^2} \left(g_{0,2}^4\right)^2 \\ \frac{2-3ca^2}{a^2} g_{0,1}^4 g_{0,2}^4 \end{pmatrix} \right], \tag{3.54d}$$

at the four separation points.

To illustrate the validity of the above formulae, we now compare the predicted separation profiles and the streamlines in figure 3-6.

We can see a surface of separation: The particles pass on top of the bubble and draw a bubble shape (for more details on the generation of separation surfaces, refer to appendix B.4). The predicted profiles appear correct, and they correctly delineate the shape of the bubble. We analyze the saddle-foci profiles numerically in appendix B.3.

In this example, the flow is given by

$$\begin{aligned} u_1 &= x_3\left(x_1^2+x_2^2-1\right)+x_3^2\left(50+10x_1-\frac{1}{6}x_3\right), \\ u_2 &= -x_1x_2x_3-\frac{1}{2}x_2x_3+10x_2x_3^2, \\ u_3 &= \frac{1}{4}x_3^2-\frac{1}{2}x_1x_3^2-\frac{20}{3}x_3^3. \end{aligned} \tag{3.55}$$

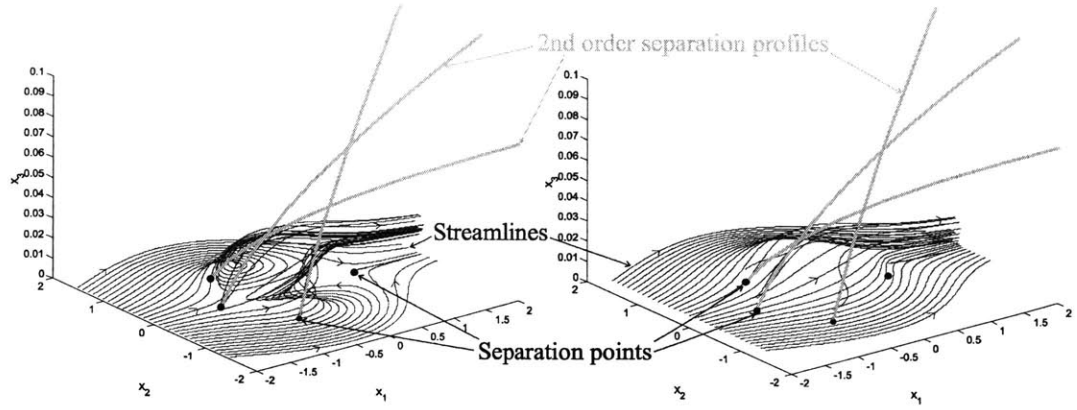

Figure 3-6: Visualization of the accuracy of the computed profiles with respect to the separation in the steady bubble flow. Left: streamlines passing under the bubble. Right: streamlines passing over the bubble.

Periodic separation bubble with moving saddle-foci

We now consider a perturbation of the steady bubble: Let us take a, b and $c > 0$ fixed, $\mathbf{F} = \mathbf{0}$, and $d = e + \varepsilon \cos \omega t$ with e, ε and $\omega > 0$ fixed. Now that we have defined the skin friction field, we set $A_{1233} = 0$ and $A_{1133} = A_{2233} = \delta$ to obtain the velocity field:

$$\begin{aligned} u_1 &= x_3 \left(\left(\frac{x_1}{a}\right)^2 + \left(\frac{x_2}{b}\right)^2 - 1 \right) + x_3^2 \left(\alpha + \delta x_1 + \frac{ca^2 - 2}{6a^2} x_3 \right), \\ u_2 &= -c x_1 x_2 x_3 - (e + \varepsilon \cos \omega t) x_2 x_3 + x_3^2 \left(\beta + \delta x_2 \right), \\ u_3 &= \frac{e + \varepsilon \cos \omega t}{2} x_3^2 + \frac{ca^2 - 2}{2a^2} x_1 x_3^2 - \frac{2\delta}{3} x_3^3. \end{aligned} \tag{3.56}$$

The first condition (3.46) for separation at $\boldsymbol{\gamma} = \begin{pmatrix} \gamma_1 \\ \gamma_2 \end{pmatrix}$ is

$$\begin{aligned} &\limsup_{t \to -\infty} \left| \int_{t_0}^{t} \begin{pmatrix} \left(\frac{\gamma_1}{a}\right)^2 + \left(\frac{\gamma_2}{b}\right)^2 - 1 \\ -c\gamma_1\gamma_2 - (e + \varepsilon \cos \omega t)\gamma_2 \end{pmatrix} d\tau \right| \\ &= \limsup_{t \to -\infty} \left[|t - t_0| \left| \begin{pmatrix} \left(\frac{\gamma_1}{a}\right)^2 + \left(\frac{\gamma_2}{b}\right)^2 - 1 \\ -c\gamma_1\gamma_2 - e\gamma_2 \end{pmatrix} \right| + \text{ a bounded term} \right] < \infty, \end{aligned}$$

which coincides with the steady condition (3.50) (with d replaced by e). Thus there are four

points of separation, defined by

$$\begin{aligned} \gamma_1 &= \begin{pmatrix} -a \\ 0 \end{pmatrix}, & \gamma_2 &= \begin{pmatrix} a \\ 0 \end{pmatrix}, \\ \gamma_3 &= \begin{pmatrix} -e/c \\ -b\sqrt{1-\left(\frac{e}{ac}\right)^2} \end{pmatrix}, & \gamma_4 &= \begin{pmatrix} -e/c \\ b\sqrt{1-\left(\frac{e}{ac}\right)^2} \end{pmatrix}. \end{aligned} \tag{3.57}$$

At these points, we express the second condition for separation (3.47): Integrating in backward time, we no longer take the periodic terms and only keep the linear terms, then the condition reads

$$\begin{aligned} C &= \lim_{t\to-\infty} \left\| \int_{t_0}^{t} \begin{pmatrix} \frac{(\gamma_1 - f_1)(6-a^2c) - a^2 e}{2a^2} & 2\frac{\gamma_2 - f_2}{b^2} \\ -c(\gamma_2 - f_2) & \frac{(\gamma_1 - f_1)(2-3a^2c) - 3a^2 e}{2a^2} \end{pmatrix} d\tau \right\| \\ &= \lim_{t\to-\infty} |t - t_0| \left\| \begin{pmatrix} \frac{(\gamma_1 - f_1)(6-a^2c) - a^2 e}{2a^2} & 2\frac{\gamma_2 - f_2}{b^2} \\ -c(\gamma_2 - f_2) & \frac{(\gamma_1 - f_1)(2-3a^2c) - 3a^2 e}{2a^2} \end{pmatrix} \right\| = \infty. \end{aligned}$$

This is again always satisfied because it is of the same form as the steady conditions (3.52).

The separation slope and curvature now do not simplify in the same way as they did in the steady case. We show (see formula (B.24) in appendix B.5) that the slopes are given by

$$\mathrm{g}_0^1 = -\begin{pmatrix} \frac{ca^2-ad-6}{2a} & 0 \\ 0 & \frac{3ca^2-3ad-2}{2a} \end{pmatrix}^{-1} \left[\begin{pmatrix} \alpha \\ \beta \end{pmatrix} + \begin{pmatrix} A_{1133} & A_{1233} \\ A_{1233} & A_{2233} \end{pmatrix} \gamma \right], \tag{3.58a}$$

$$\mathrm{g}_0^2 = -\begin{pmatrix} \frac{-ca^2-ad+6}{2a} & 0 \\ 0 & \frac{-3ca^2-3ad+2}{2a} \end{pmatrix}^{-1} \left[\begin{pmatrix} \alpha \\ \beta \end{pmatrix} + \begin{pmatrix} A_{1133} & A_{1233} \\ A_{1233} & A_{2233} \end{pmatrix} \gamma \right], \tag{3.58b}$$

$$\begin{aligned} \mathrm{g}_0^3 = &-\begin{pmatrix} -\frac{3d}{ca^2} & -\frac{2}{b}\sqrt{1-\left(\frac{d}{ac}\right)^2} \\ cb\sqrt{1-\left(\frac{d}{ac}\right)^2} & -\frac{d}{ca^2} \end{pmatrix}^{-1} \\ &\times \left[\begin{pmatrix} \alpha \\ \beta \end{pmatrix} + \begin{pmatrix} A_{1133} & A_{1233} \\ A_{1233} & A_{2233} \end{pmatrix} \gamma + \frac{\varepsilon}{\omega} \begin{pmatrix} 2\left(1-\frac{d}{ac}\right) \\ \frac{bd(2-3a^2c)\sqrt{1-\left(\frac{d}{ac}\right)^2}}{2ca^2} \end{pmatrix} \sin\omega t_0 \right], \end{aligned} \tag{3.58c}$$

$$\begin{aligned} \mathrm{g}_0^4 = &-\begin{pmatrix} -\frac{3d}{ca^2} & \frac{2}{b}\sqrt{1-\left(\frac{d}{ac}\right)^2} \\ -cb\sqrt{1-\left(\frac{d}{ac}\right)^2} & -\frac{d}{ca^2} \end{pmatrix}^{-1} \\ &\times \left[\begin{pmatrix} \alpha \\ \beta \end{pmatrix} + \begin{pmatrix} A_{1133} & A_{1233} \\ A_{1233} & A_{2233} \end{pmatrix} \gamma + \frac{\varepsilon}{\omega} \begin{pmatrix} 2\left(1-\frac{d}{ac}\right) \\ -\frac{bd(2-3a^2c)\sqrt{1-\left(\frac{d}{ac}\right)^2}}{2ca^2} \end{pmatrix} \sin\omega t_0 \right]. \end{aligned} \tag{3.58d}$$

The formulae of the curvature (B.25), rather lengthy to write at each separation point, can be found in appendix B.5.

To check the accuracy of these formulae, we can no longer use the streamlines; instead, we track particles (from the left to the right). Some slides of the movie we obtain are shown in figure 3-7. We also show the surface of separation, which the separating particles will follow (for details, refer to appendix B.4). These particles arrive near the separation bubble, pass by it, and finally leave the bubble. The bubble does not capture the particles: it releases them immediately.

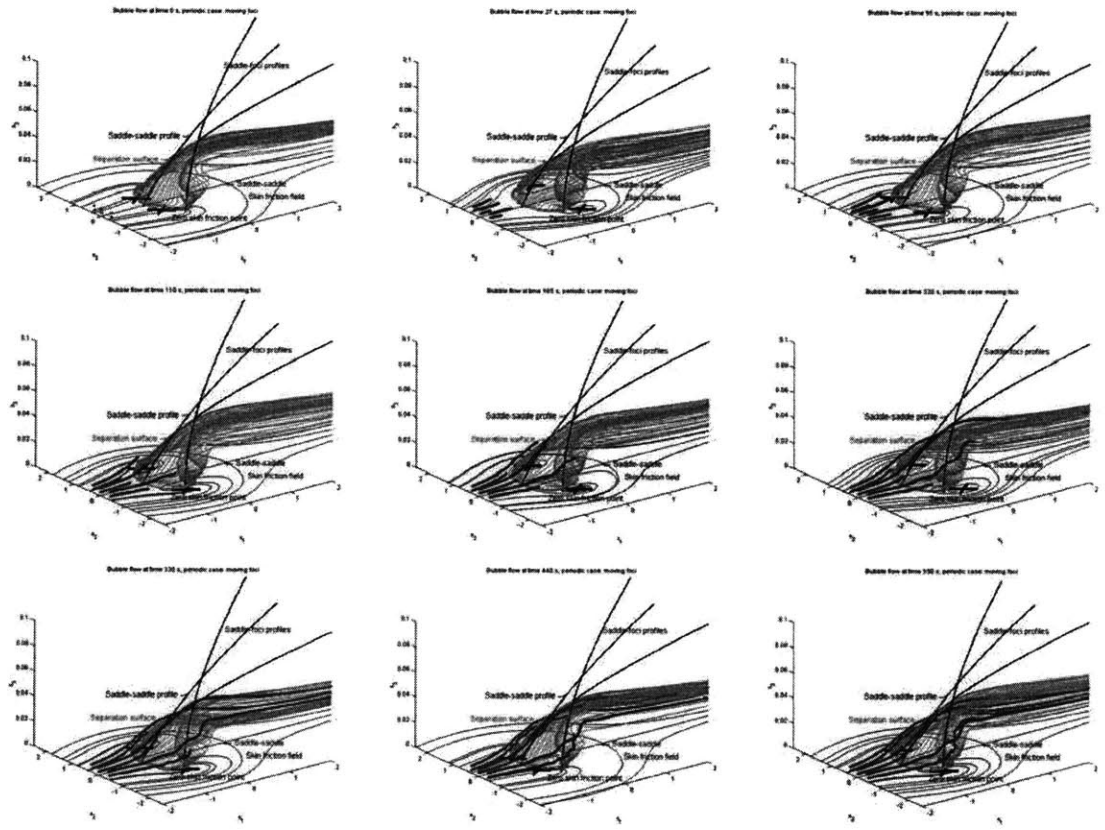

Figure 3-7: Some slides of the visualization of separation on a bubble; we showed the skin friction field, the periodic predicted profiles of separation at second-order, the periodic surfaces of separation and a few trajectories.

The time-periodic bubble flow takes the form

$$\begin{aligned} u_1 &= x_3\left(x_1^2+x_2^2-1\right)+x_3^2\left(50+10x_1-\frac{x_3}{6}\right), \\ u_2 &= -x_2x_3\left(x_1+\left(\frac{1}{2}+\frac{3}{8}\cos\left(\frac{t}{10}\right)\right)\right)+10x_2x_3^2, \\ u_3 &= \frac{4+3\cos\omega t}{16}x_3^2-\frac{x_1x_3^2}{2}-\frac{20}{3}x_3^3. \end{aligned}$$

Periodic separation bubble with moving saddle-saddles

The previous case may seem unconvincing because the separation surface appears steady in spite of the motion of the saddle-foci separation profiles. This is due to the fact that the stable manifold of the first saddle-saddle directs the separation surface, and in the previous case, even if the whole flow is unsteady, the stable manifold of the first saddle-saddle is steady. To obtain a clearly moving separation surface, we now change the flow to make the saddle-saddles move.

We set a to be periodic, and look at how separation changes: Let us take b, c and $d > 0$ fixed, $\mathbf{F} = \mathbf{0}$, and $\dfrac{1}{a^2} = \dfrac{1}{a_0^2} + \upsilon \cos \omega t$ with a_0, υ and $\omega > 0$ fixed. Now that we have defined the skin friction field, we set $A_{1233} = 0$ and $A_{1133} = A_{2233} = \delta$ to obtain the velocity field:

$$\begin{aligned} u_1 &= x_3 \left(x_1^2 \left(\frac{1}{a_0^2} + \upsilon \cos \omega t \right) + \left(\frac{x_2}{b} \right)^2 - 1 \right) + x_3^2 \left(\alpha + \delta x_1 + \left(\frac{c}{6} - \frac{1}{3a_0^2} - \frac{\upsilon}{3} \cos \omega t \right) x_3 \right), \\ u_2 &= -c x_1 x_2 x_3 - d x_2 x_3 + x_3^2 \left(\beta + \delta x_2 \right), \\ u_3 &= \frac{d}{2} x_3^2 + \left(\frac{c}{2} - \frac{1}{a_0^2} - \upsilon \cos \omega t \right) x_1 x_3^2 - \frac{2\delta}{3} x_3^3. \end{aligned} \tag{3.59}$$

The first condition for separation at $\boldsymbol{\gamma} = \begin{pmatrix} \gamma_1 \\ \gamma_2 \end{pmatrix}$ is

$$\begin{aligned} &\limsup_{t \to -\infty} \left| \int_{t_0}^{t} \begin{pmatrix} \gamma_1^2 \left(\dfrac{1}{a_0^2} + \upsilon \cos \omega t \right) + \left(\dfrac{\gamma_2}{b} \right)^2 - 1 \\ -c\gamma_1\gamma_2 - d\gamma_2 \end{pmatrix} d\tau \right| \\ &= \limsup_{t \to -\infty} \left[|t - t_0| \left| \begin{pmatrix} \left(\dfrac{\gamma_1}{a_0} \right)^2 + \left(\dfrac{\gamma_2}{b} \right)^2 - 1 \\ -c\gamma_1\gamma_2 - d\gamma_2 \end{pmatrix} \right| + \text{ a bounded term} \right] < \infty, \end{aligned}$$

which coincides with the steady condition (with a replaced by a_0). Thus, there are four separation points defined by

$$\begin{aligned} \boldsymbol{\gamma}_1 &= \begin{pmatrix} -a_0 \\ 0 \end{pmatrix}, & \boldsymbol{\gamma}_2 &= \begin{pmatrix} a_0 \\ 0 \end{pmatrix}, \\ \boldsymbol{\gamma}_3 &= \begin{pmatrix} -d/c \\ -b\sqrt{1 - \left(\frac{d}{a_0 c} \right)^2} \end{pmatrix}, & \boldsymbol{\gamma}_4 &= \begin{pmatrix} -d/c \\ b\sqrt{1 - \left(\frac{d}{a_0 c} \right)^2} \end{pmatrix}. \end{aligned} \tag{3.60}$$

At these points, we evaluate the second condition for separation, and in the integration we

only keep the dominant terms:

$$
\begin{aligned}
C &= \lim_{t\to-\infty}\left\|\int_{t_0}^{t}\begin{pmatrix} 3(\gamma_1-f_1)\left(\frac{1}{a_0^2}+\upsilon\cos\omega t-\frac{c}{6}\right)-\frac{d}{2} & 2\dfrac{\gamma_2-f_2}{b^2} \\ -c(\gamma_2-f_2) & (\gamma_1-f_1)\left(\frac{1}{a_0^2}+\upsilon\cos\omega t-\frac{3c}{2}\right)-\frac{3d}{2}\end{pmatrix} d\tau\right\| \\
&= \lim_{t\to-\infty}|t-t_0|\left\|\begin{pmatrix} \dfrac{(\gamma_1-f_1)(6-a_0^2c)-a_0^2d}{2a_0^2} & 2\dfrac{\gamma_2-f_2}{b^2} \\ -c(\gamma_2-f_2) & \dfrac{(\gamma_1-f_1)(2-3a_0^2c)-3a_0^2d}{2a_0^2}\end{pmatrix}\right\| = \infty,
\end{aligned}
$$

hence is always satisfied because it is of the same form as the steady conditions (3.52).

We show (see formula (B.26) in appendix B.6) that the slopes are given by

$$
\begin{aligned}
\mathbf{g}_0^1 &= -\begin{pmatrix} \frac{ca_0^2-a_0d-6}{2a_0} & 0 \\ 0 & \frac{3ca_0^2-3a_0d-2}{2a_0}\end{pmatrix}^{-1}\left[\begin{pmatrix}\alpha\\ \beta\end{pmatrix}+\begin{pmatrix} A_{1133} & A_{1233}\\ A_{1233} & A_{2233}\end{pmatrix}\boldsymbol{\gamma}\right. \\
&\qquad \left.-\frac{\upsilon a_0}{\omega}\begin{pmatrix}\dfrac{-6+a_0^2c-a_0d}{2a_0}\\ 0\end{pmatrix}\sin\omega t_0\right], \qquad (3.61a)\\
\mathbf{g}_0^2 &= -\begin{pmatrix} \frac{-ca_0^2-a_0d+6}{2a_0} & 0 \\ 0 & \frac{-3ca_0^2-3a_0d+2}{2a_0}\end{pmatrix}^{-1}\left[\begin{pmatrix}\alpha\\ \beta\end{pmatrix}+\begin{pmatrix} A_{1133} & A_{1233}\\ A_{1233} & A_{2233}\end{pmatrix}\boldsymbol{\gamma}\right], \\
&\qquad +\frac{\upsilon a_0}{\omega}\begin{pmatrix}\dfrac{6-a_0^2c-a_0d}{2a_0}\\ 0\end{pmatrix}\sin\omega t_0\Bigg], \qquad (3.61b)\\
\mathbf{g}_0^3 &= -\begin{pmatrix} -\frac{3d}{ca_0^2} & -\frac{2}{b}\sqrt{1-\left(\frac{d}{a_0c}\right)^2} \\ cb\sqrt{1-\left(\frac{d}{a_0c}\right)^2} & -\frac{d}{ca_0^2}\end{pmatrix}^{-1}\left[\begin{pmatrix}\alpha\\ \beta\end{pmatrix}+\begin{pmatrix} A_{1133} & A_{1233}\\ A_{1233} & A_{2233}\end{pmatrix}\boldsymbol{\gamma}\right. \\
&\qquad \left.-\frac{\upsilon e}{\omega c}\begin{pmatrix}\dfrac{-e(6-a_0^2c)-a_0^2cd}{2ca_0^2}\\ cb\sqrt{1-\left(\frac{d}{a_0c}\right)^2}\end{pmatrix}\sin\omega t_0\right], \qquad (3.61c)\\
\mathbf{g}_0^4 &= -\begin{pmatrix} -\frac{3d}{ca_0^2} & \frac{2}{b}\sqrt{1-\left(\frac{d}{a_0c}\right)^2} \\ -cb\sqrt{1-\left(\frac{d}{a_0c}\right)^2} & -\frac{d}{ca_0^2}\end{pmatrix}^{-1}\left[\begin{pmatrix}\alpha\\ \beta\end{pmatrix}+\begin{pmatrix} A_{1133} & A_{1233}\\ A_{1233} & A_{2233}\end{pmatrix}\boldsymbol{\gamma}\right. \\
&\qquad \left.-\frac{\upsilon e}{\omega c}\begin{pmatrix}\dfrac{-e(6-a_0^2c)-a_0^2cd}{2ca_0^2}\\ -cb\sqrt{1-\left(\frac{d}{a_0c}\right)^2}\end{pmatrix}\sin\omega t_0\right], \qquad (3.61d)
\end{aligned}
$$

and the formula for the curvature is given in (B.27).

To check the accuracy of these formulae, we look at two cases, which depend on the values

we give to some parameters. We also set $\beta = 0$ to preserve the symmetry of the bubble.

Closing bubble If we set α rather large and δ positive, we obtain a closing bubble; we give some slides of the motion of the particles in figure 3-8. We also show the surface of separation, which the separating particles will follow (for details, refer to appendix B.4). The particles arrive near the separation bubble, pass by it, and then leave the bubble.

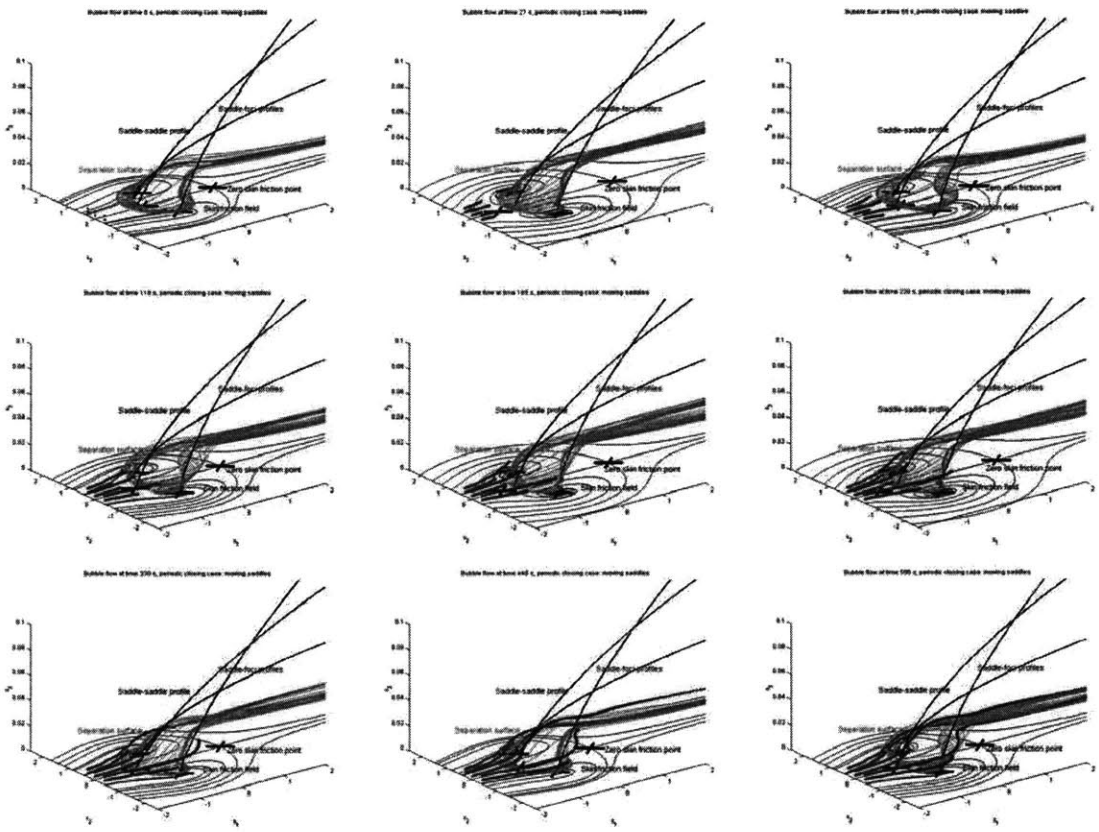

Figure 3-8: Separation on a closing bubble.

In this example, the bubble flow is

$$\begin{aligned} u_1 &= x_3\left(x_1^2\left(1+\frac{1}{2}\cos\frac{t}{10}\right)+x_2^2-1\right)+x_3^2\left(50+10x_1-\frac{1}{6}\left(1+\cos\frac{t}{10}\right)x_3\right), \\ u_2 &= -\left(x_1+\frac{1}{2}\right)x_2x_3+10x_2x_3^2, \\ u_3 &= \frac{1}{4}x_3^2-\frac{1}{2}\left(1+\cos\frac{t}{10}\right)x_1x_3^2-\frac{20}{3}x_3^3. \end{aligned} \tag{3.62}$$

Non-closing bubble If we set α not too large and δ negative, we obtain a non-closing bubble; we give some slides of the motion of the particles in figure 3-8. We also show the surface of separation, which the separating particles will follow (for details, refer to appendix B.4).

The particles arrive near the separation bubble, pass by it, eventually turn around a focus profile, and quickly leave the bubble. Even if this separation pattern does not have a bubble shape, we continue to refer to it as a bubble.

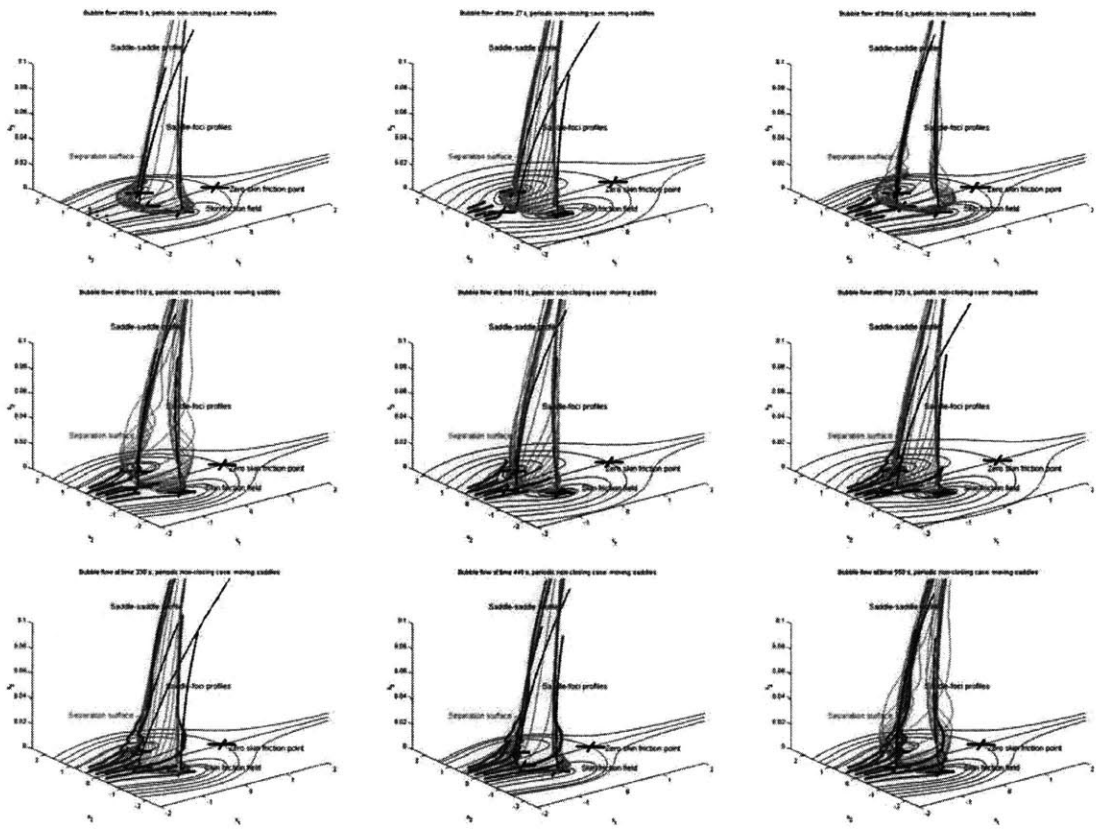

Figure 3-9: Separation on a non-closing bubble.

In this example, the bubble flow is given by

$$\begin{aligned} u_1 &= x_3\left(x_1^2\left(1+\frac{1}{2}\cos\frac{t}{10}\right)+x_2^2-1\right)+x_3^2\left(10-2x_1-\frac{1}{6}\left(1+\cos\frac{t}{10}\right)x_3\right), \\ u_2 &= -\left(x_1+\frac{1}{2}\right)x_2x_3-2x_2x_3^2, \\ u_3 &= \frac{1}{4}x_3^2-\frac{1}{2}\left(1+\cos\frac{t}{10}\right)x_1x_3^2+\frac{4x_3^3}{3}. \end{aligned} \tag{3.63}$$

3.5 Quasiperiodic compressible closing bubble

3.5.1 Method

To obtain a compressible bubble, we will use the incompressible formula obtained earlier and perturb it such that it still satisfies the boundary conditions, and its pressure gradient (obtained from the Navier-Stokes equations) remains regular; but we will not enforce the continuity equation this time. A simple way to do so is to change the first term in u_3 such that the bubble flow becomes

$$\begin{aligned}
u_1 &= x_3\left[\left(\frac{x_1-f_1}{a}\right)^2+\left(\frac{x_2-f_2}{b}\right)^2-1\right] \\
&\quad +x_3^2\left[\alpha+A_{1133}x_1+A_{1233}x_2+\left[\frac{1}{6\nu}\frac{d}{dt}\left(\left(\frac{f_1}{a}\right)^2+\left(\frac{f_2}{b}\right)^2\right)+\frac{ca^2-2}{6a^2}\right]x_3\right], \\
u_2 &= -x_3\left(c(x_1-f_1)(x_2-f_2)+d(x_2-f_2)\right) \\
&\quad +x_3^2\left[\beta+A_{1233}x_1+A_{2233}x_2+\frac{1}{6\nu}\frac{d}{dt}\left(-cf_1f_2+df_2\right)x_3\right], \\
u_3 &= \left(\frac{f_1}{a}+\frac{f_2}{b}\right)x_3^2+\frac{ca^2-2}{2a^2}x_1x_3^2-\frac{A_{1133}+A_{2233}}{3}x_3^3.
\end{aligned} \tag{3.64}$$

We still have to fix the parameters of the flow: For simplicity, we take $f_1 = f_2 = A_{1233} = 0$, $a = 1$, $b = 1$, $c = 1$, $A_{1133} = A_{2233} = \delta = \frac{1}{20}$, $\alpha = 25$ and $\beta = 0$, and we introduce quasiperiodicity within this flow by setting $d = d_0 + \varepsilon \sin(2\pi t/T_1)\sin(2\pi t/T_2)$ where $b_0 = \frac{1}{2}$ and $\varepsilon = \frac{3}{8}$. This unsteadiness is symmetrical and will preserve the saddle-saddles of the bubble, but will make move the saddle-foci in a quasiperiodic way. The two periods will have to be set accurately such that the flow attains typical unsteady behavior. Taking $T_1 = 100s$ and $T_2 = 50\pi s$ guaranties this behavior.

Now that we have the analytic compressible velocity field, we can deduce the separation points and profiles using the concepts developed in chapter 2.

3.5.2 Separation shape

We first determine the density on the wall:

$$\rho(\mathbf{x}, 0, t) = \rho(\mathbf{x}, 0, 0),$$

thus even if the density will not be constant within the whole flow, it will not depend on time on the boundary. Moreover, as this flow is not incompressible, we can not apply the incompressible formulae. We use the compressible ones (2.72).

There are four separation points, defined by

$$\begin{aligned}
\gamma_1 &= \begin{pmatrix} -a \\ 0 \end{pmatrix}, & \gamma_2 &= \begin{pmatrix} a \\ 0 \end{pmatrix}, \\
\gamma_3 &= \begin{pmatrix} -d_0/c \\ -b\sqrt{1-\left(\frac{d_0}{ac}\right)^2} \end{pmatrix}, & \gamma_4 &= \begin{pmatrix} -d_0/c \\ b\sqrt{1-\left(\frac{d_0}{ac}\right)^2} \end{pmatrix}.
\end{aligned} \tag{3.65}$$

The four separation points are fixed, but we have selected the skin friction field such that the instantaneous zero of skin friction at the saddle-foci move substantially. We will show this behavior in a later computation. The zero skin friction points move in a quasiperiodic way, while the real separation points remain steady.

We then calculate the slopes:

$$\begin{aligned}
\mathbf{g}_0^1(t) &= -\begin{pmatrix} \frac{ca^2-4}{a} & 0 \\ 0 & \frac{2(ca^2-1)-d_0 a}{a} \end{pmatrix}^{-1} \left[2\begin{pmatrix} \alpha \\ \beta \end{pmatrix} + 2\delta \begin{pmatrix} -a \\ 0 \end{pmatrix} \right. \\
&\quad \left. -\frac{\varepsilon}{\frac{2\pi}{T_1}+\frac{2\pi}{T_2}} \begin{pmatrix} 0 \\ \frac{2(ca^2-1)-d_0 a}{a} \end{pmatrix} \cos\frac{2\pi t}{T_1} \sin\frac{2\pi t}{T_2} \right], \qquad (3.66a) \\
\mathbf{g}_0^2(t) &= -\begin{pmatrix} \frac{4-ca^2}{a} & 0 \\ 0 & \frac{2(1-ca^2)-d_0 a}{a} \end{pmatrix}^{-1} \left[2\begin{pmatrix} \alpha \\ \beta \end{pmatrix} + 2\delta \begin{pmatrix} a \\ 0 \end{pmatrix} \right. \\
&\quad \left. -\frac{\varepsilon}{\frac{2\pi}{T_1}+\frac{2\pi}{T_2}} \begin{pmatrix} 0 \\ \frac{2(1-ca^2)-d_0 a}{a} \end{pmatrix} \cos\frac{2\pi t}{T_1} \sin\frac{2\pi t}{T_2} \right], \qquad (3.66b) \\
\mathbf{g}_0^3(t) &= -\begin{pmatrix} \frac{(ca^2-4)d_0}{ac} & -\frac{2}{b}\sqrt{1-\left(\frac{d_0}{ac}\right)^2} \\ bc\sqrt{1-\left(\frac{d_0}{ac}\right)^2} & \frac{d_0\left(a^2-\frac{2}{c}\right)}{a^2} \end{pmatrix}^{-1} \left[2\begin{pmatrix} \alpha \\ \beta \end{pmatrix} \right. \\
&\quad \left. +2\delta \begin{pmatrix} -\frac{d_0}{c} \\ -b\sqrt{1-\left(\frac{d_0}{ac}\right)^2} \end{pmatrix} - \frac{\varepsilon}{\frac{2\pi}{T_1}+\frac{2\pi}{T_2}} \begin{pmatrix} 0 \\ \frac{d_0\left(a^2-\frac{2}{c}\right)}{a^2} \end{pmatrix} \cos\frac{2\pi t}{T_1} \sin\frac{2\pi t}{T_2} \right], \qquad (3.66c) \\
\mathbf{g}_0^4(t) &= -\begin{pmatrix} \frac{(ca^2-4)d_0}{ac} & \frac{2}{b}\sqrt{1-\left(\frac{d_0}{ac}\right)^2} \\ -bc\sqrt{1-\left(\frac{d_0}{ac}\right)^2} & \frac{d_0\left(a^2-\frac{2}{c}\right)}{a^2} \end{pmatrix}^{-1} \left[2\begin{pmatrix} \alpha \\ \beta \end{pmatrix} \right. \\
&\quad \left. +2\delta \begin{pmatrix} -\frac{d_0}{c} \\ b\sqrt{1-\left(\frac{d_0}{ac}\right)^2} \end{pmatrix} - \frac{\varepsilon}{\frac{2\pi}{T_1}+\frac{2\pi}{T_2}} \begin{pmatrix} 0 \\ \frac{d_0\left(a^2-\frac{2}{c}\right)}{a^2} \end{pmatrix} \cos\frac{2\pi t}{T_1} \sin\frac{2\pi t}{T_2} \right]. \qquad (3.66d)
\end{aligned}$$

Because of their complexity, we do not evaluate the curvature formulae.

3.5.3 Visualization of separation

We present some slides of the motion of the particles in figure 3-10. We also show the surface of separation, followed by the separating particles.

The particles arrive near the separation bubble, pass by it, then rotate under the bubble. Here we see that some particles leave the bubble immediately, while others are trapped for a while under a bubble shape before leaving it. We refer to this model as a closing-bubble.

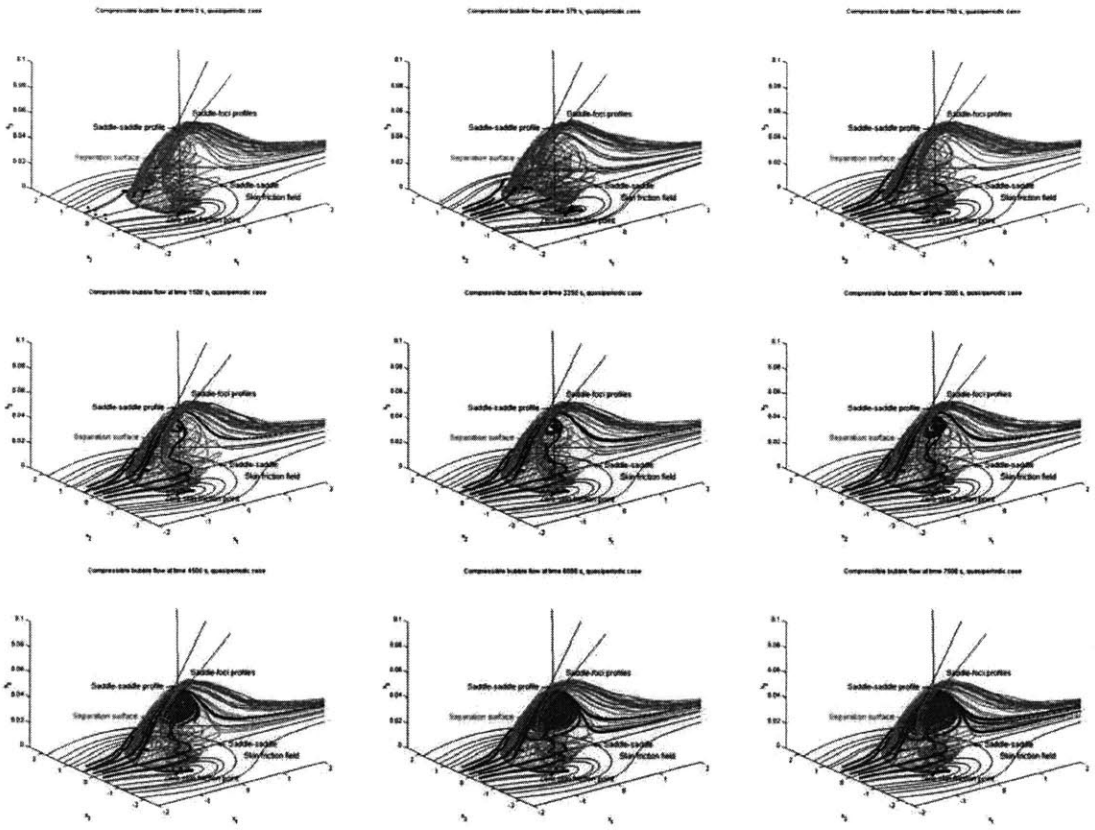

Figure 3-10: Separation under a closing bubble; the flow is compressible and quasiperiodic.

3.6 An example of aperiodic separation

Some of our results could have been predicted from previous work about two-dimensional periodic separation. We will now develop a single example of aperiodic flow which experiments steady closed separation. Nobody has never looked at such a case.

3.6.1 Velocity field

We still use a bubble non-closing model, that we simplify a lot: Let us take a, b and $c > 0$ fixed, $\mathbf{F} = \mathbf{0}$, and $d = e + \varepsilon \cos \omega t^2$ (you will remark that this term will make the flow aperiodic) with e, ε and $\omega > 0$ fixed. Now that we have defined the skin friction field, we set $\beta = 0$, $A_{1233} = 0$

and $A_{1133} = A_{2233} = \delta$ to obtain the velocity field:

$$\begin{aligned} u_1 &= x_3\left(\left(\frac{x_1}{a}\right)^2 + \left(\frac{x_2}{b}\right)^2 - 1\right) + x_3^2\left(\alpha + \delta x_1 + \frac{ca^2-2}{6a^2}x_3\right), \\ u_2 &= -cx_1x_2x_3 - (e + \varepsilon\cos\omega t^2)x_2x_3 + \delta x_2x_3^2, \\ u_3 &= \frac{e+\varepsilon\cos\omega t^2}{2}x_3^2 + \frac{ca^2-2}{2a^2}x_1x_3^2 - \frac{2\delta}{3}x_3^3. \end{aligned} \tag{3.67}$$

For numerical calculation, we will take $a_0 = 1$, $b = 1$, $c = 1$, $e = \frac{1}{2}$, $\alpha = 10$, $\delta = -2$, $\varepsilon = \frac{3}{8}$ and $\omega = \frac{1}{10}$ (the time-scale to observe separation is around $100s$, and over this time the flow is well aperiodic).

3.6.2 Analysis of separation

We remark that

$$\int_{t_0}^{t} \cos\omega\tau^2\, d\tau = G(t) - G(t_0) \text{ is uniformly bounded,}$$

where we do not have an exact value of G but we can calculate a numerical value of G. Then the first condition for separation at $\gamma = \begin{pmatrix} \gamma_1 \\ \gamma_2 \end{pmatrix}$ becomes

$$\begin{aligned} &\limsup_{t\to-\infty}\left|\int_{t_0}^{t}\begin{pmatrix} \left(\frac{\gamma_1}{a}\right)^2 + \left(\frac{\gamma_2}{b}\right)^2 - 1 \\ -c\gamma_1\gamma_2 - (e+\varepsilon\cos\omega\tau^2)\gamma_2 \end{pmatrix} d\tau\right| \\ &= \limsup_{t\to-\infty}\left[|t-t_0|\left|\begin{pmatrix} \left(\frac{\gamma_1}{a}\right)^2 + \left(\frac{\gamma_2}{b}\right)^2 - 1 \\ -c\gamma_1\gamma_2 - e\gamma_2 \end{pmatrix}\right| + \text{ a bounded term}\right] < \infty, \end{aligned}$$

which coincides with the previous steady condition (with d replaced by e). Thus there are four points of separation, defined by

$$\begin{aligned} \gamma_1 &= \begin{pmatrix} -a \\ 0 \end{pmatrix}, & \gamma_2 &= \begin{pmatrix} a \\ 0 \end{pmatrix}, \\ \gamma_3 &= \begin{pmatrix} -e/c \\ -b\sqrt{1-\left(\frac{e}{ac}\right)^2} \end{pmatrix}, & \gamma_4 &= \begin{pmatrix} -e/c \\ b\sqrt{1-\left(\frac{e}{ac}\right)^2} \end{pmatrix}. \end{aligned} \tag{3.68}$$

Thus, even if the flow is aperiodic, the separation points are fixed!

We show (we omit the calculation for brevity) that the slopes are given by

$$\mathrm{g}_0^1 = -\begin{pmatrix} \frac{ca^2-ae-6}{2a} & 0 \\ 0 & \frac{3ca^2-3ae-2}{2a} \end{pmatrix}^{-1} \left[\begin{pmatrix} \alpha \\ 0 \end{pmatrix} + \delta\boldsymbol{\gamma} \right], \tag{3.69a}$$

$$\mathrm{g}_0^2 = -\begin{pmatrix} \frac{-ca^2-ae+6}{2a} & 0 \\ 0 & \frac{-3ca^2-3ae+2}{2a} \end{pmatrix}^{-1} \left[\begin{pmatrix} \alpha \\ 0 \end{pmatrix} + \delta\boldsymbol{\gamma} \right], \tag{3.69b}$$

$$\begin{aligned} \mathrm{g}_0^3 = &-\begin{pmatrix} -\frac{3e}{ca^2} & -\frac{2}{b}\sqrt{1-\left(\frac{e}{ac}\right)^2} \\ cb\sqrt{1-\left(\frac{e}{ac}\right)^2} & -\frac{e}{ca^2} \end{pmatrix}^{-1} \\ &\times \left[\begin{pmatrix} \alpha \\ 0 \end{pmatrix} + \delta\boldsymbol{\gamma} + \varepsilon \begin{pmatrix} 2\left(1-\left(\frac{e}{ac}\right)^2\right) \\ \frac{be}{ca^2}\sqrt{1-\left(\frac{e}{ac}\right)^2} \end{pmatrix} G(t_0) \right], \end{aligned} \tag{3.69c}$$

$$\begin{aligned} \mathrm{g}_0^4 = &-\begin{pmatrix} -\frac{3e}{ca^2} & \frac{2}{b}\sqrt{1-\left(\frac{e}{ac}\right)^2} \\ -cb\sqrt{1-\left(\frac{e}{ac}\right)^2} & -\frac{e}{ca^2} \end{pmatrix}^{-1} \\ &\times \left[\begin{pmatrix} \alpha \\ 0 \end{pmatrix} + \delta\boldsymbol{\gamma} + \varepsilon \begin{pmatrix} 2\left(1-\left(\frac{e}{ac}\right)^2\right) \\ -\frac{be}{ca^2}\sqrt{1-\left(\frac{e}{ac}\right)^2} \end{pmatrix} G(t_0) \right]. \end{aligned} \tag{3.69d}$$

To check the accuracy of these formulae, we track particles. Some slides of the movie we obtain are shown in figure 3-11. We also represent the surface of separation (in green), which the separating particles will follow. These particles arrive near the separation bubble and pass over it: this is a non-closing bubble. You will remark that this time, we do not know the slope analytically but only numerically.

3.7 Conclusion

We have applied the Perry-Chong procedure to 3D flows, which has given us relevant examples of separating flows. We have explored a wide range of possible cases of 3D separation and drawn the most typical shapes of separation. We have also developed some relevant models of a 3D bubble that we have analyzed under steady and unsteady conditions. Finally, we proved the accuracy of the 3D theory of separation developed in chapter 2, and also showed its limits.

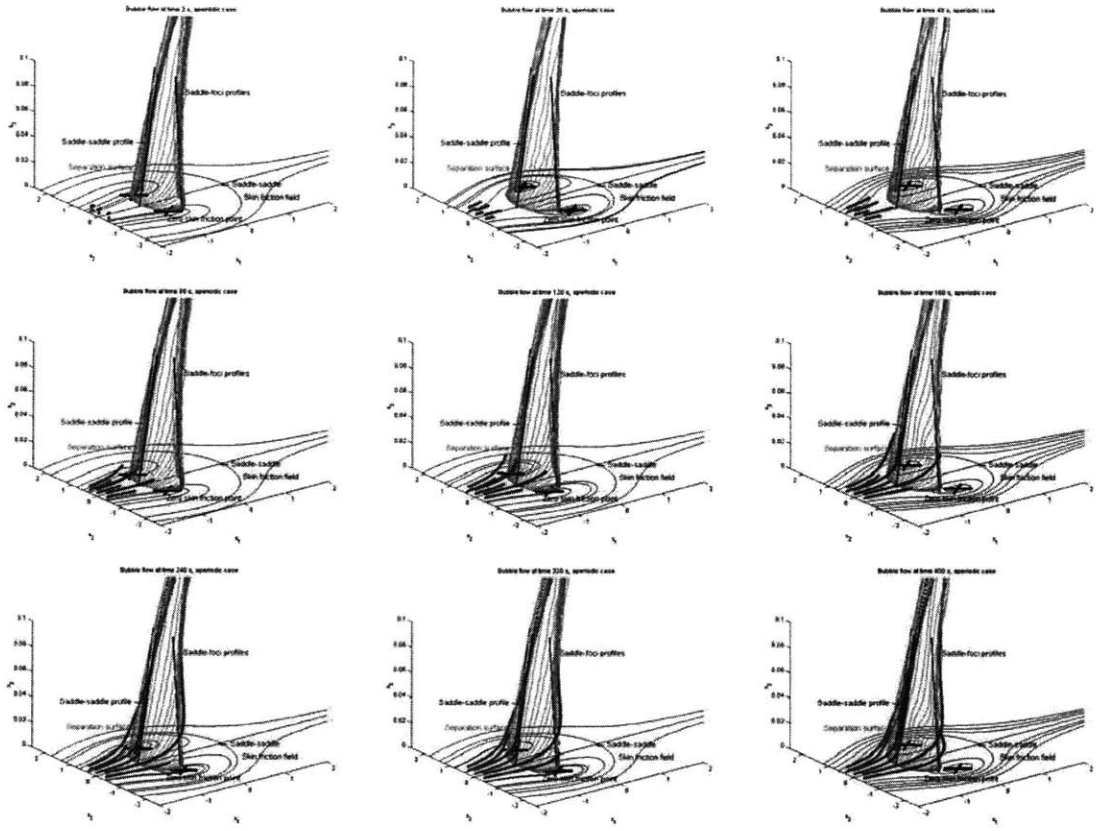

Figure 3-11: Separation over the aperiodic non-closing bubble. Even if the flow is aperiodic, separation is fixed!

Chapter 4

Open problems in the three-dimensional theory

4.1 Introduction

There are some aspects of three-dimensional separation that we have not analyzed. We will here discuss these aspects, as well as ways to study them.

The organization of this chapter is as follows: we discuss effective separation in § 4.2, separation line in § 4.3, the separation surface in § 4.4 and present our conclusions in § 4.5.

4.2 Effective separation points

Strictly speaking, we have not proved the existence of a point satisfying the concept of effective separation (2.21). Doing so would be an important step for further analysis: Firstly, it would make the theory more complete. Secondly, behind this proof is an efficient way to obtain moving separation points, as in the 2D theory (Haller 2002). But so far, this proof has defied our attempts.

4.3 Separation line

4.3.1 Introduction

As shown in figure 4-1, some separation patterns can create separation surfaces: we have given examples of such surfaces (for example in the saddle-saddle case or in the bubble case) in chapter 3. These surfaces are often created by several separation points, but sometimes they are due to open separation. We will determine the formulae giving the intersection between the wall and such surfaces, which we call the separation line. We also explain how to determine the shape of the separation surface.

4.3.2 Incompressible equation

The first step is to derive a formula for the separation line, i.e., the curve along which the separation surface attaches to the $z = 0$ boundary.

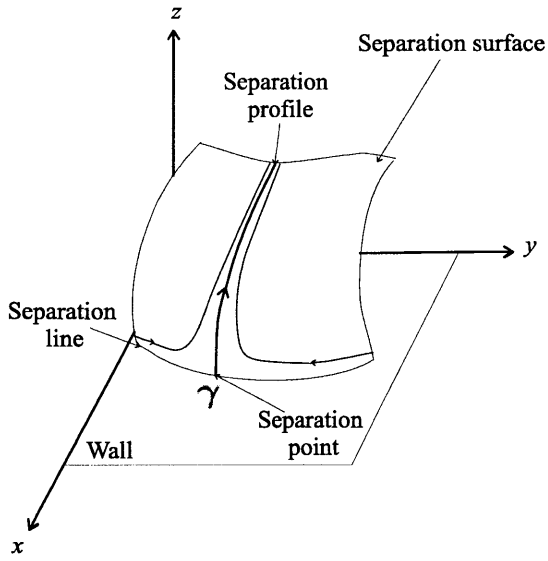

Figure 4-1: Separation surface.

Equation

Writing $\mathbf{A} = \begin{pmatrix} A^x \\ A^y \end{pmatrix}$ for better readibility, we write the equations for particle motion as

$$\begin{aligned} \dot{x} &= zA^x(x,y,z,t), \\ \dot{y} &= zA^y(x,y,z,t), \\ \dot{z} &= zB(x,y,z,t). \end{aligned} \tag{4.1}$$

Here $(A^x, A^y)(x,y,0,t)$ is the instantaneous skin friction field. We seek the separation surface locally in the form $y = p(x,z,t)$.

The intersection of the surface of separation with the wall is called the separation line, and can locally be written as $y = s(x)$ on the wall. Then $p = s$ on the wall, and we can write the separation surface as

$$p(x,z,t) = y = s(x) + zq(x,z,t). \tag{4.2}$$

We can describe any point of the surface of separation with the coordinates x and z:

$$M(x,z,t) = \begin{pmatrix} x \\ s(x) + zq(x,z,t) \\ z \end{pmatrix} = \begin{pmatrix} x \\ s(x) \\ 0 \end{pmatrix} + z \begin{pmatrix} 0 \\ q(x,0,t) \\ 1 \end{pmatrix} + O(z^2).$$

At a point $(x, s(x), 0)$ on the wall, $\frac{\partial y}{\partial z} = q(x,0,t)$ will represent the direction where this point is attracted out from the wall. The points on either side of the separation line will be repelled from the surface of separation in backward time, while this one will remain in the

surface. Thus the vector in the surface will remain uniformly bounded.

Differentiating (4.2) with respect to time:

$$\dot{y} = \dot{x}s'(x) + \dot{z}q(x,z,t) + z(\dot{x}q_x(x,z,t) + \dot{z}q_z(x,z,t) + q_t(x,z,t)), \tag{4.3}$$

and using (4.1) to replace the time derivatives:

$$zA^y = zA^x s' + zBq + z^2 A^x q_x + z^2 B q_z + zq_t,$$

we obtain an equation valid everywhere in the flow:

$$z(A^y - A^x s' - Bq - zA^x q_x - zBq_z - q_t) = 0.$$

Thus for $z > 0$, we have

$$A^y - A^x s' - Bq - zA^x q_x - zBq_z - q_t = 0, \tag{4.4}$$

and, by continuity, this equation is also valid in $z = 0$.

When the flow is incompressible, the continuity equation implies that $C = 0$ on the wall. Then setting $z = 0$ yields

$$q_t(x,0,t) = A^y(x,s(x),0,t) - A^x(x,s(x),0,t)s'(x). \tag{4.5}$$

Then, by integrating (4.5) in time, we obtain an expression for q:

$$q(x,0,t) = q(x,0,t_0) + \int_{t_0}^{t} \left[A^y(x,s(x),0,s) - A^x(x,s(x),0,s)s'(x)\right]\, ds.$$

Because q must remain uniformly bounded in backward time, we finally obtain the formula

$$\limsup_{t\to-\infty} \left| \int_{t_0}^{t} \left[A^y(x,s(x),0,t) - s'(x)A^x(x,s(x),0,t)\right]\, dt \right| < \infty \tag{4.6}$$

for the separation line $y = s(x)$.

Necessary condition

The previous formula is not sufficient to determine the separation line among all functions satisfying (4.6), thus we need another condition. We believe that the separation line is an averaged skin friction line that attracts nearby averaged skin friction trajectories.

4.3.3 Special cases

Steady flows

In the steady case, the equation (4.6) simplifies to

$$s'(x) = \frac{A^y(x,s(x))}{A^x(x,s(x))}, \tag{4.7}$$

and could have also been determined by considering that along the separation line (or any other skin friction line) $s'(x) = \dfrac{\partial y}{\partial x} = \dfrac{\partial y}{\partial t}\dfrac{\partial t}{\partial x} = \dfrac{A^y}{A^x}$, provided that $A^x(x, s(x)) \neq 0$. If it vanishes, we can reparametrize the separation line in y rather than x. If both A^x and A^y vanish, we are at a zero skin friction point, where we can apply the separation profile theory.

Time-periodic flows

When the skin friction field is periodic in time, $A^y - s'A^x$ is periodic too, thus requiring the integral of this function to be bounded is equivalent to requiring its mean to be zero. Then (4.6) simplifies to

$$\bar{A}^y(x, s(x), .) - s'(x)\bar{A}^x(x, s(x), .) = 0, \tag{4.8}$$

where $\bar{h}$ refers to the temporal mean of h. We thus obtain

$$s'(x) = \frac{\bar{A}^y(x, s(x), .)}{\bar{A}^x(x, s(x), .)},$$

which is satisfied by any trajectory of the skin friction field.

More generally, we can reparametrize these trajectories and show that $\mathbf{X} = \begin{pmatrix} x \\ y \end{pmatrix}$ satisfies the autonomous equation

$$\mathbf{X}' = \bar{\boldsymbol{\tau}}(\mathbf{X}, .)$$

along separation lines.

4.3.4 Quasi-periodic flows

We obtain the same type of formulae as in the periodic case, except that simple averaging is replaced by multi-frequency averaging.

4.4 Separation surface

We now have formulae for separation lines; understanding separation surfaces will require new ideas. An additional challenge will be the visualization of these surfaces.

4.5 Conclusions

Even if the analysis of three-dimensional closed separation is completed and validated, some difficulties remain: there are still these fully three-dimensional phenomena of effective separation and separation surface which have to be fully analyzed and understood.

Conclusion

In this thesis, we analyzed flow separation from a kinematic point of view. Despite the complexity of the analysis, the results we obtained are simple and physically appealing.

We first verified the two-dimensional theory of Haller (2002) on an unsteady example: separation over a pitching airfoil. We have shown how the theory predicts the location and the shape of separation.

After a brief review of the prior work on three-dimensional separation, we extended the kinematic separation theory of Haller (2002) to three-dimensional flows with closed separation. We then introduced model expansions of the Navier-Stokes equations and validated the three-dimensional theory on these models. The three-dimensional models we derived are of interest in their own right.

Finally, we outlined the theoretical difficulties in identifying fully three-dimensional phenomena, such as separation lines and surfaces.

Future work on 3D separation should involve the analysis of separation surfaces, the control of separation, and the use of separation theory in improving the aerodynamical performance of vehicles such as cars and airplanes.

Appendix A

Proofs of the 3D theory

A.1 Slope formula

After substituting formula (2.16) for $\mathbf{g}(s)$ in (2.24), we obtain

$$\mathbf{g}_1(t) = \frac{\mathbf{g}_1(t_0)\rho^2(t)}{\rho^2(t_0)} + \rho^2(t)\int_{t_0}^{t}\left[\mathbf{p}(s,t_0) + \mathbf{Q}(s,t_0,t)\mathbf{g}_0(t_0) - \frac{(b_{\mathbf{x}}(s)\cdot\mathbf{g}_0(t_0))\,\mathbf{g}_0(t_0)}{\rho^2(t_0)}\right]ds,$$

with $\mathbf{p}(s,t_0)$ and $\mathbf{Q}(s,t_0,t)$ defined in (2.26):

$$\begin{aligned}\mathbf{p}(s,t_0) &= \frac{\mathbf{a}_z(s)}{\rho^2(s)} + \frac{\mathbf{a}_{\mathbf{x}}(s) - b_z(s)\mathbf{I}}{\rho(s)}\int_{t_0}^{s}\frac{\mathbf{a}(r)}{\rho(r)}\,dr - b_{\mathbf{x}}(s)\left(\int_{t_0}^{s}\frac{\mathbf{a}(r)}{\rho(r)}\,dr\right)^2,\\ \mathbf{Q}(s,t_0,t) &= \frac{1}{\rho(t_0)}\left[\frac{\mathbf{a}_{\mathbf{x}}(s) - b_z(s)\mathbf{I}}{\rho(s)} - \int_{t_0}^{s}\frac{\mathbf{a}(r)\otimes b_{\mathbf{x}}(s) + b_{\mathbf{x}}(s)\cdot\mathbf{a}(r)\mathbf{I}}{\rho(r)}\,dr\right],\end{aligned}$$

with the diadic product $[\mathbf{a}\otimes b_{\mathbf{x}}]_{ij} = (\mathbf{a})_i\,(b_{\mathbf{x}})_j$.

We first observe that for material lines emanating from the separation point $(\boldsymbol{\gamma},0)$ with slopes differing from the slope of the separation profile, $|\mathbf{g}_1(t_0)|$ will tend to infinity as $t\to-\infty$. In other words, for any small vector $\boldsymbol{\varepsilon}\neq\mathbf{0}$, we have

$$\lim_{t\to-\infty}\left|\int_{t_0}^{t}\left[\mathbf{p}(s,t_0) + \mathbf{Q}(s,t_0,t)\,[\mathbf{g}_0(t_0)+\boldsymbol{\varepsilon}] - \frac{b_{\mathbf{x}}(s)\cdot(\mathbf{g}_0(t_0)+\boldsymbol{\varepsilon})\,(\mathbf{g}_0(t_0)+\boldsymbol{\varepsilon})}{\rho^2(t_0)}\right]d\tau\right| = \infty.$$

On the separation profile itself, however, $\mathbf{g}_1(t)$ remains bounded, i.e.,

$$\limsup_{t\to-\infty}\left|\int_{t_0}^{t}\left[\mathbf{p}(s,t_0) + \mathbf{Q}(s,t_0,t)\mathbf{g}_0(t_0) - \frac{(b_{\mathbf{x}}(s)\cdot\mathbf{g}_0(t_0))\,\mathbf{g}_0(t_0)}{\rho^2(t_0)}\right]d\tau\right| < \infty. \tag{A.1}$$

Comparing these two expressions we obtain that

$$\lim_{t\to-\infty}\left|\int_{t_0}^{t}\left[\mathbf{Q}(s,t_0,t) - \frac{b_{\mathbf{x}}(s)\cdot(\mathbf{g}_0(t_0)+\boldsymbol{\varepsilon})\,\mathbf{I} + \mathbf{g}_0(t_0)\otimes b_{\mathbf{x}}(s)}{\rho^2(t_0)}\right]\boldsymbol{\varepsilon}\,ds\right| = \infty. \tag{A.2}$$

By assumptions (2.6)–(2.7), we can write

$$\limsup_{t\to-\infty}\left\|\int_{t_0}^{t}\frac{b_{\mathbf{x}}(s)\cdot(\mathbf{g}_0(t_0)+\varepsilon)\,\mathbf{I}+\mathbf{g}_0(t_0)\otimes b_{\mathbf{x}}(s)}{\rho^2(t_0)}\,ds\right\|\le\frac{2\,|\mathbf{g}_0(t_0)|+|\varepsilon|}{\rho^2(t_0)}\limsup_{t\to-\infty}\left|\int_{t_0}^{t}w_{\mathbf{x}z}(\boldsymbol{\gamma},0,s)\,ds\right|<\infty, \tag{A.3}$$

therefore (A.2) simplifies to

$$\lim_{t\to-\infty}\left|\int_{t_0}^{t}\mathbf{Q}(s,t_0,t)\varepsilon\;ds\right|=\infty, \tag{A.4}$$

which holds for all nonzero ε. Equivalently, we have

$$\lim_{t\to-\infty}\left\|\int_{t_0}^{t}\left[\frac{\mathbf{a}_{\mathbf{x}}(s)-b_z(s)\mathbf{I}}{\rho(s)}-\int_{t_0}^{s}\frac{\mathbf{a}(r)\otimes b_{\mathbf{x}}(s)+b_{\mathbf{x}}(s)\cdot\mathbf{a}(r)\mathbf{I}}{\rho(r)}\,dr\right]\,ds\right\|=\infty, \tag{A.5}$$

as claimed in the necessary separation condition (2.20).

To prove formula (2.25), observe that (A.4) is equivalent to

$$\lim_{t\to-\infty}\left|\left[\int_{t_0}^{t}\mathbf{Q}(s,t_0,t)\;ds\right]\varepsilon\right|=\infty, \tag{A.6}$$

for all nonzero vector $\varepsilon\in\mathbb{R}^2$. Based on this, we want to argue that the matrix

$$\mathbf{K}(t,t_0)=\int_{t_0}^{t}\mathbf{Q}(s,t_0,t)\;ds$$

is invertible for large enough t.

Suppose the contrary. Then, for arbitrary large t, the kernel of $\mathbf{K}(t,t_0)$ is nonempty. Let $\varepsilon^*(t)\in\ker\mathbf{K}(t,t_0)\cap S^1$, where S^1 denotes the unit circle in $\mathbb{R}^2$. Any sequence of times

$$\{t_n\}_{n=1}^{\infty},\qquad\lim_{n\to+\infty}t_n=-\infty,$$

then gives rise to a bounded infinite sequence of vectors $\{\varepsilon^*(t_n)\}_{n=1}^{\infty}$, which has a convergent subsequence $\{\varepsilon^*(t_{n_k})\}_{k=1}^{\infty}$ with

$$\lim_{k\to\infty}\varepsilon^*(t_{n_k})=\varepsilon^*_{\infty}\in S^1,$$

by the compactness of S^1. Then,

$$0=\lim_{k\to+\infty}\left[\int_{t_0}^{t_{n_k}}\mathbf{Q}(s,t_0,t_{n_k})\;ds\right]\varepsilon^*(t_{n_k})=\lim_{k\to+\infty}\left[\int_{t_0}^{t_{n_k}}\mathbf{Q}(s,t_0,t_{n_k})\;ds\right]\varepsilon^*_{\infty},$$

which contradicts (A.6). Thus $\mathbf{K}(t,t_0)$ is invertible for large enough t. Also note that, by (A.4),

$$|\mathbf{K}(t,t_0)\varepsilon|^2=\left\langle\varepsilon,\mathbf{K}^T(t,t_0)\mathbf{K}(t,t_0)\varepsilon\right\rangle\to\infty,\qquad t\to-\infty,$$

for all $\varepsilon \in \mathbb{R}^2$ with $|\varepsilon| = 1$. Then an argument similar to the above implies

$$\lim_{t \to -\infty} \lambda_{\min} \left[\mathbf{K}^T(t, t_0) \mathbf{K}(t, t_0) \right] = \infty, \tag{A.7}$$

where $\lambda_{\min} \left[\mathbf{A}^T \mathbf{A} \right]$ denotes the smallest eigenvalue of the symmetric matrix $\mathbf{A}^T \mathbf{A}$.

Next we want to argue that

$$\lim_{t \to -\infty} \| \mathbf{K}^{-1}(t, t_0) \| = 0. \tag{A.8}$$

Select $\mathbf{e} \in \mathbb{R}^2 - \{\mathbf{0}\}$, and let

$$\hat{\varepsilon}(t) = \mathbf{K}^{-1}(t, t_0) \mathbf{e}.$$

Then

$$|\mathbf{e}|^2 = \langle \mathbf{K}(t, t_0) \hat{\varepsilon}(t), \mathbf{K}(t, t_0) \hat{\varepsilon}(t) \rangle = \left\langle \hat{\varepsilon}(t), \mathbf{K}^T(t, t_0) \mathbf{K}(t, t_0) \hat{\varepsilon}(t) \right\rangle \geq \lambda_{\min}(\mathbf{K}^T(t, t_0) \mathbf{K}(t, t_0)) \, |\hat{\varepsilon}(t)|^2 ,$$

thus (A.7) implies

$$\lim_{t \to -\infty} |\hat{\varepsilon}(t)| \leq |\mathbf{e}| \lim_{t \to -\infty} \frac{1}{\sqrt{\lambda_{\min}(\mathbf{K}^T(t, t_0) \mathbf{K}(t, t_0))}} = 0. \tag{A.9}$$

Because $\mathbf{e}$ was arbitrary, the expression (A.9) establishes (A.8).

Observe that (A.3) simplifies the boundedness condition (A.1) to

$$\limsup_{t \to -\infty} \left| \int_{t_0}^{t} \left[\mathbf{p}(s, t_0) + \mathbf{Q}(s, t_0, t) \mathbf{g}_0(t_0) \right] ds \right| < \infty.$$

Then the vector

$$\mathbf{q}(t) = \int_{t_0}^{t} \left[\mathbf{p}(s, t_0) + \mathbf{Q}(s, t_0, t) \mathbf{g}_0(t_0) \right] ds$$

is uniformly bounded for all $t < t_0$, thus there exists $C_0 > 0$ such that

$$|\mathbf{q}(t)| \leq C_0, \qquad t < t_0.$$

Multiplication by $\mathbf{K}^{-1}(t_0, t)$ gives

$$\left[\int_{t_0}^{t} \mathbf{Q}(s, t_0, t) \, ds \right]^{-1} \mathbf{q}(t) = \left[\int_{t_0}^{t} \mathbf{Q}(\tau, t_0, t) \, d\tau \right]^{-1} \int_{t_0}^{t} \mathbf{p}(s, t_0) \, ds + \mathbf{g}_0(t_0),$$

which in turn leads to

$$\mathbf{g}_0(t_0) = - \left[\int_{t_0}^{t} \mathbf{Q}(\tau, t_0, t) \, d\tau \right]^{-1} \int_{t_0}^{t} \mathbf{p}(s, t_0) \, ds + \left[\int_{t_0}^{t} \mathbf{Q}(s, t_0, t) \, ds \right]^{-1} \mathbf{q}(t). \tag{A.10}$$

Note that

$$\lim_{t \to -\infty} \left| \left[\int_{t_0}^{t} \mathbf{Q}(s, t_0, t) \, ds \right]^{-1} \mathbf{q}(t) \right| \leq \lim_{t \to -\infty} \| \mathbf{K}^{-1}(t, t_0) \| \, |\mathbf{q}(t)| \leq C_0 \lim_{t \to -\infty} \| \mathbf{K}^{-1}(t, t_0) \| = 0$$

by (A.8), thus (A.10) implies (2.25).

A.2 Incompressible orders of separation

Computing the $O(z, z^2, z^3)$ terms in the incompressible separation equation (2.41) leads to the set of equations

$$\dot{\mathbf{g}}_1 = (\mathbf{a}_\mathbf{x} - c\mathbf{I})\,\mathbf{g}_0 + \mathbf{a}_z, \tag{A.11}$$

$$\dot{\mathbf{g}}_2 = \mathbf{a}_{zz} + 2\,(\mathbf{a}_{\mathbf{x}z} - c_z\mathbf{I})\,\mathbf{g}_0 + [(\mathbf{a}_{\mathbf{xx}} - 2c_\mathbf{x}\cdot\mathbf{I})\,\mathbf{g}_0]\,\mathbf{g}_0 + 2\,(\mathbf{a}_\mathbf{x} - 2c\mathbf{I})\,\mathbf{g}_1, \tag{A.12}$$

$$\begin{aligned}\dot{\mathbf{g}}_3 = {} & \mathbf{a}_{zzz} + 3\,[\mathbf{a}_{\mathbf{x}zz} - c_{zz}\mathbf{I}]\,\mathbf{g}_0 + [(\mathbf{a}_{\mathbf{xxx}}\mathbf{g}_0 - 3c_{\mathbf{xx}}\mathbf{g}_0\cdot\mathbf{I})\,\mathbf{g}_0]\,\mathbf{g}_0 \\ & +3\,[(\mathbf{a}_{\mathbf{xx}z} - 2c_{\mathbf{x}z}\cdot\mathbf{I})\,\mathbf{g}_0]\,\mathbf{g}_0 + 6\,[(\mathbf{a}_{\mathbf{xx}} - 3c_\mathbf{x}\cdot\mathbf{I})\,\mathbf{g}_0]\,\mathbf{g}_1 + 6\,(\mathbf{a}_{\mathbf{x}z} - 2c_z\mathbf{I})\,\mathbf{g}_1 + 3\,(\mathbf{a}_\mathbf{x} - 3c\mathbf{I})\,\mathbf{g}_2.\end{aligned} \tag{A.13}$$

We note the following incompressibility relations derived from (2.40):

$$\operatorname{Tr}\mathbf{a}_\mathbf{x} + 2c = 0, \qquad \operatorname{Tr}\mathbf{a}_{\mathbf{x}z} + 3c_z = 0, \qquad (\operatorname{Tr}\mathbf{a}_\mathbf{x})_\mathbf{x} + 2c_\mathbf{x} = 0,$$

$$(\operatorname{Tr}\mathbf{a}_\mathbf{x})_{\mathbf{xx}} + 2c_{\mathbf{xx}} = 0, \qquad (\operatorname{Tr}\mathbf{a}_{\mathbf{x}z})_\mathbf{x} + 3c_{\mathbf{x}z} = 0, \qquad \operatorname{Tr}\mathbf{a}_{\mathbf{x}zz} + 4c_{zz} = 0,$$

$$(\operatorname{Tr}\mathbf{a}_\mathbf{x})_{\mathbf{xxx}} + 2c_{\mathbf{xxx}} = 0,\ (\operatorname{Tr}\mathbf{a}_{\mathbf{x}z})_{\mathbf{xx}} + 3c_{\mathbf{xx}z} = 0,\ (\operatorname{Tr}\mathbf{a}_{\mathbf{x}zz})_\mathbf{x} + 4c_{\mathbf{x}zz} = 0,\ \operatorname{Tr}\mathbf{a}_{\mathbf{x}zzz} + 5c_{zzz} = 0. \tag{A.14}$$

We first integrate equation (A.11), then substitute formula (2.42) and use the first equation in (A.14) to obtain

$$\begin{aligned}\mathbf{g}_1(t) = \mathbf{g}_1(t_0) + \int_{t_0}^{t} \Bigg[& \mathbf{a}_z(\tau) + \left(\mathbf{a}_\mathbf{x}(\tau) + \frac{1}{2}\mathbf{I}\operatorname{Tr}\mathbf{a}_\mathbf{x}(\tau)\right)\mathbf{g}_0(t_0) \\ & + \left(\mathbf{a}_\mathbf{x}(\tau) + \frac{1}{2}\mathbf{I}\operatorname{Tr}\mathbf{a}_\mathbf{x}(\tau)\right)\int_{t_0}^{\tau}\mathbf{a}(s)\,ds\Bigg]\,d\tau\end{aligned} \tag{A.15}$$

for the first order term in the expansion for the incompressible separation profile. Because $\mathbf{g}_1(t)$ remains bounded in backward time at a fixed separation point, we can use the argument of appendix A.1 to derive (2.47) from (A.15). The expression (2.47) can also be obtained by setting $b(\tau) \equiv 0$ and $b_z(\tau) = c(\tau)$ in its compressible counterpart (2.25).

Next we integrate (A.12) and observe that the boundedness of $\mathbf{g}_2(t)$ implies the boundedness of the integral

$$\begin{aligned}\int_{t_0}^{t} & \left[\mathbf{a}_{zz}(\tau) + 2\left[\mathbf{a}_{\mathbf{x}z}(\tau) + \frac{1}{3}\mathbf{I}\operatorname{Tr}\mathbf{a}_{\mathbf{x}z}(\tau)\right]\mathbf{g}_0 + [[\mathbf{a}_{\mathbf{xx}}(\tau) + (\operatorname{Tr}\mathbf{a}_\mathbf{x}(\tau))_\mathbf{x}\cdot\mathbf{I}]\,\mathbf{g}_0(\tau)]\,\mathbf{g}_0(\tau)\right. \\ & \left.+2\,[\mathbf{a}_\mathbf{x}(\tau) + \mathbf{I}\operatorname{Tr}\mathbf{a}_\mathbf{x}(\tau)]\,\mathbf{g}_1(\tau)]\,d\tau\right.\end{aligned} \tag{A.16}$$

for all $t \le t_0$. Invoking the arguments of appendix A.1, then substituting (A.15) and using (A.14) leads to the curvature of separation (2.48).

We now integrate (A.13) and use the incompressibility conditions in (A.14) to find that the

integral

$$\int_{t_0}^{t} \left[\mathbf{a}_{zzz} + 3\left[\mathbf{a}_{\mathbf{x}zz} + \frac{1}{4}\mathbf{I}\,\mathrm{Tr}\,\mathbf{a}_{\mathbf{x}zz}\right]\mathbf{g}_0 + \left[\left(\mathbf{a}_{\mathbf{x}\mathbf{x}\mathbf{x}}\mathbf{g}_0 + \frac{3}{2}(\mathrm{Tr}\,\mathbf{a}_{\mathbf{x}})_{\mathbf{x}\mathbf{x}}\mathbf{g}_0 \cdot \mathbf{I}\right)\mathbf{g}_0\right]\mathbf{g}_0 \right.$$
$$+3\left[\left(\mathbf{a}_{\mathbf{x}\mathbf{x}z} + \frac{2}{3}(\mathrm{Tr}\,\mathbf{a}_{\mathbf{x}z})_{\mathbf{x}} \cdot \mathbf{I}\right)\mathbf{g}_0\right]\mathbf{g}_0 + 6\left[\left(\mathbf{a}_{\mathbf{x}\mathbf{x}} + \frac{3}{2}(\mathrm{Tr}\,\mathbf{a}_{\mathbf{x}})_{\mathbf{x}} \cdot \mathbf{I}\right)\mathbf{g}_0\right]\mathbf{g}_1$$
$$\left. +6\left(\mathbf{a}_{\mathbf{x}z} + \frac{2}{3}\,\mathrm{Tr}\,\mathbf{a}_{\mathbf{x}z}\mathbf{I}\right)\mathbf{g}_1 + 3\left(\mathbf{a}_{\mathbf{x}} + \frac{3}{2}\,\mathrm{Tr}\,\mathbf{a}_{\mathbf{x}}\mathbf{I}\right)\mathbf{g}_2\right](\tau)\,d\tau \tag{A.17}$$

must be bounded for all $t \leq t_0$. Proceeding again as above, we use this boundedness to obtain (2.49).

A.3 Sharp separation

Here we prove a sufficient criterion for fixed sharp separation in incompressible flows under conditions (2.52), (2.53a) and (2.53b). Beyond these conditions, we assume that the velocity field as well as its first and second derivatives remain uniformly bounded for all times at the separation point. We will establish the existence of a unique material line that acts as an unstable manifold for the separation point $(\boldsymbol{\gamma}, 0)$.

We start by fixing $\boldsymbol{\gamma}$ and introducing the time-dependent coordinate change

$$\mathbf{q} = \mathbf{x} - \boldsymbol{\gamma} - z\left(\mathbf{g}_0(t) + z\mathbf{g}_1(t)\right), \tag{A.18}$$

with $\mathbf{g}_0(t)$ and $\mathbf{g}_1(t)$ satisfying (2.42) and (A.15). Note that this change of coordinates transforms the $\mathbf{x} = \boldsymbol{\gamma}$ coordinate axis into the new $\mathbf{q} = \mathbf{0}$ axis that has a quadratic tangency with the candidate unstable manifold (separation profile) for all times. We obtain

$$\begin{aligned}
\dot{\mathbf{q}} &= \dot{\mathbf{x}} - \dot{z}\mathbf{g}_0 - z\dot{\mathbf{g}}_0 - 2z\dot{z}\mathbf{g}_1 - z_1^2\dot{\mathbf{g}}_1 \\
&= z\mathbf{a}_{\mathbf{x}}(t)\mathbf{q} + \mathbf{m}_1(\mathbf{q}, z, \mathbf{g}_k, t)z^3 + \mathbf{m}_2(\mathbf{q}, z, \mathbf{g}_k, t)z\mathbf{q}^2 + m_3(\mathbf{q}, z, \mathbf{g}_k, t)z^2\mathbf{q}, \\
\\
\dot{z} &= z^2 C(\boldsymbol{\gamma} + z\mathbf{g}_0 + z_1^2\mathbf{g} + \mathbf{q}, z, t) \\
&= z^2\left[c(t) + zm_4(\mathbf{q}, z, \mathbf{g}_k, t) + \mathbf{q} \cdot \mathbf{m}_5(\mathbf{q}, z, \mathbf{g}_k, t)\right],
\end{aligned} \tag{A.19}$$

as new equations of motion for fluid particles, with appropriate smooth functions m_i, and with $\mathbf{g}_k$ referring to $\mathbf{g}_0$ and $\mathbf{g}_1$. The $O(z)$ and $O(z^2)$ terms in the $\dot{\mathbf{q}}$ equation vanish precisely because we chose $\mathbf{g}_0(t)$ and $\mathbf{g}_1(t)$ in our coordinate transformation to satisfy equations (2.42) and (A.15). Most importantly, $\mathbf{g}_0(t)$ and $\mathbf{g}_1(t)$ remain bounded because $\boldsymbol{\gamma}$ is a fixed separation point; as a result, all terms in the $\dot{\mathbf{q}}$ equation remain bounded for all times.

We define the "flower-cone"

$$Q = \{(\mathbf{q}, z) \mid \|\mathbf{q}\|^{\alpha} \leq z, \quad 0 \leq z \leq \beta\},$$

where α and β are positive constants to be selected below (figure A-1).

By our boundedness assumption on the velocity field, we can select a large enough constant

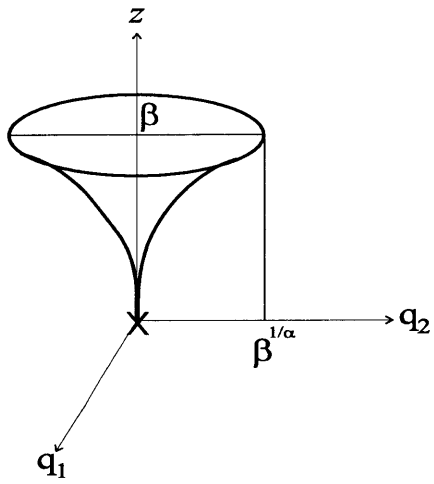

Figure A-1: The definition of the flower-cone Q.

$K > 0$ such that

$$|m_i(\mathbf{q}, z, \mathbf{g}_k, t)| \leq K, \qquad (\mathbf{q}, z) \in Q, \quad t \in \mathbb{R}. \tag{A.20}$$

Let us consider now the $z = \beta$ boundary of the flower-cone Q. Along this boundary, we have

$$\begin{aligned} \dot{z}|_{z=\beta} &= \beta^2 \left[c(t) + \beta m_4(\mathbf{q}, \beta, \mathbf{g}_k, t) + \mathbf{q} \cdot \mathbf{m}_5(\mathbf{q}, \beta, \mathbf{g}_k, t)\right] \\ &\geq \beta^2 \left[c(t) - K\left(\beta + \beta^\alpha\right)\right] > 0, \end{aligned}$$

provided that

$$c(t) > K\left(\beta + \beta^\alpha\right),$$

or, equivalently,

$$w_{zz}(\gamma, 0, t) > 2K\left(\beta + \beta^\alpha\right). \tag{A.21}$$

Therefore, solutions intersecting the $z = \beta$ boundary of Q leave Q immediately if the inequality (A.21) holds for all times (figure A-2).

Next, we consider the $\mathbf{q} = z^{1/\alpha} e^{i\theta}$ boundary of the flower-cone Q, where we define $e^{i\theta} = \begin{pmatrix} \cos\theta \\ \sin\theta \end{pmatrix}$; thus we have

$$\begin{aligned} \dot{\mathbf{q}}|_{\mathbf{q}=z^{1/\alpha}e^{i\theta}} &= z^{1+1/\alpha} a_x(t) e^{i\theta} + \mathbf{m}_1(\mathbf{q}, z, \mathbf{g}_k, t) z^3 + \mathbf{m}_2(\mathbf{q}, z, \mathbf{g}_k, t) z^{1+2/\alpha} e^{i2\theta} + m_3(\mathbf{q}, z, \mathbf{g}_k, t) z^{2+1/\alpha} e^{i\theta} \\ &\leq z^{1+1/\alpha} \left[\|a_x\| + K\left(\beta^{2-1/\alpha} + \beta^{1/\alpha} + \beta\right)\right], \end{aligned} \tag{A.22}$$

$$\begin{aligned} \dot{z}|_{\mathbf{q}=z^{1/\alpha}e^{i\theta}} &= z^2 \left[c(t) + z m_4(\mathbf{q}, z, \mathbf{g}_k, t) + z^{1/\alpha} e^{i\theta} \cdot \mathbf{m}_5(\mathbf{q}, z, \mathbf{g}_k, t)\right] \\ &\geq z^2 \left[c(t) - K\left(\beta + \beta^\alpha\right)\right], \end{aligned}$$

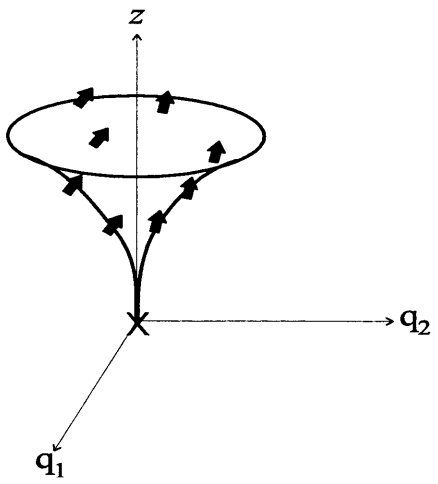

Figure A-2: Fluid particles entering and leaving the flower-cone Q.

and we want the flow to enter the flower-cone on this surface, which amounts to requiring

$$\dot{z}|_{\mathbf{q}=z^{1/\alpha}e^{i\theta}} > \alpha \left\|\mathbf{q}\right\|^{\alpha-1} \left\|\dot{\mathbf{q}}|_{\mathbf{q}=\alpha z e^{i\theta}}\right\| \text{ for any } \theta.$$

Provided that

$$c(t) - K\left(\beta+\beta^{\alpha}\right) > \alpha\left[\|a_x\| + K\left(\beta^{2-1/\alpha}+\beta^{1/\alpha}+\beta\right)\right],$$

or, equivalently,

$$w_{zz}(\boldsymbol{\gamma},0,t) > 2\alpha\left[\|a_x\| + K\left(\beta^{2-1/\alpha}+\beta^{1/\alpha}+2\beta+\beta^{\alpha}\right)\right], \tag{A.23}$$

the above entry is satisfied.

Both (A.21) and (A.23) hold if we have

$$w_{zz}(\boldsymbol{\gamma},0,t) > \max\left(2K\left(\beta+\beta^{\alpha}\right), 2\alpha\left[M + K\left(\beta^{2-1/\alpha}+\beta^{1/\alpha}+2\beta+\beta^{\alpha}\right)\right]\right),$$

where we used the fact that $\operatorname{Tr} a_x \equiv -w_{zz}(\boldsymbol{\gamma},0,t)$ by incompressibility. By conditions (2.53a), we can satisfy this last inequality by choosing the α and β parameters of the cone Q so that

$$\max\left(2K\left(\beta+\beta^{\alpha}\right), 2\alpha\left[M + K\left(\beta^{2-1/\alpha}+\beta^{1/\alpha}+2\beta+\beta^{\alpha}\right)\right]\right) < c_0.$$

A possible choice is

$$\alpha = \frac{c_0}{6M} < 1, \qquad \beta = \min\left(\frac{c_0}{5K}, \frac{M}{4K}, \sqrt{\frac{M}{K}}, \left(\frac{M}{K}\right)^{\frac{6M}{c_0}}\right), \tag{A.24}$$

for which we conclude that solutions intersecting the $\|\mathbf{q}\|^\alpha = z$ boundary of the flower-cone Q enter Q immediately by the estimates (A.22) (cf. figure A-2).

Based on the above observations, we conclude that under conditions (A.21) and (A.23), the extended equations of particle motion

$$\begin{aligned} \dot{\mathbf{q}} &= z\mathbf{a}_\mathbf{x}(t)\mathbf{q} + \mathbf{m}_1(\mathbf{q}, z, \mathbf{g}_k, t)z^3 + \mathbf{m}_2(\mathbf{q}, z, \mathbf{g}_k, t)z\mathbf{q}^2 + m_3(\mathbf{q}, z, \mathbf{g}_k, t)z^2\mathbf{q}, \\ \dot{z} &= z^2\left[c(t) + zm_4(\mathbf{q}, z, \mathbf{g}_k, t) + \mathbf{q}\cdot\mathbf{m}_5(\mathbf{q}, z, \mathbf{g}_k, t)\right], \\ \dot{t} &= 1 \end{aligned} \tag{A.25}$$

have the following properties on the closed set $\mathcal{Q} = Q \times \mathbb{R}$:

1. The set of initial particle positions $(\mathbf{q}_0, z_0, t_0)$ that immediately leave $\mathcal{Q}$ in backward time is given by $W^{im} = \{(\mathbf{q}, z, t) \in \mathcal{Q} |\ \beta \geq z > 0,\ \|\mathbf{q}\|^\alpha = z\}$. Let us remark that the origin does not belong to this set.

2. If W^{ev} denotes the set of initial conditions $(\mathbf{q}_0, z_0, t_0)$ that eventually leave $\mathcal{Q}$ in backward time, then W^{im} is a relatively closed subset of W^{ev}. (This is because a sequence within W^{im} converges to a point *outside* W^{im}, then that point is necessarily at $\mathbf{q} = z = 0$, which is *not* in W^{ev}. Therefore, all Cauchy sequences in W^{im} that converge to a point in W^{ev} necessarily have their limit points in W^{im}. By definition, this means that W^{im} is relatively closed in W^{ev}.)

These two properties, by definition, make $\mathcal{Q}$ a backward-time *Wasewsky set* for the extended system (A.25) (cf. Hale 1980). As a result, the Wasewsky principle holds for $\mathcal{Q}$: The map Γ: $W^{ev} \to W^{im}$ that maps initial positions in $\mathcal{Q}$ to the point where they leave $\mathcal{Q}$ in backward time, is continuous.

Assume now that all initial conditions with $z_0 \neq 0$ eventually leave $\mathcal{Q}$ in backward time. This would imply that

$$W^{ev} = \{(\mathbf{q}, z, t) \in \mathcal{Q} |\ z > 0\},$$

but we will prove that this is impossible.

Let us consider now the $z = \beta$ boundary of the time-dependent flower-cone $\mathcal{Q}$ that we call D_β: For a fixed time, D_β is a disc of the $z = \beta$ surface, which is topologically a closed set. Every point of D_β has to leave the cone in backward time, thus $\Gamma(D_\beta) \subset W^{im}$. As D_β is closed and Γ is a continuous function (thus has to transform a closed set into a closed set), $\Gamma(D_\beta)$ is closed. But W^{im} is not closed: the origin is a limit of a series of points of W^{im} but does not belong to W^{im}. Then there is at least one point which belongs to W^{im}, but does not belong to $\Gamma(D_\beta)$.

Let us call this point $\mathbf{r} = (\mathbf{q}_0, z_0, t_0)$: necessarily, $z_0 > 0$. In forward time, the trajectory leaving from $\mathbf{r}$ enters the cone and cannot leave it on W^{im}. We now show that the z coordinate grows and has to go beyond β in finite time: along this trajectory, we have

$$\dot{z}(t) = z^2\left[c(t) + zm_4(\mathbf{q}, z, \mathbf{g}_k, t) + \mathbf{q}\cdot\mathbf{m}_5(\mathbf{q}, z, \mathbf{g}_k, t)\right], \tag{A.26}$$

whose integration gives

$$z(t) = \frac{z_0}{1 + z_0 \int_t^{t_0} \left[c(\tau) + z(\tau) m_4(\mathbf{q}, z, \mathbf{g}_k, \tau) + \mathbf{q}(\tau) \cdot \mathbf{m}_5(\mathbf{q}, z, \mathbf{g}_k, \tau)\right] d\tau}. \tag{A.27}$$

This equation holds for $t \leq t_0$ while the trajectory we consider stays in $\mathcal{Q}$ (in forward times). Then within the flower-cone, we have

$$\begin{aligned} z(t) &\geq \frac{z_0}{1 - z_0 \int_{t_0}^{t} \left[c(\tau) - K(\beta + \beta^\alpha)\right] d\tau} \geq \frac{z_0}{1 - z_0 \int_{t_0}^{t} \left[c_0 - \frac{c_0}{2}\right] d\tau} \\ &\geq \frac{z_0}{1 - z_0 \frac{c_0}{2}(t - t_0)}, \end{aligned}$$

and necessarily the relation $z(t) \leq \beta$ cannot hold when $t \to t_0 + \frac{2}{c_0 z_0}$. Thus this trajectory has to leave the cone, and hence must intersect the disc D_β, which is impossible.

We therefore conclude that $W^{ev} \neq Q$, i.e., there is a nonempty set of initial fluid particle positions W^∞ that stays in Q for all backward times. By definition, W^∞ is an invariant set and is necessarily smooth in t because it is composed of fluid trajectories that are smooth in t.

Next we want to argue that all solutions in W^∞ tend to $\mathbf{q} = z = 0$ in backward time. Consider a specific initial position $(\bar{\mathbf{q}}_0, \bar{z}_0, \bar{t}_0) \in W^\infty$, and denote the trajectory emanating from this initial position by $(\mathbf{q}(t), z(t), t)$. Along this trajectory, the equation (A.27) holds for *all* $t \leq t_0$, because the trajectory we consider stays in $\mathcal{Q}$ for all backward times. Then (A.27) and (A.24) lead to the estimate

$$\begin{aligned} z(t) &\leq \frac{z_0}{1 + z_0 \int_t^{t_0} \left[c(\tau) - K(\beta + \beta^\alpha)\right] d\tau} \leq \frac{z_0}{1 + z_0 \int_t^{t_0} \left[c_0 - K\frac{c_0}{2K}\right] d\tau} \\ &\leq \frac{z_0}{1 + z_0 \int_t^{t_0} \frac{c_0}{2} d\tau} = \frac{z_0}{2 + z_0 \frac{c_0}{2}(t_0 - t)}, \end{aligned}$$

allowing us to conclude that

$$\lim_{t \to -\infty} z(t) = 0.$$

In other words, trajectories that never leave Q in backward time will necessarily converge to the $z = 0$ boundary of the cone Q. By the definition of Q, however, this convergence in the z direction implies

$$\lim_{t \to -\infty} \mathbf{q}(t) = 0.$$

We therefore conclude that all trajectories in W^∞ converge to $z = \mathbf{q} = 0$ in backward time, thus W^∞ is an unstable manifold for $(\gamma, 0)$. Any material curve in this manifold admits bounded and unique z derivatives according to formulae (2.47)-(2.49), therefore the unstable manifold is unique up to terms of order $O(z^3)$.

The same argument applies when higher-order terms of the candidate separation profile (2.46) are included in the initial coordinate change (A.18), leading to a unique unstable manifold up to terms of order $O(z^n)$. Here n is arbitrary integer that can be as large as the degree of differentiability of the original velocity field.

Given the existence of the separation profile, we only need to argue that the separation is indeed sharp along this profile. To prove sharp separation, it is enough to establish that the

z coordinate of fluid particles in the separation profile W^∞ grows monotonically for all times as long as the particles are in a vicinity of the boundary. Note that W^∞ has been constructed as a material line whose $z \leq \beta$ portion is fully contained in the cone Q. For all fluid particles that lie in the separation profile as well as in the $\{0 < z \leq \beta\}$ neighborhood of the boundary, equation (A.19) and (A.24) yield the estimate

$$\begin{aligned} \dot{z}(t) &= z^2 \left[c(t) + z m_4(\mathbf{q}, z, \mathbf{g}_k, t) + \mathbf{q} \cdot \mathbf{m}_5(\mathbf{q}, z, \mathbf{g}_k, t)\right] \\ &\geq z^2 \left[\frac{c_0}{2} - K(\beta + \beta^\alpha)\right] \geq z^2 \frac{c_0}{10}. \end{aligned}$$

Therefore, the z coordinate of fluid particles in W^∞ grows monotonically in the $\{0 < z \leq \beta\}$ neighborhood of the boundary, resulting in sharp separation.

A.4 Moving separation

Here we show that for general incompressible flows, (2.73) gives a sufficient condition for *finite-time* sharp separation close to the moving effective separation point $\boldsymbol{\gamma}_{eff}(t, t_0)$. We shall show this by arguing that if $\boldsymbol{\gamma}_{eff}(t, t_0)$ moves slowly enough over a finite time interval $[t_0 - T_m, t_0]$, then any point $(\boldsymbol{\gamma}, 0)$ close enough to $\boldsymbol{\gamma}_{eff}(t, t_0)$ behaves as a separation point over that time interval. From this argument, we obtain a whole set of points that can be considered finite-time separation points. The size of this set, however, tends to zero rapidly as the admissible time scale T_m increases. As a result, in numerical calculations we obtain a separation point that is unique for practical purposes.

We start by selecting a boundary point $(\boldsymbol{\gamma}, 0)$ and introducing a time-dependent coordinate change

$$\mathbf{q} = \mathbf{x} - \boldsymbol{\gamma} - z\boldsymbol{\phi}(t),$$

with $\phi(t)$ and $\psi(t)$ to be defined below. We obtain the transformed velocity field

$$\begin{aligned} \dot{\mathbf{q}} &= \dot{\mathbf{x}} - \dot{z}\boldsymbol{\phi} - z\dot{\boldsymbol{\phi}} \\ &= z(\mathbf{a} - \dot{\boldsymbol{\phi}}) + z\mathbf{a}_\mathbf{x}\mathbf{q} + z^2\left[(\mathbf{a}_\mathbf{x} - c\mathbf{I})\,\boldsymbol{\phi} + \mathbf{a}_z\right] \\ &\quad + \left(l_1 z^3 + z^2 \mathbf{l}_2 \cdot \mathbf{q} + l_3 z \mathbf{q}^2\right)(\mathbf{l}_4 + n_1\boldsymbol{\phi}), \\ \dot{z} &= z^2 C(\boldsymbol{\gamma} + \mathbf{q} + z\boldsymbol{\phi}, z, t) \\ &= z^2\left[c(t) + (\mathbf{l}_5 z + l_6\mathbf{q}) \cdot (\mathbf{l}_4 + n_2\boldsymbol{\phi})\right], \end{aligned} \tag{A.28}$$

with appropriate smooth functions $h_i(\mathbf{q}, z, \boldsymbol{\phi}, t)$. These functions are typically not globally bounded in $\boldsymbol{\phi}$, thus they will grow unbounded if $\boldsymbol{\phi}$ grows unbounded in time.

If we select the function $\boldsymbol{\phi}(t)$ to be the solution of

$$\dot{\boldsymbol{\phi}} = \mathbf{a}, \tag{A.29}$$

then the $O(z)$ term in the $\dot{\mathbf{q}}$ equation of (A.28) vanishes. By our assumptions, the $O(z\mathbf{q})$ term remains bounded regardless of the choice of $\boldsymbol{\phi}$. If $\boldsymbol{\gamma}$ were a fixed separation point, then the solution $\boldsymbol{\phi}(t)$ of (A.29) would remain bounded for all times, and hence the $O(z^3, z\mathbf{q}^2, z^2\mathbf{q})$ terms in the $\dot{\mathbf{q}}$ equation would also remain bounded for all times. But $\boldsymbol{\gamma}$ is *not* a fixed separation point in our current setting, and hence the $O(z^3, z\mathbf{q}^2, z^2\mathbf{q})$ terms in the $\dot{\mathbf{q}}$ equation will typically

grow unbounded in time

To control the above-mentioned growth of nonlinear terms in (A.28), we select

$$\boldsymbol{\gamma} = \boldsymbol{\gamma}_{eff}(t,t_0) + \boldsymbol{\Delta}(t,t_0) = \begin{pmatrix} \gamma_{x,eff}(t,t_0) + \Delta_x(t,t_0) \\ \gamma_{y,eff}(t,t_0) + \Delta_y(t,t_0) \end{pmatrix},$$

with $\boldsymbol{\gamma}_{eff}(t,t_0)$ denoting an effective separation point. In that case, any solution of the first equation in (A.29) can be written as

$$\begin{aligned} \boldsymbol{\phi}(t) &= \boldsymbol{\phi}(t_0) + \int_{t_0}^{t} \mathbf{A}(\boldsymbol{\gamma}, 0, \tau)\, d\tau \\ &= \boldsymbol{\phi}(t_0) + \int_{t_0}^{t} \mathbf{A}(\gamma_{x,eff}(t,t_0) + \Delta_x(t,t_0), \gamma_{y,eff}(t,t_0) + \Delta_y(t,t_0), 0, \tau)\, d\tau. \end{aligned}$$

Applying two consecutive times the one-dimensional mean-value theorem yields

$$\begin{aligned} & \mathbf{A}(\gamma_{x,eff}(t,t_0) + \Delta_x(t,t_0), \gamma_{y,eff}(t,t_0) + \Delta_y(t,t_0), 0, \tau) \\ = \; & \mathbf{A}(\gamma_{x,eff}(t,t_0), \gamma_{y,eff}(t,t_0) + \Delta_y(t,t_0), 0, \tau) + \mathbf{A}_x(\gamma_x^*(\tau), \gamma_{y,eff}(t,t_0) + \Delta_y(t,t_0), 0, \tau)\Delta_x(t,t_0) \\ = \; & \mathbf{A}(\gamma_{x,eff}(t,t_0), \gamma_{y,eff}(t,t_0), 0, \tau) + \mathbf{A}_y(\gamma_{x,eff}(t,t_0), \gamma_y^*(\tau), 0, \tau)\Delta_y(t,t_0) \\ & + \mathbf{A}_x(\gamma_x^*(\tau), \gamma_{y,eff}(t,t_0) + \Delta_y(t,t_0), 0, \tau)\Delta_x(t,t_0), \end{aligned}$$

for some γ_x^* and γ_y^*, respectively between γ_x and $\gamma_{x,eff}(t,t_0)$, and γ_y and $\gamma_{y,eff}(t,t_0)$.

The integration of this expression over $[t_0,t]$ gives the expression

$$\begin{aligned} \boldsymbol{\phi}(t) &= \boldsymbol{\phi}(t_0) + \Delta_x(t,t_0) \int_{t_0}^{t} \mathbf{u}_{xz}(\gamma_x^*(\tau), \gamma_{y,eff}(t,t_0) + \Delta_y(t,t_0), 0, \tau)\, d\tau \\ & \quad + \Delta_y(t,t_0) \int_{t_0}^{t} \mathbf{u}_{yz}(\gamma_{x,eff}(t,t_0), \gamma_y^*(\tau), 0, \tau)\, d\tau. \end{aligned}$$

Let $\mathbf{I}'(t,t_0)$ denote the $\mathbf{x}$ interval covered by the moving separation point $\boldsymbol{\gamma}_{eff}(s,t_0)$ while s varies over the time interval $[t,t_0]$. We define $\mathbf{I}(t,t_0)$ as the smallest rectangle containing $\mathbf{I}'(t,t_0)$, and we denote the length of $\mathbf{I}(t,t_0)$ by $\delta(t,t_0)$. If we select $\boldsymbol{\gamma}$ from the interval $I(t,t_0)$,

then for any $t < t_0$, we have the estimate

$$\begin{aligned}
|\phi(t)| &= \left|\phi(t_0) + \Delta_x(t,t_0)\int_{t_0}^{t} \mathbf{u}_{xz}(\gamma_x^*(\tau), \gamma_{y,eff}(t,t_0) + \Delta_y(t,t_0), 0, \tau)\, d\tau \right. \\
&\quad \left. + \Delta_y(t,t_0)\int_{t_0}^{t} \mathbf{u}_{yz}(\gamma_{x,eff}(t,t_0), \gamma_y^*(\tau), 0, \tau)\, d\tau\right| \\
&\leq |\phi(t_0)| + |\Delta_x(t,t_0)|\left|\int_{t_0}^{t} \mathbf{u}_{xz}(\gamma_x^*(\tau), \gamma_{y,eff}(t,t_0) + \Delta_y(t,t_0), 0, \tau)\, d\tau\right| \\
&\quad + |\Delta_y(t,t_0)|\left|\int_{t_0}^{t} \mathbf{u}_{yz}(\gamma_{x,eff}(t,t_0), \gamma_y^*(\tau), 0, \tau)\, d\tau\right| \\
&\leq |\phi(t_0)| + (|\Delta_x(t,t_0)| + |\Delta_y(t,t_0)|)\left\|\int_{t_0}^{t} \max_{\mathbf{x}\in I(t,t_0)} \mathbf{u}_{\mathbf{x}z}(\mathbf{x}, 0, \tau)\, d\tau\right\| \\
&\leq |\phi(t_0)| + \sqrt{2}\,\|\Delta(t,t_0)\|_2 \left\|\int_{t_0}^{t} \max_{\mathbf{x}\in I(t,t_0)} \mathbf{u}_{\mathbf{x}z}(\mathbf{x}, 0, \tau)\, d\tau\right\| \\
&\leq |\phi(t_0)| + \delta(t,t_0)\sqrt{2}\left\|\int_{t_0}^{t} \max_{\mathbf{x}\in I(t,t_0)} \mathbf{u}_{\mathbf{x}z}(\mathbf{x}, 0, \tau)\, d\tau\right\|. \qquad \text{(A.30)}
\end{aligned}$$

As in appendix A.3, we now define the flower-cone

$$Q = \{(\mathbf{q}, z) \mid \|\mathbf{q}\|^\alpha \leq z, \quad 0 \leq z \leq \beta\},$$

where α and β are positive constants to be selected below. Modifying the functions l_j, n_k, ϕ smoothly outside a time interval $[t_0 - T_m, t_0]$ with T_m to be determined below , we can select a constant $K > 0$ such that the modified functions satisfy

$$|l_j(\mathbf{q}, z, \phi, t)|, \ |n_k(\mathbf{q}, z, \phi, t)\phi| \leq K, \qquad (\mathbf{q}, z) \in Q, \quad t \in \mathbb{R}.$$

Along the $z = \beta$ boundary, we now have

$$\begin{aligned}
\dot{z}|_{z=\beta} &= \beta^2\left[c(t) + (\mathbf{l}_5 z + l_6\mathbf{q})\cdot(\mathbf{l}_7 + n_2\phi)\right] \\
&\geq \beta^2\left[c(t) - 2K^2\left(\beta + \beta^{1/\alpha}\right)\right] > 0,
\end{aligned}$$

provided that

$$c(t) > 2K^2\left(\beta + \beta^{1/\alpha}\right),$$

or, equivalently,

$$w_{zz}(\boldsymbol{\gamma}, 0, t) > 4K^2\left(\beta + \beta^{1/\alpha}\right). \qquad \text{(A.31)}$$

Therefore, solutions intersecting the $z = \beta$ boundary of Q leave Q immediately if the inequality (A.31) holds for all times.

Next, we consider the $\mathbf{q} = z^{1/\alpha}e^{i\theta}$ boundary of the flower-cone Q, where we use $e^{i\theta} =$

$\begin{pmatrix} \cos\theta \\ \sin\theta \end{pmatrix}$:

$$\begin{aligned}
\dot{\mathbf{q}}|_{\mathbf{q}=z^{1/\alpha}e^{i\theta}} &= z^{1+1/\alpha}\left[\mathbf{a}_{\mathbf{x}}(t)e^{i\theta} + z^{1-1/\alpha}\left[\left(\mathbf{a}_{\mathbf{x}} - c\mathbf{I}\right)\boldsymbol{\phi} + \mathbf{a}_z\right]\right. \\
&\quad \left. + \left(l_1 z^{2-1/\alpha} + z\mathbf{l}_2 \cdot e^{i\theta} + l_3 z^{1/\alpha}e^{i2\theta}\right)\left(\mathbf{l}_4 + n_1\boldsymbol{\phi}\right)\right] \\
&\leq z^{1+1/\alpha}\left[\left\|\mathbf{a}_{\mathbf{x}}(t)\right\| + z^{1-1/\alpha}\left[\left(\mathbf{a}_{\mathbf{x}} - c\mathbf{I}\right)\boldsymbol{\phi} + \mathbf{a}_z\right] + 2K^2\left(\beta^{2-1/\alpha} + \beta + \beta^{1/\alpha}\right)\right], \\
\dot{z}|_{\mathbf{q}=z^{1/\alpha}e^{i\theta}} &= z^2\left[c(t) + \left(\mathbf{l}_5 z + l_6 z^{1/\alpha}e^{i\theta}\right)\cdot\left(\mathbf{l}_4 + n_2\boldsymbol{\phi}\right)\right] > z^2\left[c(t) - 2K^2\left(\beta + \beta^{1/\alpha}\right)\right],
\end{aligned}$$

and we want the flow to enter the flower-cone on this surface, which requires

$$\dot{z}|_{\mathbf{q}=\alpha z e^{i\theta}} > \alpha\left\|\mathbf{q}\right\|^{\alpha-1}\left\|\dot{\mathbf{q}}|_{\mathbf{q}=\alpha z e^{i\theta}}\right\| \text{ for any } \theta.$$

Provided that

$$\begin{aligned}
&\alpha z^{\frac{\alpha-1}{\alpha}} z^{1+1/\alpha}\left[\left\|\mathbf{a}_{\mathbf{x}}(t)\right\| + \beta^{1-1/\alpha}\left[\left(\mathbf{a}_{\mathbf{x}} - c\mathbf{I}\right)\boldsymbol{\phi} + \mathbf{a}_z\right] + 2K^2\left(\beta^{2-1/\alpha} + \beta + \beta^{1/\alpha}\right)\right] \\
< \;& z^2\left[c(t) - 2K^2\left(\beta + \beta^{1/\alpha}\right)\right],
\end{aligned}$$

which simplifies to

$$\alpha\left[\left\|\mathbf{a}_{\mathbf{x}}(t)\right\| + \beta^{1-1/\alpha}\left[\left(\mathbf{a}_{\mathbf{x}} - c\mathbf{I}\right)\boldsymbol{\phi} + \mathbf{a}_z\right]\right] + 2K^2\left[\alpha\beta^{2-1/\alpha} + (1+\alpha)\left(\beta + \beta^{1/\alpha}\right)\right] < c(t), \quad \text{(A.32)}$$

the above entry condition is satisfied.

We first select the coefficient $\alpha < 1$ such that

$$\left(2 + 2\left|\boldsymbol{\phi}(t_0)\right| + (\kappa+1)\frac{\left\|\mathbf{u}_{zz}(t)\right\|}{\left\|\mathbf{u}_{\mathbf{x}z}(t)\right\|}\right)\alpha\left\|a_x(t)\right\| < c(t),$$

with κ to be a selected positive constant in our system. For this fixed $\alpha > 0$, we can always select an appropriately small $1 > \beta > 0$ such that the previous inequalities hold, provided that

$$\begin{aligned}
\left(\mathbf{a}_{\mathbf{x}} - c\mathbf{I}\right)\boldsymbol{\phi} + \mathbf{a}_z &< \left(2\left|\boldsymbol{\phi}(t_0)\right| + (\kappa+1)\frac{\left\|\mathbf{u}_{zz}(t)\right\|}{\left\|\mathbf{u}_{\mathbf{x}z}(t)\right\|}\right)\left\|\mathbf{a}_{\mathbf{x}}(t)\right\|, \quad \text{(A.33)} \\
2K^2\left[\alpha\beta^{2-1/\alpha} + (1+\alpha)\left(\beta + \beta^{1/\alpha}\right)\right] &< \left\|\mathbf{a}_{\mathbf{x}}(t)\right\|.
\end{aligned}$$

The condition in (A.33) holds if we require

$$\begin{aligned}
&\left\|\mathbf{a}_{\mathbf{x}}(t) + \frac{\operatorname{Tr}\mathbf{a}_{\mathbf{x}}(t)}{2}\mathbf{I}\right\|\left(\left|\boldsymbol{\phi}(t_0)\right| + \delta(t,t_0)\sqrt{2}\left\|\int_{t_0}^{t}\max_{\mathbf{x}\in I(t,t_0)}\mathbf{u}_{\mathbf{x}z}(\mathbf{x},0,\tau)\,d\tau\right\|\right) + \left\|\mathbf{a}_z(t)\right\| \\
< \;& \left(2\left|\boldsymbol{\phi}(t_0)\right| + (\kappa+1)\frac{\left\|\mathbf{u}_{zz}(t)\right\|}{\left\|\mathbf{u}_{\mathbf{x}z}(t)\right\|}\right)\left\|\mathbf{a}_{\mathbf{x}}(t)\right\|,
\end{aligned}$$

where we used the incompressibility relation $\operatorname{Tr} \mathbf{a}_{\mathbf{x}} + 2c = 0$. Using the relation

$$\left| \frac{\operatorname{Tr} \mathbf{a}_{\mathbf{x}}(t)}{2} \right| < \|\mathbf{a}_{\mathbf{x}}(t)\|,$$

the condition holds if we require

$$\delta(t, t_0) \int_{t_0}^{t} \max_{\mathbf{x} \in I(t,t_0)} \|\mathbf{u}_{\mathbf{x}z}(\mathbf{x}, 0, \tau)\| \, d\tau < \frac{\sqrt{2}}{2} \kappa \max_{\mathbf{x} \in I(t,t_0)} \frac{\|\mathbf{u}_{zz}(t)\|}{\|\mathbf{u}_{\mathbf{x}z}(t)\|}. \tag{A.34}$$

The choice of κ will be very important: Selecting a small κ will guarantee a great accuracy but will enforce the separation point to move fast. Typically, we select $\kappa = 1$.

We must also have

$$\max_{\mathbf{x} \in I(t,t_0)} \operatorname{Tr} \mathbf{u}_{\mathbf{x}z}(\mathbf{x}, 0, t) < 0. \tag{A.35}$$

With this last conclusion, the rest of our argument is identical to that of appendix A.3. Following that argument, we obtain that $\boldsymbol{\gamma}$ is a fixed sharp separation point for the modified system that admits all the uniform bounds that we have assumed. As a result, the original unmodified system also admits sharp finite-time separation at $\boldsymbol{\gamma}$ *as long as it agrees with the modified system.*

Appendix B

Proofs for the flow expansions

B.1 Tensor term of the curvature

As

$$\mathbf{u}_z = \begin{pmatrix} u_{1,3} \\ u_{2,3} \end{pmatrix}, \quad \mathbf{u}_{\mathbf{x}z} = \begin{pmatrix} u_{1,13} & u_{1,23} \\ u_{2,13} & u_{2,23} \end{pmatrix},$$
$$\mathbf{u}_{\mathbf{x}\mathbf{x}z} = \begin{pmatrix} u_{1,13} & u_{1,23} \\ u_{2,13} & u_{2,23} \end{pmatrix}_{\mathbf{x}},$$

the tensor term (3.25) can be rewritten

$$\left[\left[\frac{\partial}{\partial x_i}\begin{pmatrix} \frac{\partial^2 u_1}{\partial x_1 \partial x_3} & \frac{\partial^2 u_1}{\partial x_2 \partial x_3} \\ \frac{\partial^2 u_2}{\partial x_1 \partial x_3} & \frac{\partial^2 u_2}{\partial x_2 \partial x_3} \end{pmatrix}_{i=1,2} + \frac{\partial}{\partial x_i}\left(\mathrm{Tr}\begin{pmatrix} \frac{\partial^2 u_1}{\partial x_1 \partial x_3} & \frac{\partial^2 u_1}{\partial x_2 \partial x_3} \\ \frac{\partial^2 u_2}{\partial x_1 \partial x_3} & \frac{\partial^2 u_2}{\partial x_2 \partial x_3} \end{pmatrix}\right)_{i=1,2} \cdot \mathbf{I}\right] \mathbf{g}_0\right] \mathbf{g}_0.$$

We first write the matrix

$$\mathbf{u}_{\mathbf{x}\mathbf{x}z}\mathbf{g}_0 = \begin{pmatrix} u_{1,113}g_{0,1} + u_{1,123}g_{0,2} & u_{1,123}g_{0,1} + u_{1,223}g_{0,2} \\ u_{2,113}g_{0,1} + u_{2,123}g_{0,2} & u_{2,123}g_{0,1} + u_{2,223}g_{0,2} \end{pmatrix},$$

and we deduce the vector

$$\mathbf{u}_{\mathbf{x}\mathbf{x}z}\mathbf{g}_0\mathbf{g}_0 = \begin{pmatrix} u_{1,113}\left(g_{0,1}\right)^2 + 2u_{1,123}g_{0,1}g_{0,2} + u_{1,223}\left(g_{0,2}\right)^2 \\ u_{2,113}\left(g_{0,1}\right)^2 + 2u_{2,123}g_{0,1}g_{0,2} + u_{2,223}\left(g_{0,2}\right)^2 \end{pmatrix}. \tag{B.1}$$

We also have

$$\mathrm{Tr}\,\mathbf{u}_{\mathbf{x}z} = u_{1,13} + u_{2,23},$$

which yields the vector

$$\left(\mathrm{Tr}\,\mathbf{u}_{\mathbf{x}z}\right)_{\mathbf{x}} = \begin{pmatrix} u_{1,113} + u_{2,123} \\ u_{1,123} + u_{2,223} \end{pmatrix}.$$

Taking the scalar product with $\mathbf{g}_0$, we obtain

$$\left(\mathrm{Tr}\,\mathbf{u}_{\mathbf{x}z}\right)_{\mathbf{x}} \cdot \mathbf{g}_0 = \left(u_{1,113} + u_{2,123}\right) g_{0,1} + \left(u_{1,123} + u_{2,223}\right) g_{0,2},$$

which is also equal to $\mathrm{Tr}(\mathbf{u_{xxz}g_0})$.

Then we obtain

$$[(\mathrm{Tr}\,\mathbf{u_{xz}})_{\mathbf{x}}\cdot\mathbf{g_0}]\,\mathbf{g_0} = \begin{pmatrix} (u_{1,113}+u_{2,123})\,(g_{0,1})^2 + (u_{1,123}+u_{2,223})\,g_{0,1}g_{0,2} \\ (u_{1,113}+u_{2,123})\,g_{0,1}g_{0,2} + (u_{1,123}+u_{2,223})\,(g_{0,2})^2 \end{pmatrix}, \tag{B.2}$$

and summing the contributions, we obtain

$$\begin{aligned} &[(\mathbf{u_{xxz}} + (\mathrm{Tr}\,\mathbf{u_{xz}})_{\mathbf{x}}\cdot\mathbf{I})\,\mathbf{g_0}]\,\mathbf{g_0} \\ = &\begin{pmatrix} (2u_{1,113}+u_{2,123})\,(g_{0,1})^2 + (3u_{1,123}+u_{2,223})\,g_{0,1}g_{0,2} + +u_{1,223}\,(g_{0,2})^2 \\ u_{2,113}\,(g_{0,1})^2 + (u_{1,113}+3u_{2,123})\,g_{0,1}g_{0,2} + (u_{1,123}+2u_{2,223})\,(g_{0,2})^2 \end{pmatrix}. \end{aligned} \tag{B.3}$$

In the first case, the skin friction field is linear, which implies that this term vanishes. But in the case of the bubble, this term will be nonzero.

B.2 A word on the saddle-focus profile

In chapter 3, we showed that the predicted profile of separation at a saddle-focus approximates the true profile poorly. As it turns out, the radius of convergence for a Taylor-series expansion of the profile can be zero or small, which prevents a good approximation of the separation shape unless we compute higher-order terms.

B.2.1 Numerical method to calculate the orders of separation

We present here a method which allows, for any steady flow whose velocity is analytically known near the separation point, to numerically calculate all the orders of separation.

This method only works for the steady case, and cannot be directly extended to the unsteady case. We find an algorithm which allows to obtain recurrently all the orders of separation.

Analysis of a non-analytic saddle-focus

Let us consider the steady saddle-focus flow such as $\mathbf{K} = \begin{pmatrix} 0 & 1 \\ -1 & 0 \end{pmatrix}$ (thus corresponding to the case when $\lambda = 1$ and $\theta = \frac{\pi}{2}$), $\mathbf{F} = \mathbf{0}$, $A_{1233} = 0$, and $A_{1133} = A_{2233} = \delta < 0$: under these conditions, the model velocity field (3.20) takes the form

$$\begin{aligned} u_1 &= x_2x_3 + (\alpha + \delta x_1)x_3^2, \\ u_2 &= -x_1x_3 + (\beta + \delta x_2)x_3^2, \\ u_3 &= -\frac{2\delta}{3}x_3^3. \end{aligned} \tag{B.4}$$

For this particular flow, we obtain $\mathbf{g_0}(t_0) = -\begin{pmatrix} -\beta \\ \alpha \end{pmatrix}$ and $\mathbf{g_1} = -\frac{5\delta}{3}\begin{pmatrix} \alpha \\ \beta \end{pmatrix}$; trajectories

emanating from a vicinity of the separation point follow the separation profile

$$\begin{pmatrix} x_1 \\ x_2 \end{pmatrix} = -x_3 \begin{pmatrix} x_3\frac{5\delta}{3} & -1 \\ 1 & x_3\frac{5\delta}{3} \end{pmatrix} \begin{pmatrix} \alpha \\ \beta \end{pmatrix} + O(x_3^3). \tag{B.5}$$

By comparing streamlines of this flow and the predicted separation profile at first and second order, we validate formula (B.5) in figure B-1.

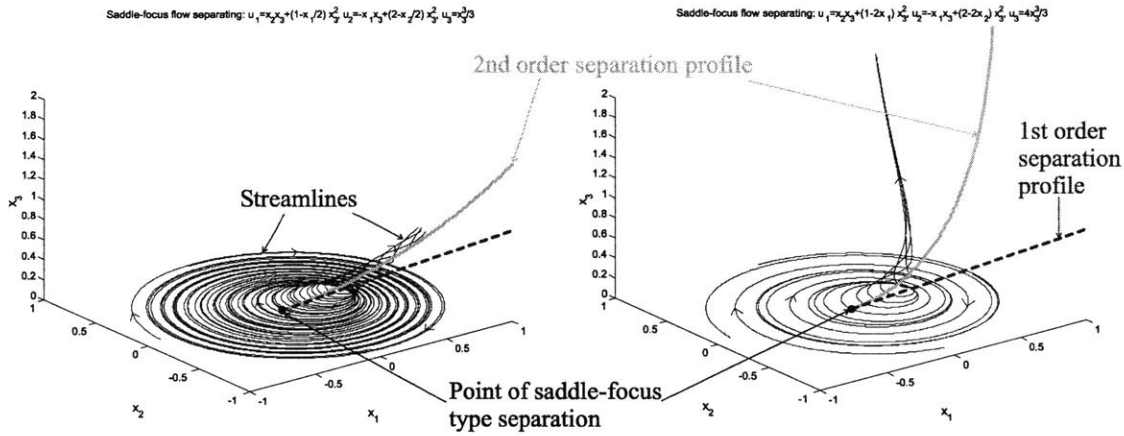

Figure B-1: Predicted and real saddle-focus separation profiles.

In the steady case, the motion of the particles is given by the streamlines, and we see in the two cases of figure B-1 that all the particles of the wall are attracted to a single line, the separation profile, which is approximated by our first and second order approximations.

The left image represents the case of $\delta = -1/2$, then the high-order terms are negligible and the slope and curvature are sufficient to approximate the shape of separation. The right image represents the case of $\delta = -2$, then the curvature of the separation profile is not sufficient to obtain the real shape of separation.

The low-order saddle-focus profile is not as accurate as the saddle-sink or saddle-saddle profiles. We will show that the following orders of separation grow unbounded, and this prevents a good approximation of the separation profile, unless we compute a large number of separation orders. Moreover, we will show that this separation profile turns out not to be analytic.

Numerical orders of separation

Let us explain our algorithm on a specific case, the steady focus case (B.4): the differential equations that the particles of the flow have to satisfy are

$$\dot{x}_1 = x_2x_3 + (\alpha + \delta x_1)x_3^2, \tag{B.6}$$
$$\dot{x}_2 = -x_1x_3 + (\beta + \delta x_2)x_3^2, \tag{B.7}$$
$$\dot{x}_3 = -\frac{2\delta}{3}x_3^3, \tag{B.8}$$

and the separation profile is (B.5) at second order.

Time-scale We see in (B.8) that x_3 has a simple dependence on time that can be integrated directly. Let us take the initial conditions at $\begin{pmatrix} x_1 \\ x_2 \\ x_3 \end{pmatrix} = \begin{pmatrix} \epsilon_1 \\ \epsilon_2 \\ \epsilon_3 \end{pmatrix}$ close to the origin, in which case (B.8) implies that

$$x_3 = \frac{\epsilon_3}{\sqrt{1 + \frac{4\delta\epsilon_3^2}{3}t}}.$$

Then we define the natural new time-scale by setting

$$\boxed{\tilde{t} = x_3,} \tag{B.9}$$

which implies that for $i = 1, 2$ we have

$$\dot{x}_i = \frac{\partial x_i}{\partial t} = \frac{\partial x_i}{\partial x_3}\frac{\partial x_3}{\partial t} = -x_i'\frac{2\delta}{3}\tilde{t}^3.$$

Differential equations With this new time-scale, the system of differential equation becomes

$$\begin{aligned} x_1' &= -\frac{3}{2\delta}\frac{x_2 + (\alpha + \delta x_1)\tilde{t}}{\tilde{t}^2}, \\ x_2' &= -\frac{3}{2\delta}\frac{-x_1 + (\beta + \delta x_2)\tilde{t}}{\tilde{t}^2}. \end{aligned} \tag{B.10}$$

In the steady case, the separation profile corresponds to the streamline emanating from the separation point, then searching the first orders of separation is the same thing as looking at the solution of this system expanded at a certain order in power series. One can expand the C^∞ solutions of (B.10) in Taylor series at any order: considering the k^{th} order, we can write

$$\begin{aligned} x_1 &= \sum_{n=0}^{k} y_n\tilde{t}^n + O(\tilde{t}^{k+1}), \\ x_2 &= \sum_{n=0}^{k} z_n\tilde{t}^n + O(\tilde{t}^{k+1}), \end{aligned}$$

We replace these expansions in (B.10) and we obtain the system

$$\begin{aligned}
\sum_{n=1}^{k+1}(n-1)y_{n-1}\tilde{t}^n &= -\frac{3}{2\delta}\left[\sum_{n=0}^{k} z_n\tilde{t}^n + \alpha\tilde{t} + \delta\sum_{n=1}^{k+1} y_{n-1}\tilde{t}^n\right] + O(\tilde{t}^{k+1}),\\
\sum_{n=1}^{k+1}(n-1)z_{n-1}\tilde{t}^n &= -\frac{3}{2\delta}\left[-\sum_{n=0}^{k} y_n\tilde{t}^n + \beta\tilde{t} + \delta\sum_{n=1}^{k+1} z_{n-1}\tilde{t}^n\right] + O(\tilde{t}^{k+1}).
\end{aligned} \tag{B.11}$$

We now have to equate all the terms of this expansion to determine the separation profile.

Verification on the first terms We write the separation profile in the form

$$\begin{pmatrix} x_1 \\ x_2 \end{pmatrix} = x_3\left(\sum_{n=0}^{k}\frac{1}{n!}\mathbf{g}_n x_3^n + O(\tilde{t}^{k+1})\right),$$

and replacing x_3 with $\tilde{t}$ in this expression, we expect for $n \geq 1$

$$\begin{pmatrix} y_n \\ z_n \end{pmatrix} = \frac{1}{(n-1)!}\mathbf{g}_{n-1}. \tag{B.12}$$

Taking the constant terms of (B.11) yields $y_0 = 0$ and $z_0 = 0$, which we expected.

Then the linear terms of (B.11) yields $y_1 = \beta$ and $z_1 = -\alpha$, corresponding to the slope of separation determined in (B.5).

The quadratic terms of (B.11) give $y_2 = -\frac{5\delta\alpha}{3}$ and $z_2 = -\frac{5\delta\beta}{3}$, corresponding to the curvature of separation determined in (B.5).

Thus this method gives the correct orders of separation, at least for the first terms.

Practical algorithm Taking the terms corresponding to $\tilde{t}^n$ when $2 \leq n \leq k$ yields the system of equations

$$\begin{aligned}
\left(n+\frac{1}{2}\right)y_{n-1} &= -\frac{3}{2\delta}z_n,\\
\left(n+\frac{1}{2}\right)z_{n-1} &= +\frac{3}{2\delta}y_n,
\end{aligned}$$

which is true for any k. Thus this implies when $n \geq 3$:

$$\begin{aligned}
y_n &= -\left(\frac{2\delta}{3}\right)^2\left(n^2-\frac{1}{4}\right)y_{n-2},\\
z_n &= -\left(\frac{2\delta}{3}\right)^2\left(n^2-\frac{1}{4}\right)z_{n-2}.
\end{aligned}$$

Then we have when $n \geq 2$

$$\mathbf{g}_n = -\left(\frac{2\delta}{3}\right)^2 \left((n+1)^2 - \frac{1}{4}\right) n\,(n-1)\,\mathbf{g}_{n-2}. \tag{B.13}$$

Knowing the first two orders of separation, we can now recursively calculate all the orders.

Growing orders of separation Expression (B.13) shows that the orders of separation increase fast, which implies that the successive derivatives of the flow at the separation point become important. This will prevent a good approximation of the separation profile by only a few terms. We see on figure B-2 the profiles computed at different orders: Each number corresponds to the order up to which the separation profile is expanded, from the first to the sixth. Apparently, the shape of separation is not better predicted with more terms. In reality it is better predicted, but the convergence is slow, and the predicted profile diverges fast from the real shape of separation.

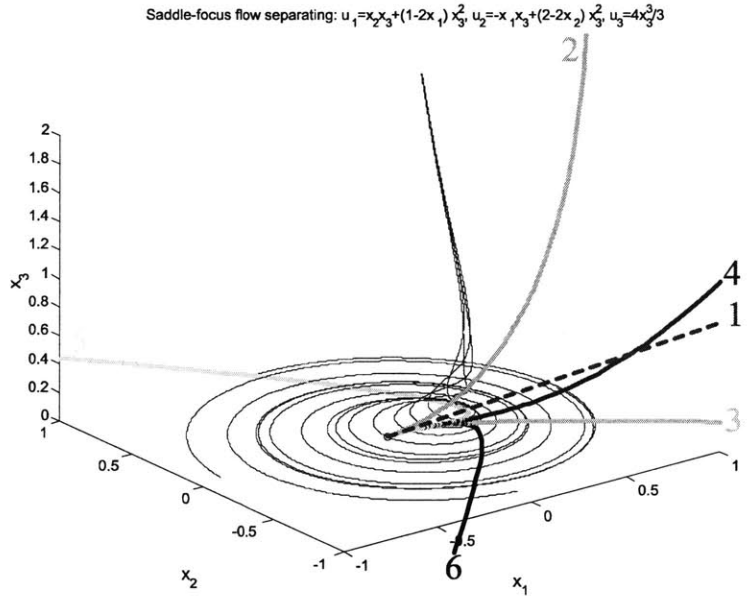

Figure B-2: Saddle-focus separation profiles at different orders.

B.2.2 Analyticity

Non-analyticity of the previous case

As we are about to show, the previous profile can not be predicted well because it is not analytic.

Writing the infinite power series

$$\begin{aligned} x_1 &= \sum_{n\geq 0} y_n \tilde{t}^n, \\ x_2 &= \sum_{n\geq 0} z_n \tilde{t}^n, \end{aligned}$$

which is true at least at the separation point, we seek the radius of convergence of this series, which corresponds to the radius of the disc around the separation point where this infinite expansion remains valid. We substitute these expansions into (B.10) to obtain

$$\begin{aligned} \sum_{n\geq 1}(n-1)y_{n-1}\tilde{t}^n &= -\frac{3}{2\delta}\left[\sum_{n\geq 0} z_n\tilde{t}^n + \alpha\tilde{t} + \delta\sum_{n\geq 1} y_{n-1}\tilde{t}^n\right], \\ \sum_{n\geq 1}(n-1)z_{n-1}\tilde{t}^n &= -\frac{3}{2\delta}\left[-\sum_{n\geq 0} y_n\tilde{t}^n + \beta\tilde{t} + \delta\sum_{n\geq 1} z_{n-1}\tilde{t}^n\right]. \end{aligned}$$

Equating each term at the n^{th} power, we obtain the system of equations valid for $n \geq 2$

$$\begin{aligned} \left(n+\frac{1}{2}\right) y_{n-1} &= -\frac{3}{2\delta} z_n, \\ \left(n+\frac{1}{2}\right) z_{n-1} &= +\frac{3}{2\delta} y_n, \end{aligned}$$

which implies when $n \geq 3$:

$$\begin{aligned} y_n &= -\left(\frac{2\delta}{3}\right)^2 \left(n^2-\frac{1}{4}\right) y_{n-2}, \\ z_n &= -\left(\frac{2\delta}{3}\right)^2 \left(n^2-\frac{1}{4}\right) z_{n-2}. \end{aligned}$$

Then we have

$$\begin{aligned} \lim_{n\to\infty}\left|\frac{y_n}{y_{n-2}}\right| &= \infty, \\ \lim_{n\to\infty}\left|\frac{z_n}{z_{n-2}}\right| &= \infty, \end{aligned}$$

and by D'Alembert's rule, the radius of convergence of the sequence is zero.

As the radius of convergence vanishes, the separation profile is never equal (except at the separation point) to its infinite power series, and this is going to prevent a good approximation of the real separation profile by finite truncations.

Comparison with another case

Apparently, the separation profile is not always analytic. But is it ever? Let us analyze a particular example, the flow given in (3.42): using the equivalent change of time-scale $\tilde{t} = x_3$ and writing

$$\begin{pmatrix} x_1 \\ x_2 \end{pmatrix} = \sum_{n\geq 0} G_n \tilde{t}^n \text{ with } G_n = \begin{pmatrix} y_n \\ z_n \end{pmatrix},$$

we have the equation

$$\sum_{n\geq 0} n G_n \tilde{t}^{n-1} \left(\tilde{t}^2 - \frac{2\delta}{3}\tilde{t}^3\right) = \begin{pmatrix} -1 & 1 \\ -1 & -1 \end{pmatrix} \sum_{n\geq 0} G_n \tilde{t}^n + \left(\begin{pmatrix} \alpha \\ \beta \end{pmatrix} + \delta \sum_{n\geq 0} G_n \tilde{t}^n \right) \tilde{t}^2,$$

then we deduce the equation in G_n for n large enough:

$$(n-1)\, G_{n-1} - \frac{2\delta}{3}(n-2)\, G_{n-2} = \begin{pmatrix} -1 & 1 \\ -1 & -1 \end{pmatrix} G_n + \delta G_{n-2},$$

that we rewrite

$$\begin{pmatrix} -1 & 1 \\ -1 & -1 \end{pmatrix} G_n - (n-1)\, G_{n-1} + \delta \left[\frac{2}{3}(n-2) + 1\right] G_{n-2} = 0. \tag{B.14}$$

The above equations give the system

$$\begin{aligned} -y_n + z_n &= (n-1)\, y_{n-1} - \delta \left[\frac{2}{3}(n-2) + 1\right] y_{n-2}, \\ -y_n - z_n &= (n-1)\, z_{n-1} - \delta \left[\frac{2}{3}(n-2) + 1\right] z_{n-2}. \end{aligned}$$

Looking for the limits of $\dfrac{y_n}{y_{n-1}}$ and $\dfrac{z_n}{z_{n-1}}$, we find that

$$\begin{aligned} \lim_{n\to\infty} \left| \frac{y_n}{y_{n-1}} \right| &= \frac{3}{2\delta}, \\ \lim_{n\to\infty} \left| \frac{z_n}{z_{n-1}} \right| &= \frac{3}{2\delta}, \end{aligned}$$

thus D'Alembert's rule implies that the radius of convergence is equal to $\dfrac{2\delta}{3}$.

As this flow is analytic, we will see that the following orders of separation will tend to come closer to the real separation, as shown in figure B-3. The profiles computed at different orders (each number corresponds to the order up to which the separation profile is expanded) always give a better approximation of the real separation.

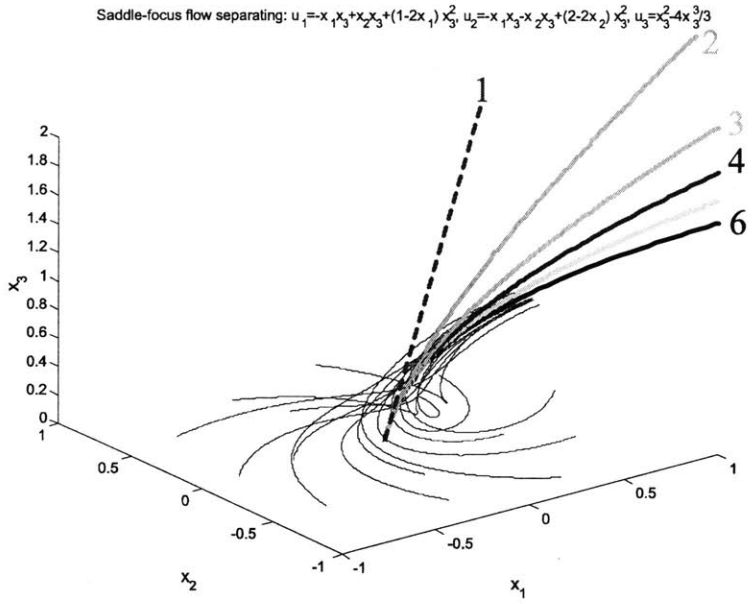

Figure B-3: Saddle-focus separation profiles at increasing orders.

General case

Considering the general equation (3.20), we once again perform the change of time-scale $\tilde{t} = x_3$ and write the power series in G_n, then we deduce the equation in G_n for n large enough:

$$-\frac{k_{11}+k_{22}}{2}(n-1)\,G_{n-1} - \frac{A_{1133}+A_{2233}}{3}(n-2)\,G_{n-2} = \mathbf{K}G_n + \begin{pmatrix} A_{1133} & A_{1233} \\ A_{1233} & A_{2233} \end{pmatrix} G_{n-2},$$

that we rewrite

$$\mathbf{K}G_n + \frac{\operatorname{Tr}\mathbf{K}}{2}(n-1)\,G_{n-1} + \left[\frac{\operatorname{Tr}\mathbf{A}}{3}(n-2) + \mathbf{A}\right] G_{n-2} = 0, \tag{B.15}$$

with $\operatorname{Tr}\mathbf{K} = k_{11}+k_{22}$ and $\mathbf{A} = \begin{pmatrix} A_{1133} & A_{1233} \\ A_{1233} & A_{2233} \end{pmatrix}$.

Defining $R =$ the radius of convergence of the power sequence, we can analyze the different cases when $\mathbf{K}$ is invertible.

When $\operatorname{Tr}\mathbf{K} = 0$ and $\mathbf{A} = 0$, the solution is a polynomial, $R = \infty$.

When $\operatorname{Tr}\mathbf{K} = 0$, $\mathbf{A} \neq 0$ and $\operatorname{Tr}\mathbf{A} = 0$, then $\dfrac{y_n}{y_{n-2}} \sim \dfrac{z_n}{z_{n-2}} \sim$ constants, thus $0 < R < \infty$.

When $\operatorname{Tr}\mathbf{K} = 0$ and $\operatorname{Tr}\mathbf{A} \neq 0$ (first case analyzed), then $\dfrac{y_n}{y_{n-2}} \sim \dfrac{z_n}{z_{n-2}} \sim n$ or n^2, which implies that $R = 0$.

When $\mathrm{Tr}\,\mathbf{K} \neq 0$ and $\mathbf{A} = 0$, then $\dfrac{y_n}{y_{n-2}} \sim \dfrac{z_n}{z_{n-2}} \sim n$ or n^2, which implies that $R = 0$.

When $\mathrm{Tr}\,\mathbf{K} \neq 0$, $\mathbf{A} \neq 0$ and $\mathrm{Tr}\,\mathbf{A} = 0$, then once again $\dfrac{y_n}{y_{n-2}} \sim \dfrac{z_n}{z_{n-2}} \sim n$ or n^2, which implies that $R = 0$.

Finally, when $\mathrm{Tr}\,\mathbf{K} \neq 0$ and $\mathrm{Tr}\,\mathbf{A} \neq 0$, we cannot directly determine the radius if convergence, but we still can see that it is finite: $0 \leq R < \infty$.

Conclusion

We have generalized these two examples and shown that the radius of convergence depends on the values of the parameters of the flow. Thus, in steady flows, we can determine the radius; and if it vanishes, the separation profile determined by the theory is not analytic, and is likely not to fit the real separation.

B.3 Steady saddle-foci of the bubble

B.3.1 Saddle-foci profile

We have already experienced some problems with saddle-foci profiles. If the saddle-saddle profile still seems accurate and draws well the bubble shape, once again we wonder if the saddle-foci profiles of the bubble at second order accurately fit the real separation. Thus we would like to numerically calculate the following orders of separation.

B.3.2 Change of variables

We re-center the differential equations around the saddle-foci. For example, let us consider $\mathbf{F} = \mathbf{0}$, and look at the first saddle-focus $\boldsymbol{\gamma}^3 = \begin{pmatrix} -d/c \\ -b\sqrt{1-\left(\frac{d}{ac}\right)^2} \end{pmatrix}$: setting

$$\begin{aligned} x_1 &= \gamma_1^3 + \zeta_1, \\ x_2 &= \gamma_2^3 + \zeta_2, \\ x_3 &= \zeta_3, \end{aligned} \tag{B.16}$$

we re-center the equations (3.45) around the separation point to obtain the new differential system

$$
\begin{aligned}
\dot{\zeta}_1 &= \zeta_3 \left[-\frac{2d\zeta_1}{ca^2} + \left(\frac{\zeta_1}{a}\right)^2 - \frac{2\sqrt{1-\left(\frac{d}{ac}\right)^2}\zeta_2}{b} + \left(\frac{\zeta_2}{b}\right)^2 \right] \\
&\quad + \zeta_3^2 \left[\alpha - A_{1133}\frac{d}{c} - A_{1233}b\sqrt{1-\left(\frac{d}{ac}\right)^2} + A_{1133}\zeta_1 + A_{1233}\zeta_2 + \frac{ca^2-2}{6a^2}\zeta_3 \right], \\
\dot{\zeta}_2 &= -\zeta_3 \left(-bc\sqrt{1-\left(\frac{d}{ac}\right)^2}\zeta_1 + c\zeta_1\zeta_2 \right) \\
&\quad + \zeta_3^2 \left[\beta - A_{1233}\frac{d}{c} - A_{2233}b\sqrt{1-\left(\frac{d}{ac}\right)^2} + A_{1233}\zeta_1 + A_{2233}\zeta_2 \right], \\
\dot{\zeta}_3 &= \left(\frac{d}{2} - \frac{cda^2-2d}{2ca^2} \right)\zeta_3^2 + \frac{ca^2-2}{2a^2}\zeta_1\zeta_3^2 - \frac{A_{1133}+A_{2233}}{3}\zeta_3^3.
\end{aligned}
\tag{B.17}
$$

Then we apply the usual change of time-scale $\tilde{t} = \zeta_3$, expand ζ_1 and ζ_2 in $\tilde{t}-$series, and with the previous notations we obtain the equation in y_n and z_n, the Taylor terms of the series of ζ_1 and ζ_2:

$$
\begin{aligned}
&\sum_{n=0}^{k} n y_n \tilde{t}^{n-1} \left(\left(\frac{d}{2} - \frac{cda^2-2d}{2ca^2} \right)\tilde{t}^2 + \frac{ca^2-2}{2a^2}\sum_{n=0}^{k} y_n \tilde{t}^{n+2} - \frac{A_{1133}+A_{2233}}{3}\tilde{t}^3 \right) + O(\tilde{t}^{k+1}) \\
&= \tilde{t} \left[-\frac{2d}{ca^2}\sum_{n=0}^{k} y_n \tilde{t}^n + \frac{1}{a^2}\left(\sum_{n=0}^{k} y_n \tilde{t}^n\right)^2 - \frac{2\sqrt{1-\left(\frac{d}{ac}\right)^2}}{b}\sum_{n=0}^{k} z_n \tilde{t}^n + \frac{1}{b^2}\left(\sum_{n=0}^{k} z_n \tilde{t}^n\right)^2 \right] \\
&+ \tilde{t}^2 \left[\alpha - A_{1133}\frac{d}{c} - A_{1233}b\sqrt{1-\left(\frac{d}{ac}\right)^2} + A_{1133}\sum_{n=0}^{k} y_n \tilde{t}^n + A_{1233}\sum_{n=0}^{k} z_n \tilde{t}^n + \frac{ca^2-2}{6a^2}\tilde{t} \right], \\
&\sum_{n=0}^{k} n z_n \tilde{t}^{n-1} \left(\left(\frac{d}{2} - \frac{cda^2-2d}{2ca^2} \right)\tilde{t}^2 + \frac{ca^2-2}{2a^2}\sum_{n=0}^{k} y_n \tilde{t}^{n+2} - \frac{A_{1133}+A_{2233}}{3}\tilde{t}^3 \right) + O(\tilde{t}^{k+1}) \\
&= -\tilde{t} \left(-bc\sqrt{1-\left(\frac{d}{ac}\right)^2}\sum_{n=0}^{k} y_n \tilde{t}^n + c\sum_{n=0}^{k} y_n \tilde{t}^n \sum_{n=0}^{k} z_n \tilde{t}^n \right) \\
&+ \tilde{t}^2 \left[\beta - A_{1233}\frac{d}{c} - A_{2233}b\sqrt{1-\left(\frac{d}{ac}\right)^2} + A_{1233}\sum_{n=0}^{k} y_n \tilde{t}^n + A_{2233}\sum_{n=0}^{k} z_n \tilde{t}^n \right].
\end{aligned}
\tag{B.18}
$$

B.3.3 First terms

Linear term

Looking at the linear term in (B.18), which corresponds to the first nonzero term in $\tilde{t}$, yields

$$-\frac{2d}{ca^2}y_0 + \frac{1}{a^2}(y_0)^2 - \frac{2\sqrt{1-\left(\frac{d}{ac}\right)^2}}{b}z_0 + \frac{1}{b^2}(z_0)^2 = 0,$$
$$-b\sqrt{1-\left(\frac{d}{ac}\right)^2}\,y_0 + y_0 z_0 = 0.$$

$\begin{pmatrix} y_0 \\ z_0 \end{pmatrix} = \begin{pmatrix} 0 \\ 0 \end{pmatrix}$ is a solution of this equation, and is the one we expect, but it is not the only one: there are also $\begin{pmatrix} y_0 \\ z_0 \end{pmatrix} = \begin{pmatrix} 0 \\ 2b\sqrt{1-\left(\frac{d}{ac}\right)^2} \end{pmatrix}$, $\begin{pmatrix} y_0 \\ z_0 \end{pmatrix} = \begin{pmatrix} \frac{d}{c} - a\sqrt{1-\left(\frac{d}{ac}\right)^2} \\ b\sqrt{1-\left(\frac{d}{ac}\right)^2} \end{pmatrix}$ and $\begin{pmatrix} y_0 \\ z_0 \end{pmatrix} = \begin{pmatrix} \frac{d}{c} + a\sqrt{1-\left(\frac{d}{ac}\right)^2} \\ b\sqrt{1-\left(\frac{d}{ac}\right)^2} \end{pmatrix}$, which correspond to the three other separation profiles of the three other separation points. Here, we only consider the first saddle-focus.

Quadratic term

Looking at the quadratic term in (B.18), which corresponds to the second nonzero term in $\tilde{t}$, yields

$$y_1\left(\frac{d}{2} - \frac{cda^2-2d}{2ca^2} + \frac{ca^2-2}{2a^2}y_0\right) = -\frac{2d}{ca^2}y_1 + \frac{2}{a^2}y_0 y_1 - \frac{2\sqrt{1-\left(\frac{d}{ac}\right)^2}}{b}z_1$$
$$+\frac{1}{b^2}z_0 z_1 + \alpha - A_{1133}\frac{d}{c} - A_{1233}b\sqrt{1-\left(\frac{d}{ac}\right)^2} + A_{1133}y_0 + A_{1233}z_0,$$
$$z_1\left(\frac{d}{2} - \frac{cda^2-2d}{2ca^2} + \frac{ca^2-2}{2a^2}y_0\right) = bc\sqrt{1-\left(\frac{d}{ac}\right)^2}\,y_1 - cy_0 z_1 - cy_1 z_0$$
$$+\beta - A_{1233}\frac{d}{c} - A_{2233}b\sqrt{1-\left(\frac{d}{ac}\right)^2} + A_{1233}y_0 + A_{2233}z_0.$$

Using the previous condition $\begin{pmatrix} y_0 \\ z_0 \end{pmatrix} = \begin{pmatrix} 0 \\ 0 \end{pmatrix}$ implies

$$\left(\frac{d}{2} + \frac{-cda^2 + 6d}{2ca^2}\right) y_1 + \frac{2\sqrt{1 - \left(\frac{d}{ac}\right)^2}}{b} z_1 = \alpha - A_{1133}\frac{d}{c} - A_{1233}b\sqrt{1 - \left(\frac{d}{ac}\right)^2},$$
$$-bc\sqrt{1 - \left(\frac{d}{ac}\right)^2}\, y_1 + \left(\frac{d}{2} - \frac{cda^2 - 2d}{2ca^2}\right) z_1 = \beta - A_{1233}\frac{d}{c} - A_{2233}b\sqrt{1 - \left(\frac{d}{ac}\right)^2},$$

corresponding to

$$\begin{pmatrix} \frac{3d}{ca^2} & \frac{2\sqrt{1-\left(\frac{d}{ac}\right)^2}}{b} \\ -bc\sqrt{1 - \left(\frac{d}{ac}\right)^2} & \frac{d}{ca^2} \end{pmatrix} \begin{pmatrix} y_1 \\ z_1 \end{pmatrix}$$
$$= \begin{pmatrix} \alpha \\ \beta \end{pmatrix} + \begin{pmatrix} A_{1133} & A_{1233} \\ A_{1233} & A_{2233} \end{pmatrix} \begin{pmatrix} -\frac{d}{c} \\ -b\sqrt{1 - \left(\frac{d}{ac}\right)^2} \end{pmatrix},$$

thus to the slope equation (3.53c).

Cubic term

Looking at the cubic term in (B.18), which corresponds to the third nonzero term in $\tilde{t}$, yields

$$y_1\left(\frac{ca^2 - 2}{2a^2} y_1 - \frac{A_{1133} + A_{2233}}{3}\right) + 2y_2\left(\frac{d}{2} - \frac{cda^2 - 2d}{2ca^2}\right)$$
$$= \left[-\frac{2d}{ca^2} y_2 + \frac{1}{a^2} y_1^2 - \frac{2\sqrt{1 - \left(\frac{d}{ac}\right)^2}}{b} z_2 + \frac{1}{b^2} z_1^2\right] + \left[A_{1133} y_1 + A_{1233} z_1 + \frac{ca^2 - 2}{6a^2}\right],$$
$$z_1\left(\frac{ca^2 - 2}{2a^2} y_1 - \frac{A_{1133} + A_{2233}}{3}\right) + 2z_2\left(\frac{d}{2} - \frac{cda^2 - 2d}{2ca^2}\right)$$
$$= -\left(-bc\sqrt{1 - \left(\frac{d}{ac}\right)^2}\, y_2 + c y_1 z_1\right) + \left[A_{1233} y_1 + A_{2233} z_1\right].$$

Rearranging the equations, we have

$$\begin{pmatrix} 2\dfrac{2d}{2ca^2}+\frac{2d}{ca^2} & \dfrac{2\sqrt{1-\left(\frac{d}{ac}\right)^2}}{b} \\ -bc\sqrt{1-\left(\frac{d}{ac}\right)^2} & 2\dfrac{2d}{2ca^2} \end{pmatrix}\begin{pmatrix} y_2 \\ z_2 \end{pmatrix} = \begin{pmatrix} \dfrac{ca^2-2}{6a^2} \\ 0 \end{pmatrix}$$
$$+\begin{pmatrix} A_{1133}+\dfrac{A_{1133}+A_{2233}}{3} & A_{1233} \\ A_{1233} & A_{2233}+\dfrac{A_{1133}+A_{2233}}{3} \end{pmatrix}\begin{pmatrix} y_1 \\ z_1 \end{pmatrix}$$
$$+\begin{pmatrix} \left(-\dfrac{ca^2-2}{2a^2}+\dfrac{1}{a^2}\right)y_1^2+\dfrac{1}{b^2}z_1^2 \\ \left(-\dfrac{ca^2-2}{2a^2}-c\right)y_1z_1 \end{pmatrix},$$

which is the same equation as (3.54c).

Any term

If we now consider any order $n \geq 4$ of the expansion, we have the equation

$$\begin{aligned}
&(n-1)\,y_{n-1}\left(\frac{d}{2}-\frac{cda^2-2d}{2ca^2}\right)+\frac{ca^2-2}{2a^2}\sum_{i=1}^{n-2} iy_iy_{n-1-i}-\frac{A_{1133}+A_{2233}}{3}(n-2)\,y_{n-2} \\
&=-\frac{2d}{ca^2}y_{n-1}+\frac{1}{a^2}\sum_{i=1}^{n-2}y_iy_{n-1-i}-\frac{2\sqrt{1-\left(\frac{d}{ac}\right)^2}}{b}z_{n-1}+\frac{1}{b^2}\sum_{i=1}^{n-2}z_iz_{n-1-i}+A_{1133}y_{n-2}+A_{1233}z_{n-2}, \\
&(n-1)\,z_{n-1}\left(\frac{d}{2}-\frac{cda^2-2d}{2ca^2}\right)\tilde{t}^2+\frac{ca^2-2}{2a^2}\sum_{i=1}^{n-2} iz_iy_{n-1-i}-\frac{A_{1133}+A_{2233}}{3}(n-2)\,z_{n-2} \quad \text{(B.19)} \\
&=bc\sqrt{1-\left(\frac{d}{ac}\right)^2}\,y_{n-1}-c\sum_{i=1}^{n-2}y_iz_{n-1-i}+A_{1233}y_{n-2}+A_{2233}z_{n-2},
\end{aligned}$$

which allows to recurrently calculate the different orders of separation.

B.3.4 Conclusion

It appears on our images that the second order separation profile draws well the shape of separation and is accurate enough. We still have a numerical model that we can use in case we would like higher accuracy.

B.4 Separation surfaces

B.4.1 Complicated shape of the attracting surfaces

On the left of figure 3-6, we see that particles near the separation points are first attracted to the separation points, then are attracted near the plane $x_2 = 0$. They come closer and closer

to this plane, rotating, and they finally leave it in a line which attracts all the particles away from the bubble.

On the right, we see the particles passing on top of the bubble, then they rotate, come back near the attracting surface in the plane $x_2 = 0$, and leave it following the same attracting line.

B.4.2 Theory

The analysis and creation of this surface are explained in chapter 4.

B.4.3 Steady bubble

In the steady case, the separation line satisfies the differential equation

$$s'(x) = \frac{B(x, s(x))}{A(x, s(x))}, \tag{B.20}$$

and joins the saddle-saddle, thus the point $\begin{pmatrix} -a \\ 0 \end{pmatrix}$, when $t \to -\infty$, to a saddle-focus, say the point $\begin{pmatrix} -d/c \\ b\sqrt{1-\left(\frac{d}{ac}\right)^2} \end{pmatrix}$, when $t \to +\infty$.

Formula (B.20) is local and allows obtaining the entire separation line by part. Indeed, we see that the trajectory joining the saddle-saddle to the saddle-focus will wind round the saddle-focus, which implies we can no longer define a bijection between x_1 and x_2 near this point . Locally, s satisfies

$$s' = \frac{-cx_1 s - ds}{\left(\frac{x_1}{a}\right)^2 + \left(\frac{s}{b}\right)^2 - 1}, \tag{B.21}$$

but we can not integrate directly this nonlinear differential equation.

Analytic solution

When we look at the trajectory connecting the saddle to the foci, we see that it leaves in the direction x_2. Thus we expect x_2 to vary faster than $x_1 + a$, and we can begin with solving the equation (B.21) when $\left(\frac{x_1}{a}\right)^2 - 1 \ll \left(\frac{s}{b}\right)^2$: then

$$s' \simeq -\frac{s\,(cx_1 + d)}{s^2} = -\frac{cx_1 + d}{s},$$

which integrates to

$$\frac{s^2(x_1)}{2} \simeq -\left(c\frac{x_1^2}{2} + dx_1\right) + \left(\frac{ca^2}{2} - da\right) = -\frac{c}{2}\left(x_1 + \frac{d}{c}\right)^2 + \frac{c}{2}\left(-a + \frac{d}{c}\right)^2,$$

thus we obtain the equation of an ellipse

$$\left(\frac{x_1^2 + \frac{d}{c}}{a - \frac{d}{c}}\right)^2 + \left(\frac{s}{\sqrt{c}\,(a - \frac{d}{c})}\right)^2 \simeq 1.$$

Then we can draw this ellipse and check how well it fits the real separation line.

Numerical solution

In the general case, we cannot solve (B.21) analytically, but we can still solve it numerically, as shown in figure B-4. Here we compare the shape of the separation line (we solve this equation by part, changing the sense of variation of x_1 each time s' vanishes: the separation line turns around the focus) with its approximation analytically obtained and the simple shape of an ellipse going from the saddle-saddle to each saddle-focus. Even if an ellipse is a simple analytic shape, it is a good approximation which fits well the true separation line .

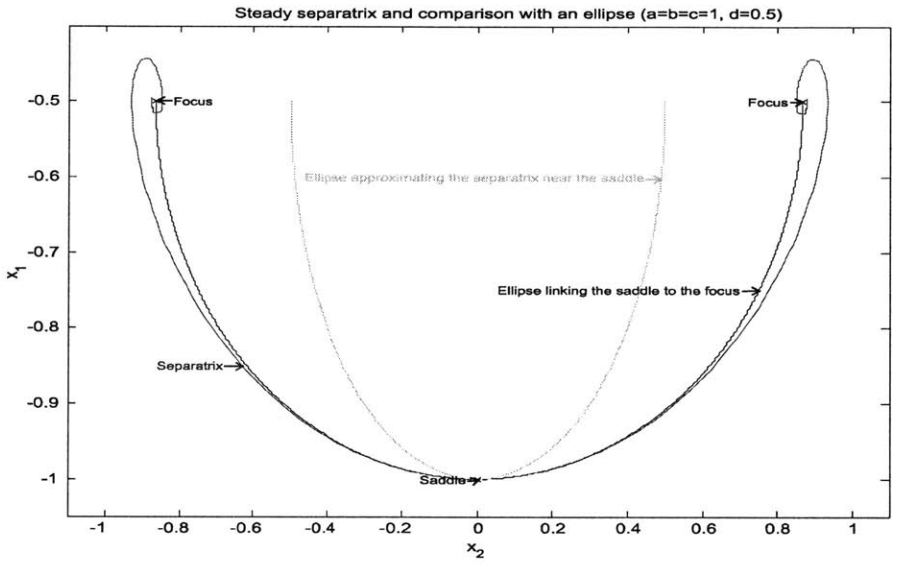

Figure B-4: Numerical separation line and comparison with ellipse shapes.

B.4.4 Periodic bubble

The equation of the separation line writes

$$\bar{B}(x, s(x), .) - s'(x)\bar{A}(x, s(x), .) = 0, \tag{B.22}$$

where $\bar{h}$ refers to the temporal mean of h. When the coefficients a, b, c and d are periodic, we replace them by their mean value to obtain

$$s' = \frac{-\bar{c}\, x_1\, s - \bar{d}\, s}{x_1^2 \overline{\left(\frac{1}{a}\right)^2} + s^2 \overline{\left(\frac{1}{b}\right)^2} - 1}. \tag{B.23}$$

This equation has already been analyzed in the steady case.

B.5 Periodic moving saddle-foci

B.5.1 Periodic slope

If we look at the slope in a separation point γ of (3.57), we have

$$\int_{t_0}^{s} \begin{pmatrix} \left(\frac{\gamma_1 - f_1}{a}\right)^2 + \left(\frac{\gamma_2 - f_2}{b}\right)^2 - 1 \\ -c(\gamma_1 - f_1)(\gamma_2 - f_2) - d(\gamma_2 - f_2) \end{pmatrix} dr = \begin{pmatrix} 0 \\ -\frac{\varepsilon(\gamma_2 - f_2)}{\omega}(\sin\omega t - \sin\omega t_0) \end{pmatrix},$$

then

$$\begin{pmatrix} \frac{(\gamma_1 - f_1)(6 - a^2c) - a^2d}{2a^2} & 2\frac{\gamma_2 - f_2}{b^2} \\ -c(\gamma_2 - f_2) & \frac{(\gamma_1 - f_1)(2 - 3a^2c) - 3a^2d}{2a^2} \end{pmatrix}$$
$$\times \int_{t_0}^{s} \begin{pmatrix} \left(\frac{\gamma_1 - f_1}{a}\right)^2 + \left(\frac{\gamma_2 - f_2}{b}\right)^2 - 1 \\ -c(\gamma_1 - f_1)(\gamma_2 - f_2) - d(\gamma_2 - f_2) \end{pmatrix} dr$$
$$= \begin{pmatrix} -2\frac{\varepsilon(\gamma_2 - f_2)^2}{\omega b^2}(\sin\omega t - \sin\omega t_0) \\ -\left((\gamma_1 - f_1)(2 - 3a^2c) - 3a^2d\right)\frac{\varepsilon(\gamma_2 - f_2)}{2a^2\omega}(\sin\omega t - \sin\omega t_0) \end{pmatrix},$$

thus

$$\int_{t_0}^{t} \left[\begin{pmatrix} \alpha \\ \beta \end{pmatrix} + \begin{pmatrix} A_{1133} & A_{1233} \\ A_{1233} & A_{2233} \end{pmatrix} \gamma \right.$$
$$+ \begin{pmatrix} \frac{(\gamma_1 - f_1)(6 - a^2c) - a^2d}{2a^2} & 2\frac{\gamma_2 - f_2}{b^2} \\ -c(\gamma_2 - f_2) & \frac{(\gamma_1 - f_1)(2 - 3a^2c) - 3a^2d}{2a^2} \end{pmatrix}$$
$$\left. x \int_{t_0}^{s} \begin{pmatrix} \left(\frac{\gamma_1 - f_1}{a}\right)^2 + \left(\frac{\gamma_2 - f_2}{b}\right)^2 - 1 \\ -c(\gamma_1 - f_1)(\gamma_2 - f_2) - d(\gamma_2 - f_2) \end{pmatrix} dr \right] ds$$
$$= (t - t_0) \left[\begin{pmatrix} \alpha \\ \beta \end{pmatrix} + \begin{pmatrix} A_{1133} & A_{1233} \\ A_{1233} & A_{2233} \end{pmatrix} \gamma + \begin{pmatrix} 2\frac{\varepsilon(\gamma_2 - f_2)^2}{\omega b^2}\sin\omega t_0 \\ \left((\gamma_1 - f_1)(2 - 3a^2c) - 3a^2e\right)\frac{\varepsilon(\gamma_2 - f_2)}{2a^2\omega}\sin\omega t_0 \end{pmatrix} \right]$$
$+$ terms in $\cos\omega t$, $\sin\omega t$ and $\cos 2\omega t$.

Taking the limit $t \longrightarrow -\infty$, we only keep the linear terms of this vector and of the matrix

$$\left[\int_{t_0}^{t} \begin{pmatrix} \dfrac{(\gamma_1 - f_1)(6 - a^2c) - a^2d}{2a^2} & 2\dfrac{\gamma_2 - f_2}{b^2} \\ -c(\gamma_2 - f_2) & \dfrac{(\gamma_1 - f_1)(2 - 3a^2c) - 3a^2d}{2a^2} \end{pmatrix} d\tau\right]^{-1},$$

we eliminate the periodic terms in the slope formula to finally get

$$\begin{aligned} \mathrm{g}_0(t_0) = &- \lim_{t\to-\infty} \left[(t - t_0) \begin{pmatrix} \dfrac{(\gamma_1 - f_1)(6 - a^2c) - a^2e}{2a^2} & 2\dfrac{\gamma_2 - f_2}{b^2} \\ -c(\gamma_2 - f_2) & \dfrac{(\gamma_1 - f_1)(2 - 3a^2c) - 3a^2e}{2a^2} \end{pmatrix} d\tau\right]^{-1} \\ &\times (t - t_0)\left[\begin{pmatrix} \alpha \\ \beta \end{pmatrix} + \begin{pmatrix} A_{1133} & A_{1233} \\ A_{1233} & A_{2233} \end{pmatrix}\gamma + \begin{pmatrix} 2\dfrac{\varepsilon(\gamma_2 - f_2)^2}{\omega b^2}\sin\omega t_0 \\ ((\gamma_1 - f_1)(2 - 3a^2c) - 3a^2e)\dfrac{\varepsilon(\gamma_2 - f_2)}{2a^2\omega}\sin\omega t_0 \end{pmatrix}\right] \\ = &- \begin{pmatrix} \dfrac{(\gamma_1 - f_1)(6 - a^2c) - a^2e}{2a^2} & 2\dfrac{\gamma_2 - f_2}{b^2} \\ -c(\gamma_2 - f_2) & \dfrac{(\gamma_1 - f_1)(2 - 3a^2c) - 3a^2e}{2a^2} \end{pmatrix}^{-1} \qquad \text{(B.24)} \\ &\times \left[\begin{pmatrix} \alpha \\ \beta \end{pmatrix} + \begin{pmatrix} A_{1133} & A_{1233} \\ A_{1233} & A_{2233} \end{pmatrix}\gamma + \begin{pmatrix} 2\dfrac{\varepsilon(\gamma_2 - f_2)^2}{\omega b^2}\sin\omega t_0 \\ ((\gamma_1 - f_1)(2 - 3a^2c) - 3a^2e)\dfrac{\varepsilon(\gamma_2 - f_2)}{2a^2\omega}\sin\omega t_0 \end{pmatrix}\right]. \end{aligned}$$

We remark that when $\gamma_2 - f_2 = 0$, the periodic terms disappear, thus there will not be any periodic terms in the saddle-saddle separation points.

B.5.2 Periodic curvature

In the same way, we can analyze the terms of the curvature formula: we first have

$$\begin{aligned} &\begin{pmatrix} \dfrac{(\gamma_1 - f_1)(6 - a^2c) - a^2d}{2a^2} & 2\dfrac{\gamma_2 - f_2}{b^2} \\ -c(\gamma_2 - f_2) & \dfrac{(\gamma_1 - f_1)(2 - 3a^2c) - 3a^2d}{2a^2} \end{pmatrix} \mathrm{g}_0(s) \\ = &- \left[\begin{pmatrix} \alpha \\ \beta \end{pmatrix} + \begin{pmatrix} A_{1133} & A_{1233} \\ A_{1233} & A_{2233} \end{pmatrix}\gamma + \begin{pmatrix} 2\dfrac{\varepsilon(\gamma_2 - f_2)^2}{\omega b^2}\sin\omega s \\ ((\gamma_1 - f_1)(2 - 3a^2c) - 3a^2e)\dfrac{\varepsilon(\gamma_2 - f_2)}{2a^2\omega}\sin\omega s \end{pmatrix}\right], \end{aligned}$$

which implies

$$\begin{aligned}
&\int_{t_0}^{\tau} \left[\begin{pmatrix} \alpha \\ \beta \end{pmatrix} + \begin{pmatrix} A_{1133} & A_{1233} \\ A_{1233} & A_{2233} \end{pmatrix} \gamma \right. \\
&\left. + \begin{pmatrix} \dfrac{(\gamma_1 - f_1)(6 - a^2c) - a^2d}{2a^2} & 2\dfrac{\gamma_2 - f_2}{b^2} \\ -c(\gamma_2 - f_2) & \dfrac{(\gamma_1 - f_1)(2 - 3a^2c) - 3a^2d}{2a^2} \end{pmatrix} \mathrm{g}_0(s) \right] ds \\
= & -\int_{t_0}^{\tau} \begin{pmatrix} 2\dfrac{\varepsilon(\gamma_2 - f_2)^2}{\omega b^2} \sin \omega s \\ ((\gamma_1 - f_1)(2 - 3a^2c) - 3a^2e)\dfrac{\varepsilon(\gamma_2 - f_2)}{2a^2\omega} \sin \omega s \end{pmatrix} ds \\
= & \begin{pmatrix} 2\dfrac{\varepsilon(\gamma_2 - f_2)^2}{\omega b^2}(\cos \omega\tau - \cos \omega t_0) \\ (\gamma_1 - f_1)(2 - 3a^2c)\dfrac{\varepsilon(\gamma_2 - f_2)}{2a^2\omega}(\cos \omega\tau - \cos \omega t_0) \end{pmatrix}.
\end{aligned}$$

Then in the following term

$$\begin{aligned}
&\int_{t_0}^{t} 2 \begin{pmatrix} \dfrac{(\gamma_1 - f_1)(4 - a^2c) - a^2d}{a^2} & 2\dfrac{\gamma_2 - f_2}{b^2} \\ -c(\gamma_2 - f_2) & 2\dfrac{(\gamma_1 - f_1)(1 - a^2c) - a^2d}{a^2} \end{pmatrix} \\
&\times \int_{t_0}^{\tau} \left[\begin{pmatrix} \alpha \\ \beta \end{pmatrix} + \begin{pmatrix} A_{1133} & A_{1233} \\ A_{1233} & A_{2233} \end{pmatrix} \gamma \right. \\
&\left. \left. + \begin{pmatrix} \dfrac{(\gamma_1 - f_1)(6 - a^2c) - a^2d}{2a^2} & 2\dfrac{\gamma_2 - f_2}{b^2} \\ -c(\gamma_2 - f_2) & \dfrac{(\gamma_1 - f_1)(2 - 3a^2c) - 3a^2d}{2a^2} \end{pmatrix} \mathrm{g}_0(s) \right] ds \right] d\tau \\
= & \; 2\int_{t_0}^{t} \left[\begin{pmatrix} \dfrac{(\gamma_1 - f_1)(4 - a^2c) - a^2e}{a^2} & 2\dfrac{\gamma_2 - f_2}{b^2} \\ -c(\gamma_2 - f_2) & 2\dfrac{(\gamma_1 - f_1)(1 - a^2c) - a^2e}{a^2} \end{pmatrix} \right. \\
&\left. -\varepsilon \begin{pmatrix} 1 & 0 \\ 0 & 2 \end{pmatrix} \cos \omega\tau \right] \times \begin{pmatrix} 2\dfrac{\varepsilon(\gamma_2 - f_2)^2}{\omega b^2}(\cos \omega\tau - \cos \omega t_0) \\ (\gamma_1 - f_1)(2 - 3a^2c)\dfrac{\varepsilon(\gamma_2 - f_2)}{2a^2\omega}(\cos \omega\tau - \cos \omega t_0) \end{pmatrix},
\end{aligned}$$

we only keep the dominant terms

$$2(t-t_0)\begin{pmatrix} \dfrac{(\gamma_1-f_1)(4-a^2c)-a^2e}{a^2} & 2\dfrac{\gamma_2-f_2}{b^2} \\ -c(\gamma_2-f_2) & 2\dfrac{(\gamma_1-f_1)(1-a^2c)-a^2e}{a^2} \end{pmatrix}$$
$$\times\begin{pmatrix} -2\dfrac{\varepsilon(\gamma_2-f_2)^2}{\omega b^2}\cos\omega t_0 \\ -(\gamma_1-f_1)(2-3a^2c)\dfrac{\varepsilon(\gamma_2-f_2)}{2a^2\omega}\cos\omega t_0 \end{pmatrix}$$
$$-(t-t_0)\varepsilon\begin{pmatrix} 1 & 0 \\ 0 & 2 \end{pmatrix}\times\begin{pmatrix} 2\dfrac{\varepsilon(\gamma_2-f_2)^2}{\omega b^2} \\ (\gamma_1-f_1)(2-3a^2c)\dfrac{\varepsilon(\gamma_2-f_2)}{2a^2\omega} \end{pmatrix}.$$

We also have to analyze the nonlinear term

$$\int_{t_0}^{t} \mathbf{g}_0^T\mathbb{T}\mathbf{g}_0\ dt,$$

with the tensor $\mathbb{T}$ defined by

$$\mathbf{g}_0^T\mathbb{T}\mathbf{g}_0 = \begin{pmatrix} \dfrac{4-ca^2}{a^2}(g_{0,1})^2+\dfrac{2}{b^2}(g_{0,2})^2 \\ \dfrac{2-3ca^2}{a^2}g_{0,1}g_{0,2} \end{pmatrix},$$

and we can decompose $\mathbf{g}_0$ as

$$\mathbf{g}_0 = \mathbf{g}_0^S+\mathbf{g}_0^P\sin\omega t_0 = \begin{pmatrix} g_{0,1}^S \\ g_{0,2}^S \end{pmatrix}+\begin{pmatrix} g_{0,1}^P \\ g_{0,2}^P \end{pmatrix}\sin\omega t_0.$$

Thus we have

$$
\begin{aligned}
& \int_{t_0}^{t} \mathbf{g}_0^T \mathbb{T} \mathbf{g}_0 \, dt \\
= & \int_{t_0}^{t} \begin{pmatrix} \frac{4-ca^2}{a^2} \left(\mathbf{g}_{0,1}^S + \mathbf{g}_{0,1}^P \sin\omega t_0\right)^2 + \frac{2}{b^2} \left(\mathbf{g}_{0,2}^S + \mathbf{g}_{0,2}^P \sin\omega t_0\right)^2 \\ \frac{2-3ca^2}{a^2} \left(\mathbf{g}_{0,1}^S + \mathbf{g}_{0,1}^P \sin\omega t_0\right) \left(\mathbf{g}_{0,2}^S + \mathbf{g}_{0,2}^P \sin\omega t_0\right) \end{pmatrix} \\
= & \int_{t_0}^{t} \begin{pmatrix} \frac{4-ca^2}{a^2} \left(\mathbf{g}_{0,1}^S\right)^2 + \frac{2}{b^2} \left(\mathbf{g}_{0,2}^S\right)^2 \\ \frac{2-3ca^2}{a^2} \mathbf{g}_{0,1}^S \mathbf{g}_{0,2}^S \end{pmatrix} + \sin\omega t_0 \begin{pmatrix} \frac{8-2ca^2}{a^2} \mathbf{g}_{0,1}^S \mathbf{g}_{0,1}^P + \frac{4}{b^2} \mathbf{g}_{0,2}^S \mathbf{g}_{0,2}^P \\ \frac{2-3ca^2}{a^2} \left(\mathbf{g}_{0,1}^S \mathbf{g}_{0,2}^P + \mathbf{g}_{0,1}^P \mathbf{g}_{0,2}^S\right) \end{pmatrix} \\
& + \sin^2\omega t_0 \begin{pmatrix} \frac{4-ca^2}{a^2} \left(\mathbf{g}_{0,1}^P\right)^2 + \frac{2}{b^2} \left(\mathbf{g}_{0,2}^P\right)^2 \\ \frac{2-3ca^2}{a^2} \mathbf{g}_{0,1}^P \mathbf{g}_{0,2}^P \end{pmatrix} \end{pmatrix} dt \\
= & (t-t_0) \begin{pmatrix} \frac{4-ca^2}{a^2} \left(\mathbf{g}_{0,1}^S\right)^2 + \frac{2}{b^2} \left(\mathbf{g}_{0,2}^S\right)^2 \\ \frac{2-3ca^2}{a^2} \mathbf{g}_{0,1}^S \mathbf{g}_{0,2}^S \end{pmatrix} \\
& - \frac{\cos\omega t - \cos\omega t_0}{\omega} \begin{pmatrix} \frac{8-2ca^2}{a^2} \mathbf{g}_{0,1}^S \mathbf{g}_{0,1}^P + \frac{4}{b^2} \mathbf{g}_{0,2}^S \mathbf{g}_{0,2}^P \\ \frac{2-3ca^2}{a^2} \left(\mathbf{g}_{0,1}^S \mathbf{g}_{0,2}^P + \mathbf{g}_{0,1}^P \mathbf{g}_{0,2}^S\right) \end{pmatrix} \\
& + \left(\frac{t-t_0}{2} - \frac{\sin 2\omega t - \sin 2\omega t_0}{4\omega}\right) \begin{pmatrix} \frac{4-ca^2}{a^2} \left(\mathbf{g}_{0,1}^P\right)^2 + \frac{2}{b^2} \left(\mathbf{g}_{0,2}^P\right)^2 \\ \frac{2-3ca^2}{a^2} \mathbf{g}_{0,1}^P \mathbf{g}_{0,2}^P \end{pmatrix}.
\end{aligned}
$$

Finally, we can write the curvature, keeping only the linear terms

$$
\begin{aligned}
\mathrm{g}_1(t_0) \;=\; & -\lim_{t\to-\infty}\left[2(t-t_0)\begin{pmatrix} \dfrac{(\gamma_1-f_1)(4-a^2c)-a^2e}{a^2} & 2\dfrac{\gamma_2-f_2}{b^2} \\ -c(\gamma_2-f_2) & 2\dfrac{(\gamma_1-f_1)(1-a^2c)-a^2e}{a^2}\end{pmatrix}\right]^{-1} \\
& \times\left[2(t-t_0)\begin{pmatrix} \dfrac{ca^2-2}{6a^2} \\ 0\end{pmatrix}\right. \\
& +2\begin{pmatrix} \frac{4A_{1133}+A_{2233}}{3} & A_{1233} \\ A_{1233} & \frac{A_{1133}+4A_{2233}}{3}\end{pmatrix}\int_{t_0}^{t}\mathrm{g}_0\,dt \\
& +(t-t_0)\begin{pmatrix} \dfrac{4-ca^2}{a^2}\left(\mathrm{g}^S_{0,1}\right)^2+\dfrac{2}{b^2}\left(\mathrm{g}^S_{0,2}\right)^2 \\ \dfrac{2-3ca^2}{a^2}\mathrm{g}^S_{0,1}\mathrm{g}^S_{0,2}\end{pmatrix} \\
& +\frac{t-t_0}{2}\begin{pmatrix} \dfrac{4-ca^2}{a^2}\left(\mathrm{g}^P_{0,1}\right)^2+\dfrac{2}{b^2}\left(\mathrm{g}^P_{0,2}\right)^2 \\ \dfrac{2-3ca^2}{a^2}\mathrm{g}^P_{0,1}\mathrm{g}^P_{0,2}\end{pmatrix} \\
& +2(t-t_0)\begin{pmatrix} \dfrac{(\gamma_1-f_1)(4-a^2c)-a^2e}{a^2} & 2\dfrac{\gamma_2-f_2}{b^2} \\ -c(\gamma_2-f_2) & 2\dfrac{(\gamma_1-f_1)(1-a^2c)-a^2e}{a^2}\end{pmatrix} \\
& \times\begin{pmatrix} -2\dfrac{\varepsilon(\gamma_2-f_2)^2}{\omega b^2}\cos\omega t_0 \\ -(\gamma_1-f_1)(2-3a^2c)\dfrac{\varepsilon(\gamma_2-f_2)}{2a^2\omega}\cos\omega t_0\end{pmatrix} \\
& \left.-(t-t_0)\varepsilon\begin{pmatrix} 2\dfrac{\varepsilon(\gamma_2-f_2)^2}{\omega b^2} \\ (\gamma_1-f_1)(2-3a^2c)\dfrac{\varepsilon(\gamma_2-f_2)}{a^2\omega}\end{pmatrix}\right],
\end{aligned}
$$

which simplifies to the still complicated formula

$$
\begin{aligned}
\mathbf{g}_1(t_0) \;=\; & -\left[2\begin{pmatrix} \dfrac{(\gamma_1-f_1)(4-a^2c)-a^2e}{a^2} & 2\dfrac{\gamma_2-f_2}{b^2} \\ -c(\gamma_2-f_2) & 2\dfrac{(\gamma_1-f_1)(1-a^2c)-a^2e}{a^2}\end{pmatrix}\right]^{-1} \\
& \times\left[2\begin{pmatrix} \dfrac{ca^2-2}{6a^2} \\ 0\end{pmatrix}+2\begin{pmatrix} \frac{4A_{1133}+A_{2233}}{3} & A_{1233} \\ A_{1233} & \frac{A_{1133}+4A_{2233}}{3}\end{pmatrix}\mathbf{g}_0^S\right. \\
& +\begin{pmatrix} \dfrac{4-ca^2}{a^2}\left(\mathbf{g}_{0,1}^S\right)^2+\dfrac{2}{b^2}\left(\mathbf{g}_{0,2}^S\right)^2 \\ \dfrac{2-3ca^2}{a^2}\mathbf{g}_{0,1}^S\mathbf{g}_{0,2}^S\end{pmatrix}+\frac{1}{2}\begin{pmatrix} \dfrac{4-ca^2}{a^2}\left(\mathbf{g}_{0,1}^P\right)^2+\dfrac{2}{b^2}\left(\mathbf{g}_{0,2}^P\right)^2 \\ \dfrac{2-3ca^2}{a^2}\mathbf{g}_{0,1}^P\mathbf{g}_{0,2}^P\end{pmatrix} \\
& -\varepsilon\begin{pmatrix} 2\dfrac{\varepsilon(\gamma_2-f_2)^2}{\omega b^2} \\ (\gamma_1-f_1)(2-3a^2c)\dfrac{\varepsilon(\gamma_2-f_2)}{a^2\omega}\end{pmatrix} \qquad\qquad (B.25) \\
& +2\begin{pmatrix} \dfrac{(\gamma_1-f_1)(4-a^2c)-a^2e}{a^2} & 2\dfrac{\gamma_2-f_2}{b^2} \\ -c(\gamma_2-f_2) & 2\dfrac{(\gamma_1-f_1)(1-a^2c)-a^2e}{a^2}\end{pmatrix} \\
& \left.\times\begin{pmatrix} -2\dfrac{\varepsilon(\gamma_2-f_2)^2}{\omega b^2} \\ -(\gamma_1-f_1)(2-3a^2c)\dfrac{\varepsilon(\gamma_2-f_2)}{2a^2\omega}\cos\end{pmatrix}\cos\omega t_0\right]
\end{aligned}
$$

Once again, when $\gamma_2 = f_2$, $\mathbf{g}_1$ does not depend on time. Only the profiles of the saddle-foci will move.

B.6 Periodic moving saddle-saddles

B.6.1 Periodic slope

If we look at the slope in a separation point $\boldsymbol{\gamma}$ of (3.60), we have

$$
\int_{t_0}^{s}\begin{pmatrix} \left(\dfrac{\gamma_1-f_1}{a}\right)^2+\left(\dfrac{\gamma_2-f_2}{b}\right)^2-1 \\ -c(\gamma_1-f_1)(\gamma_2-f_2)-d(\gamma_2-f_2)\end{pmatrix}dr=\begin{pmatrix} -\dfrac{\upsilon(\gamma_1-f_1)}{\omega}(\sin\omega t-\sin\omega t_0) \\ 0\end{pmatrix},
$$

then

$$\begin{pmatrix} \dfrac{(\gamma_1 - f_1)(6 - a^2c) - a^2d}{2a^2} & 2\dfrac{\gamma_2 - f_2}{b^2} \\ -c(\gamma_2 - f_2) & \dfrac{(\gamma_1 - f_1)(2 - 3a^2c) - 3a^2d}{2a^2} \end{pmatrix}$$
$$\times \int_{t_0}^{s} \begin{pmatrix} \left(\dfrac{\gamma_1 - f_1}{a}\right)^2 + \left(\dfrac{\gamma_2 - f_2}{b}\right)^2 - 1 \\ -c(\gamma_1 - f_1)(\gamma_2 - f_2) - d(\gamma_2 - f_2) \end{pmatrix} dr$$
$$= \begin{pmatrix} -\dfrac{(\gamma_1 - f_1)(6 - a^2c) - a^2d}{2a^2} \dfrac{\upsilon(\gamma_1 - f_1)}{\omega}(\sin\omega t - \sin\omega t_0) \\ c(\gamma_2 - f_2)\dfrac{\upsilon(\gamma_1 - f_1)}{\omega}(\sin\omega t - \sin\omega t_0) \end{pmatrix},$$

thus

$$\int_{t_0}^{t} \left[\begin{pmatrix} \alpha \\ \beta \end{pmatrix} + \begin{pmatrix} A_{1133} & A_{1233} \\ A_{1233} & A_{2233} \end{pmatrix} \gamma \right.$$
$$+ \begin{pmatrix} \dfrac{(\gamma_1 - f_1)(6 - a^2c) - a^2d}{2a^2} & 2\dfrac{\gamma_2 - f_2}{b^2} \\ -c(\gamma_2 - f_2) & \dfrac{(\gamma_1 - f_1)(2 - 3a^2c) - 3a^2d}{2a^2} \end{pmatrix}$$
$$\left. x \int_{t_0}^{s} \begin{pmatrix} \left(\dfrac{\gamma_1 - f_1}{a}\right)^2 + \left(\dfrac{\gamma_2 - f_2}{b}\right)^2 - 1 \\ -c(\gamma_1 - f_1)(\gamma_2 - f_2) - d(\gamma_2 - f_2) \end{pmatrix} dr \right] ds$$
$$= (t - t_0) \left[\begin{pmatrix} \alpha \\ \beta \end{pmatrix} + \begin{pmatrix} A_{1133} & A_{1233} \\ A_{1233} & A_{2233} \end{pmatrix} \gamma + \begin{pmatrix} \dfrac{(\gamma_1 - f_1)(6 - a_0^2c) - a_0^2d}{2a_0^2} \dfrac{\upsilon(\gamma_1 - f_1)}{\omega} \sin\omega t_0 \\ -c(\gamma_2 - f_2)\dfrac{\upsilon(\gamma_1 - f_1)}{\omega} \sin\omega t_0 \end{pmatrix} \right]$$
$$+ \text{ terms in } \cos\omega t,\ \sin\omega t \text{ and } \cos 2\omega t.$$

Taking the limit $t \longrightarrow -\infty$, we only keep the dominant terms of this vector and of the matrix

$$\left[\int_{t_0}^{t} \begin{pmatrix} \dfrac{(\gamma_1 - f_1)(6 - a^2c) - a^2d}{2a^2} & 2\dfrac{\gamma_2 - f_2}{b^2} \\ -c(\gamma_2 - f_2) & \dfrac{(\gamma_1 - f_1)(2 - 3a^2c) - 3a^2d}{2a^2} \end{pmatrix} d\tau \right]^{-1},$$

we eliminate the periodic terms in the slope formula to finally get

$$
\begin{aligned}
\mathbf{g}_0(t_0) = &- \lim_{t\to-\infty} \left[(t-t_0) \begin{pmatrix} \dfrac{(\gamma_1-f_1)(6-a_0^2c)-a_0^2d}{2a_0^2} & 2\dfrac{\gamma_2-f_2}{b^2} \\ -c(\gamma_2-f_2) & \dfrac{(\gamma_1-f_1)(2-3a_0^2c)-3a_0^2d}{2a_0^2} \end{pmatrix} d\tau \right]^{-1} \\
&\times (t-t_0) \left[\begin{pmatrix} \alpha \\ \beta \end{pmatrix} + \begin{pmatrix} A_{1133} & A_{1233} \\ A_{1233} & A_{2233} \end{pmatrix} \boldsymbol{\gamma} + \begin{pmatrix} \dfrac{(\gamma_1-f_1)(6-a_0^2c)-a_0^2d}{2a_0^2} \dfrac{\upsilon(\gamma_1-f_1)}{\omega} \sin\omega t_0 \\ -c(\gamma_2-f_2)\dfrac{\upsilon(\gamma_1-f_1)}{\omega}\sin\omega t_0 \end{pmatrix} \right] \\
&= - \begin{pmatrix} \dfrac{(\gamma_1-f_1)(6-a_0^2c)-a_0^2d}{2a_0^2} & 2\dfrac{\gamma_2-f_2}{b^2} \\ -c(\gamma_2-f_2) & \dfrac{(\gamma_1-f_1)(2-3a_0^2c)-3a_0^2d}{2a_0^2} \end{pmatrix}^{-1} \qquad \text{(B.26)} \\
&\times \left[\begin{pmatrix} \alpha \\ \beta \end{pmatrix} + \begin{pmatrix} A_{1133} & A_{1233} \\ A_{1233} & A_{2233} \end{pmatrix} \boldsymbol{\gamma} + \begin{pmatrix} \dfrac{(\gamma_1-f_1)(6-a_0^2c)-a_0^2d}{2a_0^2} \dfrac{\upsilon(\gamma_1-f_1)}{\omega} \sin\omega t_0 \\ -c(\gamma_2-f_2)\dfrac{\upsilon(\gamma_1-f_1)}{\omega}\sin\omega t_0 \end{pmatrix} \right].
\end{aligned}
$$

B.6.2 Periodic curvature

In the same way, we can analyze the terms of the curvature formula: we first have

$$
\begin{aligned}
&\begin{pmatrix} \dfrac{(\gamma_1-f_1)(6-a^2c)-a^2d}{2a^2} & 2\dfrac{\gamma_2-f_2}{b^2} \\ -c(\gamma_2-f_2) & \dfrac{(\gamma_1-f_1)(2-3a^2c)-3a^2d}{2a^2} \end{pmatrix} \mathbf{g}_0(s) \\
= &- \left[\begin{pmatrix} \alpha \\ \beta \end{pmatrix} + \begin{pmatrix} A_{1133} & A_{1233} \\ A_{1233} & A_{2233} \end{pmatrix} \boldsymbol{\gamma} + \begin{pmatrix} \left(-\dfrac{3(\gamma_1-f_1)}{a_0^2} + \dfrac{(\gamma_1-f_1)c+d}{2}\right) \dfrac{\upsilon(\gamma_1-f_1)}{\omega} \sin\omega s \\ -c(\gamma_2-f_2)\dfrac{\upsilon(\gamma_1-f_1)}{\omega}\sin\omega s \end{pmatrix} \right],
\end{aligned}
$$

which implies

$$\begin{aligned}
&\int_{t_0}^{\tau} \left[\begin{pmatrix} \alpha \\ \beta \end{pmatrix} + \begin{pmatrix} A_{1133} & A_{1233} \\ A_{1233} & A_{2233} \end{pmatrix} \boldsymbol{\gamma} \right. \\
&\left. + \begin{pmatrix} \dfrac{(\gamma_1 - f_1)(6 - a^2 c) - a^2 d}{2a^2} & 2\dfrac{\gamma_2 - f_2}{b^2} \\ -c(\gamma_2 - f_2) & \dfrac{(\gamma_1 - f_1)(2 - 3a^2 c) - 3a^2 d}{2a^2} \end{pmatrix} \mathbf{g}_0(s) \right] ds \\
= &\int_{t_0}^{\tau} \left[- \begin{pmatrix} \left(-\dfrac{3(\gamma_1 - f_1)}{a_0^2} + \dfrac{(\gamma_1 - f_1)c + d}{2} \right) \dfrac{\upsilon(\gamma_1 - f_1)}{\omega} \sin \omega s \\ -c(\gamma_2 - f_2) \dfrac{\upsilon(\gamma_1 - f_1)}{\omega} \sin \omega s \end{pmatrix} \right. \\
= &\begin{pmatrix} \left(-\dfrac{3(\gamma_1 - f_1)}{a_0^2} + \dfrac{(\gamma_1 - f_1)c + d}{2} \right) \dfrac{\upsilon(\gamma_1 - f_1)}{\omega} (\cos \omega \tau - \cos \omega t_0) \\ -c(\gamma_2 - f_2) \dfrac{\upsilon(\gamma_1 - f_1)}{\omega} (\cos \omega \tau - \cos \omega t_0) \end{pmatrix}.
\end{aligned}$$

Then in the following term

$$\begin{aligned}
&\int_{t_0}^{t} 2 \begin{pmatrix} \dfrac{(\gamma_1 - f_1)(4 - a^2 c) - a^2 d}{a^2} & 2\dfrac{\gamma_2 - f_2}{b^2} \\ -c(\gamma_2 - f_2) & 2\dfrac{(\gamma_1 - f_1)(1 - a^2 c) - a^2 d}{a^2} \end{pmatrix} \\
&\times \int_{t_0}^{\tau} \left[\begin{pmatrix} \alpha \\ \beta \end{pmatrix} + \begin{pmatrix} A_{1133} & A_{1233} \\ A_{1233} & A_{2233} \end{pmatrix} \boldsymbol{\gamma} \right. \\
&\left. + \begin{pmatrix} \dfrac{(\gamma_1 - f_1)(6 - a^2 c) - a^2 d}{2a^2} & 2\dfrac{\gamma_2 - f_2}{b^2} \\ -c(\gamma_2 - f_2) & \dfrac{(\gamma_1 - f_1)(2 - 3a^2 c) - 3a^2 d}{2a^2} \end{pmatrix} \mathbf{g}_0(s) \right] ds \Bigg] d\tau \\
= \; &2 \int_{t_0}^{t} \left[\begin{pmatrix} \dfrac{(\gamma_1 - f_1)(4 - a_0^2 c) - a_0^2 d}{a_0^2} & 2\dfrac{\gamma_2 - f_2}{b^2} \\ -c(\gamma_2 - f_2) & 2\dfrac{(\gamma_1 - f_1)(1 - a_0^2 c) - a_0^2 d}{a_0^2} \end{pmatrix} + 2(\gamma_1 - f_1) \begin{pmatrix} 2 & 0 \\ 0 & 1 \end{pmatrix} \upsilon \cos \omega t \right] \\
&\times \begin{pmatrix} \left(-\dfrac{3(\gamma_1 - f_1)}{a_0^2} + \dfrac{(\gamma_1 - f_1)c + d}{2} \right) \dfrac{\upsilon(\gamma_1 - f_1)}{\omega} (\cos \omega t - \cos \omega t_0) \\ -c(\gamma_2 - f_2) \dfrac{\upsilon(\gamma_1 - f_1)}{\omega} (\cos \omega t - \cos \omega t_0) \end{pmatrix},
\end{aligned}$$

we only keep the linear terms

$$2(t-t_0)\begin{pmatrix} \dfrac{(\gamma_1-f_1)(4-a_0^2c)-a_0^2d}{a_0^2} & 2\dfrac{\gamma_2-f_2}{b^2} \\ -c(\gamma_2-f_2) & 2\dfrac{(\gamma_1-f_1)(1-a_0^2c)-a_0^2d}{a_0^2} \end{pmatrix}$$
$$\times\begin{pmatrix} -\left(-\dfrac{3(\gamma_1-f_1)}{a_0^2}+\dfrac{(\gamma_1-f_1)c+d}{2}\right)\dfrac{\upsilon(\gamma_1-f_1)}{\omega}\cos\omega t_0 \\ c(\gamma_2-f_2)\dfrac{\upsilon(\gamma_1-f_1)}{\omega}\cos\omega t_0 \end{pmatrix}$$
$$+2\upsilon(t-t_0)(\gamma_1-f_1)\begin{pmatrix} 2 & 0 \\ 0 & 1 \end{pmatrix}\begin{pmatrix} \left(-\dfrac{3(\gamma_1-f_1)}{a_0^2}+\dfrac{(\gamma_1-f_1)c+d}{2}\right)\dfrac{\upsilon(\gamma_1-f_1)}{\omega} \\ -c(\gamma_2-f_2)\dfrac{\upsilon(\gamma_1-f_1)}{\omega} \end{pmatrix}.$$

We also have to analyze the term

$$\int_{t_0}^{t} \mathbf{g}_0^T \mathbb{T}\mathbf{g}_0 \, dt.$$

Decomposing $\mathbf{g}_0$ as

$$\mathbf{g}_0 = \mathbf{g}_0^S + \mathbf{g}_0^P \sin\omega t_0 = \begin{pmatrix} g_{0,1}^S \\ g_{0,2}^S \end{pmatrix} + \begin{pmatrix} g_{0,1}^P \\ g_{0,2}^P \end{pmatrix} \sin\omega t_0,$$

we have

$$
\begin{aligned}
&\int_{t_0}^{t} \mathbf{g}_0^T \mathbb{T} \mathbf{g}_0 \, dt \\
= &\int_{t_0}^{t} \begin{pmatrix} \left(\frac{4}{a^2} - c\right)\left(\mathbf{g}_{0,1}^S + \mathbf{g}_{0,1}^P \sin\omega t_0\right)^2 + \frac{2}{b^2}\left(\mathbf{g}_{0,2}^S + \mathbf{g}_{0,2}^P \sin\omega t_0\right)^2 \\ \frac{2-3ca^2}{a^2}\left(\mathbf{g}_{0,1}^S + \mathbf{g}_{0,1}^P \sin\omega t_0\right)\left(\mathbf{g}_{0,2}^S + \mathbf{g}_{0,2}^P \sin\omega t_0\right) \end{pmatrix} \\
= &\int_{t_0}^{t} \begin{pmatrix} \left(\frac{4}{a_0^2} - c\right)\left(\mathbf{g}_{0,1}^S\right)^2 + \frac{2}{b^2}\left(\mathbf{g}_{0,2}^S\right)^2 \\ \frac{2-3ca^2}{a^2}\mathbf{g}_{0,1}^S \mathbf{g}_{0,2}^S \end{pmatrix} \\
&+ \sin\omega t_0 \begin{pmatrix} \left(\frac{8}{a_0^2} - 2c\right)\mathbf{g}_{0,1}^S \mathbf{g}_{0,1}^P + 4\upsilon\left(\mathbf{g}_{0,1}^S\right)^2 + \frac{4}{b^2}\mathbf{g}_{0,2}^S \mathbf{g}_{0,2}^P \\ \frac{2-3ca^2}{a^2}\left(\mathbf{g}_{0,1}^S \mathbf{g}_{0,2}^P + \mathbf{g}_{0,1}^P \mathbf{g}_{0,2}^S\right) \end{pmatrix} \\
&+ \sin^2\omega t_0 \begin{pmatrix} \frac{4-ca_0^2}{a_0^2}\left(\mathbf{g}_{0,1}^P\right)^2 + 8\upsilon \mathbf{g}_{0,1}^S \mathbf{g}_{0,1}^P + \frac{2}{b^2}\left(\mathbf{g}_{0,2}^P\right)^2 \\ \frac{2-3ca^2}{a^2}\mathbf{g}_{0,1}^P \mathbf{g}_{0,2}^P \end{pmatrix} \\
&+ \sin^3\omega t_0 \begin{pmatrix} 4\upsilon\left(\mathbf{g}_{0,1}^P\right)^2 \\ 0 \end{pmatrix} \Bigg) \, dt \\
= &(t-t_0) \begin{pmatrix} \left(\frac{4}{a_0^2} - c\right)\left(\mathbf{g}_{0,1}^S\right)^2 + \frac{2}{b^2}\left(\mathbf{g}_{0,2}^S\right)^2 \\ \frac{2-3ca^2}{a^2}\mathbf{g}_{0,1}^S \mathbf{g}_{0,2}^S \end{pmatrix} \\
&- \frac{\cos\omega t - \cos\omega t_0}{\omega} \begin{pmatrix} \left(\frac{8}{a_0^2} - 2c\right)\mathbf{g}_{0,1}^S \mathbf{g}_{0,1}^P + 4\upsilon\left(\mathbf{g}_{0,1}^S\right)^2 + \frac{4}{b^2}\mathbf{g}_{0,2}^S \mathbf{g}_{0,2}^P \\ \frac{2-3ca^2}{a^2}\left(\mathbf{g}_{0,1}^S \mathbf{g}_{0,2}^P + \mathbf{g}_{0,1}^P \mathbf{g}_{0,2}^S\right) \end{pmatrix} \\
&+ \left(\frac{t-t_0}{2} - \frac{\sin 2\omega t - \sin 2\omega t_0}{4\omega}\right) \begin{pmatrix} \frac{4-ca_0^2}{a_0^2}\left(\mathbf{g}_{0,1}^P\right)^2 + 8\upsilon \mathbf{g}_{0,1}^S \mathbf{g}_{0,1}^P + \frac{2}{b^2}\left(\mathbf{g}_{0,2}^P\right)^2 \\ \frac{2-3ca^2}{a^2}\mathbf{g}_{0,1}^P \mathbf{g}_{0,2}^P \end{pmatrix} \\
&+ \left(\frac{\cos 3\omega t - \cos 3\omega t_0}{12\omega} - \frac{3}{4}\frac{\cos\omega t - \cos\omega t_0}{\omega}\right) \begin{pmatrix} 4\upsilon\left(\mathbf{g}_{0,1}^P\right)^2 \\ 0 \end{pmatrix}.
\end{aligned}
$$

Finally, we can write the curvature, keeping only the dominant terms

$$
\begin{aligned}
\mathbf{g}_1(t_0) \;=\; & -\lim_{t\to-\infty}\left[2(t-t_0)\begin{pmatrix} \dfrac{(\gamma_1-f_1)(4-a_0^2c)-a_0^2d}{a_0^2} & 2\dfrac{\gamma_2-f_2}{b^2} \\ -c(\gamma_2-f_2) & 2\dfrac{(\gamma_1-f_1)(1-a_0^2c)-a_0^2d}{a_0^2}\end{pmatrix}\right]^{-1} \\
& \times\left[2(t-t_0)\begin{pmatrix} \dfrac{c}{6}-\dfrac{1}{3a^2} \\ 0\end{pmatrix}\right. \\
& +2\begin{pmatrix} \frac{4A_{1133}+A_{2233}}{3} & A_{1233} \\ A_{1233} & \frac{A_{1133}+4A_{2233}}{3}\end{pmatrix}\int_{t_0}^{t}\mathbf{g}_0\,dt \\
& +(t-t_0)\begin{pmatrix} \left(\dfrac{4}{a_0^2}-c\right)\left(\mathbf{g}_{0,1}^S\right)^2+\dfrac{2}{b^2}\left(\mathbf{g}_{0,2}^S\right)^2 \\ \dfrac{2-3ca^2}{a^2}\mathbf{g}_{0,1}^S\mathbf{g}_{0,2}^S\end{pmatrix} \\
& +\frac{t-t_0}{2}\begin{pmatrix} \dfrac{4-ca_0^2}{a_0^2}\left(\mathbf{g}_{0,1}^P\right)^2+8\upsilon\mathbf{g}_{0,1}^S\mathbf{g}_{0,1}^P+\dfrac{2}{b^2}\left(\mathbf{g}_{0,2}^P\right)^2 \\ \dfrac{2-3ca^2}{a^2}\mathbf{g}_{0,1}^P\mathbf{g}_{0,2}^P\end{pmatrix} \\
& +2(t-t_0)\begin{pmatrix} \dfrac{(\gamma_1-f_1)(4-a_0^2c)-a_0^2d}{a_0^2} & 2\dfrac{\gamma_2-f_2}{b^2} \\ -c(\gamma_2-f_2) & 2\dfrac{(\gamma_1-f_1)(1-a_0^2c)-a_0^2d}{a_0^2}\end{pmatrix} \\
& \times\begin{pmatrix} -\left(-\dfrac{3(\gamma_1-f_1)}{a_0^2}+\dfrac{(\gamma_1-f_1)c+d}{2}\right)\dfrac{\upsilon(\gamma_1-f_1)}{\omega}\cos\omega t_0 \\ c(\gamma_2-f_2)\dfrac{\upsilon(\gamma_1-f_1)}{\omega}\cos\omega t_0\end{pmatrix} \\
& \left.+2(t-t_0)\frac{(\upsilon(\gamma_1-f_1))^2}{\omega}\begin{pmatrix} 2\left(-\dfrac{3(\gamma_1-f_1)}{a_0^2}+\dfrac{(\gamma_1-f_1)c+d}{2}\right) \\ -c(\gamma_2-f_2)\end{pmatrix}\right],
\end{aligned}
$$

which simplifies to the still complicated formula

$$
\begin{aligned}
\mathrm{g}_1(t_0) \;=\; & -\left[2\begin{pmatrix} \dfrac{(\gamma_1-f_1)(4-a_0^2c)-a_0^2d}{a_0^2} & 2\dfrac{\gamma_2-f_2}{b^2} \\ -c(\gamma_2-f_2) & 2\dfrac{(\gamma_1-f_1)(1-a_0^2c)-a_0^2d}{a_0^2}\end{pmatrix}\right]^{-1} \\
& \times\left[2\begin{pmatrix} \dfrac{c}{6}-\dfrac{1}{3a_0^2} \\ 0\end{pmatrix}+2\begin{pmatrix} \frac{4A_{1133}+A_{2233}}{3} & A_{1233} \\ A_{1233} & \frac{A_{1133}+4A_{2233}}{3}\end{pmatrix}\mathrm{g}_0^S\right. \\
& +\begin{pmatrix} \left(\dfrac{4}{a_0^2}-c\right)\left(\mathrm{g}_{0,1}^S\right)^2+\dfrac{2}{b^2}\left(\mathrm{g}_{0,2}^S\right)^2 \\ \dfrac{2-3ca^2}{a^2}\mathrm{g}_{0,1}^S\mathrm{g}_{0,2}^S\end{pmatrix}+\frac{1}{2}\begin{pmatrix} \dfrac{4-ca_0^2}{a_0^2}\left(\mathrm{g}_{0,1}^P\right)^2+8\upsilon\mathrm{g}_{0,1}^S\mathrm{g}_{0,1}^P+\dfrac{2}{b^2}\left(\mathrm{g}_{0,2}^P\right)^2 \\ \dfrac{2-3ca^2}{a^2}\mathrm{g}_{0,1}^P\mathrm{g}_{0,2}^P\end{pmatrix} \\
& +2\frac{(\upsilon(\gamma_1-f_1))^2}{\omega}\begin{pmatrix} 2\left(-\dfrac{3(\gamma_1-f_1)}{a_0^2}+\dfrac{(\gamma_1-f_1)c+d}{2}\right) \\ -c(\gamma_2-f_2)\end{pmatrix} \qquad \text{(B.27)} \\
& +2\begin{pmatrix} \dfrac{(\gamma_1-f_1)(4-a_0^2c)-a_0^2d}{a_0^2} & 2\dfrac{\gamma_2-f_2}{b^2} \\ -c(\gamma_2-f_2) & 2\dfrac{(\gamma_1-f_1)(1-a_0^2c)-a_0^2d}{a_0^2}\end{pmatrix} \\
& \left.\times\begin{pmatrix} -\left(-\dfrac{3(\gamma_1-f_1)}{a_0^2}+\dfrac{(\gamma_1-f_1)c+d}{2}\right) \\ c(\gamma_2-f_2)\end{pmatrix}\frac{\upsilon(\gamma_1-f_1)}{\omega}\cos\omega t_0.\right.
\end{aligned}
$$

Bibliography

[1] Ahmed S. R., Ramm R., Faltin G. 1984 Some salient features of the time-averaged ground vehicle wake. SAE Technical paper series 840300.

[2] Arnold V. I. 1978 Ordinary Differential Equations, MIT Press, Cambridge.

[3] Bakker P.G., Winkel M.E.M. 1989 On the topology of three-dimensional flow structures and local solutions of the Navier-Stokes equations. Proc. IUTAM Symp. Topol. Fluid Mech., Cambridge, pp. 13-18.

[4] Chapman C. T. 1986 Topological classification of flow separation on three-dimensional bodies. NASA

[5] Dallmann U. 1983 Topological structures of three-dimensional flow separation, DFVLR 1B: 221-82.

[6] Délery J.M. 2001 Robert Legendre and Henri Werlé: Toward the elucidation of three-dimensional separation. Annu Rev. Fluid Mech 2001. 33:129-54

[7] Ghosh S., Leonard A., Wiggins S. 1998 Diffusion of a passive scalar from a no-slip boundary into a two-dimensional chaotic advection field. J. Fluid Mech. **372,** 119–163.

[8] Hale J. K. 1980 Ordinary Differential Equations. Kreiger.

[9] Haller G., Poje A. 1998 Finite-time transport in aperiodic flows. Physica D **119,** 352–380.

[10] Haller G. 2000 Finding finite-time invariant manifolds in two-dimensional velocity fields. Chaos **10,** 99–108.

[11] Haller G. 2001 Lagrangian structures and the rate of strain in two-dimensional turbulence. Phys. Fluids A **13,** 3365–3385.

[12] Haller G. 2002 Kinematic theory of unsteady separation for two-dimensional flows. J. Fluid Mech, submitted.

[13] Hesthaven J.S. 1998 A stable penalty method for the compressible Navier-Stokes equations.III. Multi dimensional domain decomposition schemes. SIAM J. Sci. Comp. 20(1), pp. 62-93.

[14] Hornung H., Perry AE. 1984 Some aspects of three-dimensional separation. Part1: Streamsurface bifurcations. Z. Flugwiss. Weltraumforsch. 8(Heft 2): 77-87.

[15] Hunt JCR, Abell CJ, Peterka JA, Woo H. 1978 Kinematical studies of the flows around free or surface mounted obstacle; applying topology to flow visualization. J. Fluid Mech. 86: 179-200.

[16] Insperger T. 2003 Flow control - effect of time delay. Preprint.

[17] Legendre R. 1956 Séparation de l'écoulement laminaire tridimensionnel. La Rech. Aéronaut. 54: 3-8.

[18] Lekien F., Insperger T., Haller G. 2003 Control of 2D separation. Preprint.

[19] Lighthill M.J. 1963 Attachment and separation in three-dimensional flows. In Laminar Bound. Layer Theory, Sect. II 2.6, ed L Rosenhead, pp. 72-82. New York: Oxford Univ. Press

[20] Lighthill M.J. 1963 Boundary layer theory. In Laminar Boundary Layers (ed. L. Rosenhead). Dover.

[21] Perry A.E., Fairlie BD. 1974 Critical points in flow patterns. Adv. Geophys. B 18-200-15

[22] Perry A.E., Chong M.S. 1986 A series expansion study of the Navier-Stokes equations with applications to three-dimensional separation patterns. J. Fluid Mech. **173,** 207–223.

[23] Perry A.E., Chong M. S.1987 A description of eddying motions and flow patterns using critical-point concepts. Ann. Rev. Fluid Mech. 1987. 19:125-55

[24] Prandtl, L. 1904 Über Flüssigkeitsbewegung bei sehr kleiner Reibung. Verh. III, Int. Math. Kongr., Heidelberg, 484–491.

[25] Salman H., Wang Y., Haller G., Hesthaven J.S. 2002 A feedback control law for unsteady separation in two-dimensional flows. J. Flow, Turbulence and Combust. submitted.

[26] Shariff K., Pulliam T.H., Ottino J.M. 1991 A dynamical systems analysis of kinematics in the time-periodic wake of a circular cylinder. Lect. Appl. Math. **28**, 613–646.

[27] Sinha S.K., Pandey M., Wang H., Pal D. 1997 Using an array of transducers under a compliant wall to detect and control dynamic stall on a pitching airfoil. AIAA 98-0678.

[28] Tobak M., Peake D.J. 1982 Topology of three-dimensional separated flows. Annu. Rev. Fluid Mech. 14:61-85

[29] Tobak M., Coon M. D. 1996 Topology of pressure surfaces in three-dimensional surfaces in three-dimensional separated flows AIAA 96-0319

[30] Tobak M. 1997 Topologically derived separation onset conditions for two- and three-dimensional laminar flows. AIAA 97-0866

[31] Wang K.C. 1970 Three-dimensional boundary layer near the plane of symmetry of a spheroid at incidence. J. Fluid Mech. 43, 187 (1970)

[32] Wang K.C. 1983 On the dispute about open separation. AIAA Pap. 83-0296

[33] Wang Y., Haller G., Banaszuk, Tadmor G. 2003 Closed-loop lagrangian separation control in a bluff body shear flow model. Physics of Fluids, 15-8.

[34] Wu J.Z., Gu J.W. 1987 Steady three-dimensional fluid particle separation from arbitrary smooth surface and formation of free vortex layers. 87-2348

[35] Wu J.Z., Tramel R.W., Zhu F.L., Yin X.Y. 2000 A vorticity dynamics theory of three-dimensional flow separation. Physics of Fluids, 12-8.

[36] Yates L.A., Chapman G.T. 1992 Streamlines, vorticity lines, and vortices around three-dimensional bodies. AIAA J. 30:1819-26

[37] Yuster T., Hackborn W.W. 1997 On invariant manifolds attached to oscillating boundaries of Stokes flows. Chaos **7,** 769–776.